5-2016

ORGANIZATION AND REGULATION OF PROTEINS REQUIRED FOR INITIATION OF CELL DIVISION IN ESCHERICHIA COLI

Veronica W. Rowlett

ORGANIZATION AND REGULATION OF PROTEINS REQUIRED FOR INITIATION OF CELL DIVISION IN ESCHERICHIA COLI

By

Veronica Wells Rowlett, B.S.

APPROVED:

Supervisory Professor
William Margolin, Ph.D.

Kevin A. Morano, Ph.D.

Theresa M. Koehler, Ph.D.

Heidi B. Kaplan, Ph.D.

Joseph L. Alcorn, Ph.D.

APPROVED:

Dean, The University of Texas
Graduate School of Biomedical Sciences at Houston

ORGANIZATION AND REGULATION OF PROTEINS REQUIRED FOR INITIATION OF CELL DIVISION IN ESCHERICHIA COLI

A

Dissertation

Presented to the Faculty of

The University of Texas

Health Science Center at Houston

and

The University of Texas

M.D. Anderson Cancer Center

Graduate School of Biomedical Sciences

in Partial Fulfillment

of the Requirements

for the Degree of

DOCTOR OF PHILOSOPHY

By

Veronica Wells Rowlett, B.S.

Houston, TX

May, 2016

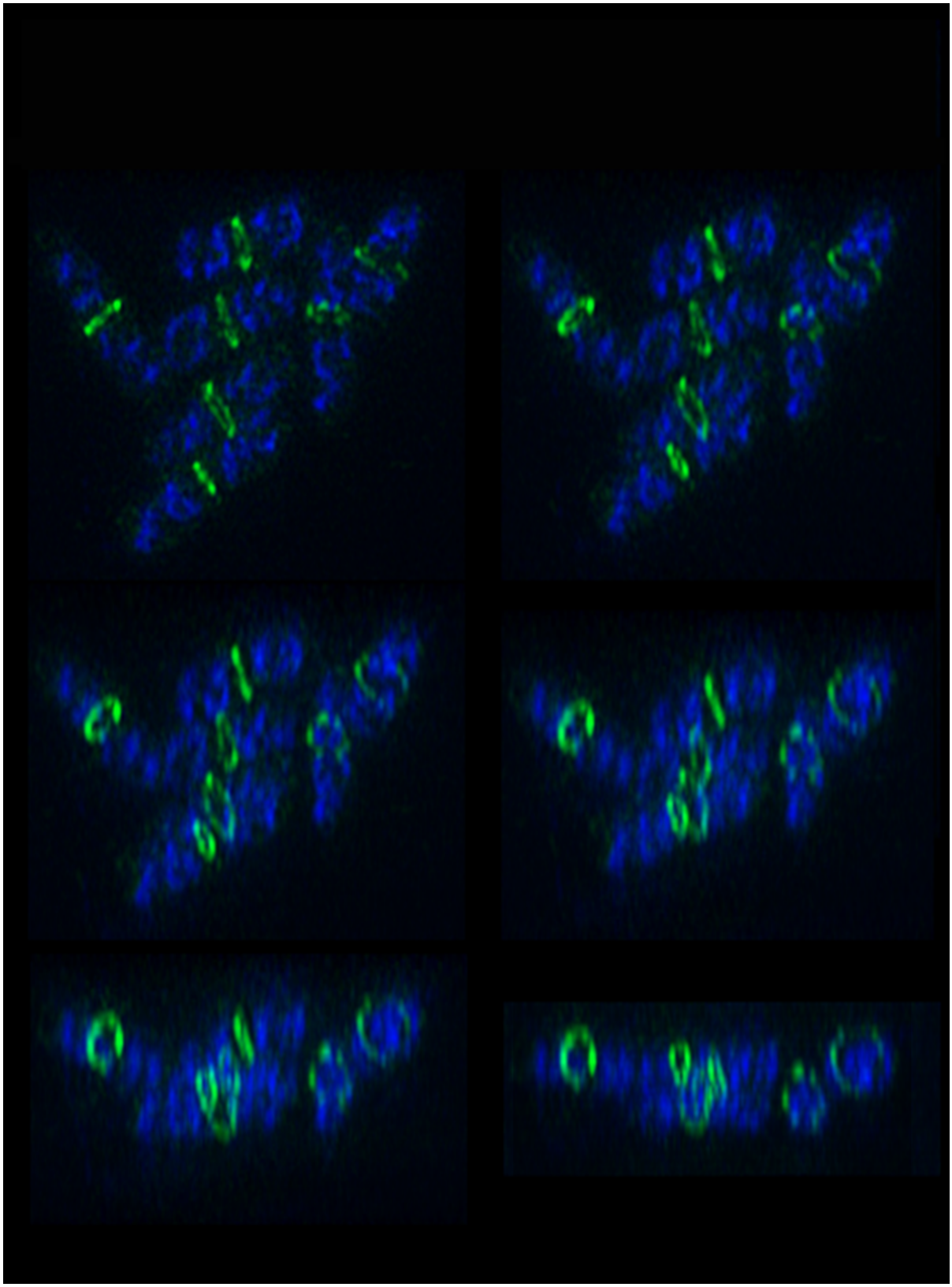

DEDICATION

This work is dedicated to my family.

ACKNOWLEDGMENTS

I would like to thank my mentor William Margolin for being an outstanding advisor throughout my graduate career. Bill gave me guidance and support while allowing me to develop as an independent researcher, and I am grateful for the training I have received. Bill's enthusiasm and excitement for science made it easy to remain optimistic through challenging times. I appreciate his support of my career goals and the opportunities that he provided to strengthen my scientific writing and communication skills.

I would like to thank all past and present members of the Margolin laboratory for insightful comments and technical advice. I am grateful to Daniel Haeusser, Jennifer Herricks, Kim Busiek, and Jesus Eraso for their feedback on results, presentations, and written work. Daniel was my mentor during my rotation in the lab, and I learned so much from him during my rotation and after joining the lab. Jennifer was willing to have discussions about experiments and provide encouragement. Kim always made me laugh and gave excellent advice. It has been a pleasure to work with new members Marcin Krupka and Kara Schoenemann. Marcin is willing to share ideas and technical advice. Kara has been a ray of sunshine in the lab and a source of encouragement, and I would like to acknowledge Kara for her help with multiple protein purifications.

I would like to thank Kevin Morano, Theresa Koehler, Heidi Kaplan, and Joseph Alcorn for serving on my advisory and supervisory committees and for their helpful suggestions that guided my research plans. I am grateful for their letters of recommendation for scholarship applications and for their encouragement and support over the years. I'd also like to thank Kevin Morano for chairing, and Heidi Kaplan, Danielle Garsin, Ambro van Hoof, and Jeffrey Frost for serving on my candidacy exam committee; I learned so much from this process.

I am grateful to all of the faculty, students, and postdocs in the Microbiology and Molecular Genetics (MMG) Department for discussions about research and careers, and readily sharing reagents and equipment. I am also thankful to the MMG staff for their support. I'm very thankful to Veronica

Garcia for being a great friend, workout partner, and collaborator. I would like to thank William Dowhan and members of his lab, Eugenia Mileykovskaya, Venkata Mallampalli, and especially Heidi Vitrac for their biochemistry and lipid advice. Heidi has been a great collaborator and her advice on biochemical experiments was invaluable.

I am grateful for the support of the scholarships I have received while at the Graduate School of Biomedical Sciences (GSBS), including the Gigli Family Endowed Scholarship, the Investing in Student Futures Scholarship, and GSBS Travel Awards. I would like to thank the ASM Texas Branch and Millicent Goldschmidt for choosing me as a recipient of the Eugene and Millicent Goldschmidt Graduate Student Award. Thank you to the Graduate Student Education Committee (GSEC) for selecting me to receive the Dean's Research Scholarship, a GSEC Poster Award, and a GSEC Travel Award. Thank you to the MMG Department for the MMG Travel Award for career development. I would also like to thank the ASM for a travel grant to attend the 2015 Prokaryotic Cell Biology and Development Meeting. Thank you to the National Institutes of Health for a Diversity Supplement that supported some of my research.

I would like to thank Renato Aguilera and the Research Initiative for Scientific Enhancement (RISE) program at The University of Texas at El Paso for supporting my undergraduate research in Marc Cox's laboratory. It was through this research experience that I decided to pursue graduate education, and I am very grateful to Marc for the opportunity to work in his lab and present a poster at a conference where I learned about the wonderful MMG Program at the GSBS from my poster judge, Kevin Morano.

I would like to thank my husband, Daniel Adam Rowlett. I am so proud of his ten-year career in the U.S. military. He has been incredibly supportive, caring, and understanding. I love you and I am so excited for our future together. I would like to thank my parents, Russel and Phyllis Wells, who believed in me and encouraged me to pursue the career of my dreams. Thank you both for being great role models and for your support. Thank you to my sister Melissa Rangel for encouraging me and being a great friend. Phone conversations with my sister and my mom always cheered me up. Thank

you to my brothers, Rusty and Jeff Wells for their encouragement over the years. I am very grateful to have such a close and supportive family. I'd like to thank my grandparents, aunts, uncles and cousins for their encouragement. Finally, thank you to all my nieces and nephews; you can do anything you set your mind to!

ORGANIZATION AND REGULATION OF PROTEINS REQUIRED FOR INITIATION OF CELL DIVISION IN ESCHERICHIA COLI

Veronica Wells Rowlett, B.S.

Supervisory Professor: William Margolin, Ph.D.

The process of bacterial cell division relies on the assembly of multiple proteins to form the cell division machine, or "divisome." FtsZ, a bacterial homolog of eukaryotic tubulin, forms a ring-like structure, the "Z ring," at midcell and serves as a scaffold for divisome assembly and potential force generator during synthesis of the division septum. Both FtsA, a bacterial homolog of eukaryotic actin, and ZipA, a single-pass transmembrane protein, anchor the Z ring to the inner membrane, are required for the localization of other divisome proteins to midcell, and likely influence the assembly state of FtsZ. Positioning of the Z ring at midcell must be precise in order to ensure efficient cell division, and the MinCDE proteins have an important role in restricting the Z ring to midcell. I found that an artificial fusion of the C-terminus of MinC with MinD, instead of inhibiting Z ring formation as expected, restricted FtsA localization to only part of an intact Z ring. This resulted in many cells with division septa mostly on the side where FtsA localized, causing jackknifing of dividing cells and supporting the importance of a symmetrical FtsA ring for normal cell division. I then investigated localization patterns for FtsZ, FtsA, and ZipA in normal cells using 3D-SIM super-resolution microscopy, which showed that they generally colocalize in puncta instead of a uniformly continuous ring. Finally, I investigated the assembly of purified FtsA and FtsA mutant proteins by electron microscopy and assessed their ability to bind membranes. These studies have refined our view of the organization of the proto-ring proteins FtsZ, FtsA, and ZipA.

Table of Contents

Approval Sheet	i
Title Page	ii
Cover art by Veronica W. Rowlett and William Margolin	iii
Dedication	iv
Acknowledgements	v
Abstract	viii
Table of Contents	ix
List of Figures	xi
List of Tables	xiii
Chapter I: Introduction	**1**
Division site positioning	2
Divisome assembly	9
Proto-ring proteins	12
Gaps in knowledge and significance of research	16
Chapter II: Materials and Methods	**18**
Chapter III: Asymmetric constriction of dividing *Escherichia coli* cells induced by expression of a fusion between two Min proteins	**33**
Introduction	34
Results	37
Discussion	59
Chapter IV: 3D-SIM super-resolution of FtsZ and its membrane tethers in *Escherichia coli* cells	**62**
Introduction	63

Results 66

Discussion 77

Chapter V: *In vitro* biochemical analysis of FtsA **79**

Introduction 80

Results 83

Discussion 95

Chapter VI: Discussion and Future Directions **98**

An FtsA ring is essential for symmetrical septum constriction 99

FtsZ, FtsA, and ZipA localize into punctate rings 101

Debate over the ultrastructure and force generation of the Z ring 102

FtsA forms rings *in vitro* similar to a functional homolog, SepF 104

FtsA and FtsA mutant proteins polymerize and bind to liposomes without added ATP 106

Importance of reversible membrane binding 108

Targeting the divisome for novel antimicrobial therapies 108

Bibliography **110**

Vita **133**

List of Figures

Figure 1-1. The mechanism of the Min system 4

Figure 1-2. Roles of FtsA and ZipA during cell division 10

Figure 1-3. Domain organization and assembly of FtsZ 14

Figure 2-1. Quantitation of immunofluorescence localization patterns of *E. coli* cells overproducing MinCc-MinD 30

Figure 3-1. A MinCc-MinD fusion causes bending in Δ*minCDE E. coli* cells 38

Figure 3-2. Viability of various fusion constructs 41

Figure 3-3. Growing and dividing cells overproducing MinCc-MinD in time-lapse images 43

Figure 3-4. Transmission electron microscopy of thin sections of dividing WM2738 cells 44

Figure 3-5. Localization of His_6-MinCc-MinD fusions in Δ*minCDE* (WM1032) cells 46

Figure 3-6. Membrane targeting, septal interaction, and self-interaction contribute to the effects of MinCc-MinD on cell bending 48

Figure 3-7. Western blot of fusions 49

Figure 3-8. Aggregated His_6-MinCc-MinD fusion proteins preferentially displace FtsA from the Z ring 54

Figure 3-9. Colony viability assays 57

Figure 3-10. Morphologies of MinCc-MinD cells overproducing FtsQAZ or carrying chromosomal *ftsA** 58

Figure 4-1. Examples of Z ring localization using different methods of super-resolution microscopy 64

Figure 4-2. 3D-SIM localization of FtsZ in *E. coli* 67

Figure 4-3. Quantitation of fluorescence intensities around the circumference of Z rings 68

Figure 4-4. 3D-SIM localization of FtsZ after overproduction of SulA 69

Figure 4-5. 3D-SIM localization of FtsA and ZipA 71

Figure 4-6. Quantitation of FtsA and ZipA colocalization 73

Figure 4-7. 3D-SIM localization and transmission electron micrographs of FtsZ and $FtsZ_{L169R}$ 74

Figure 5-1. Dimer crystal structure of *Thermotoga maritima* FtsA 81

Figure 5-2. Purification of His_6-FtsA from *E. coli* cells 84

Figure 5-3. Transmission electron micrographs of FtsA and FtsA mutant proteins stained with uranyl acetate 85

Figure 5-4. FtsA purifies with ATP bound to the nucleotide-binding site 86

Figure 5-5. Sedimentation analysis of liposome bound FtsA proteins 88

Figure 5-6. Turbidity assay of FtsA 93

Figure 6-1. Model of ZipA and FtsA activity during cell division 100

List of Tables

Table 2-1. Strains and plasmids used in this study 20

Table 2-2. Oligonucleotides used for plasmid construction 24

Table 3-1. Percentage of bent division septa 39

Table 3-2. Phenotypes of protein fusions in different Min deletion backgrounds 51

Table 5-1. Growth of FtsA mutants in an *ftsA12* background and with *ftsA-null* transduction 90

Chapter I

Introduction

The process of cell division occurs in all organisms, from bacteria to eukaryotes, and is essential for the continuation of life. Most bacteria divide by binary fission, in which a single cell grows and duplicates its genetic material, and then separates into two daughter cells. This process must be tightly regulated to ensure that division occurs at the right place and time. Here, I present a brief overview of the proteins involved in the regulation of cell division, with a focus on the Gram-negative model organism *Escherichia coli*.

Rod shaped *E. coli* cells double in size and duplicate and partition their chromosomes, prior to separation into two genetically identical daughter cells. It is very important to regulate when and where cell division occurs to ensure that both daughter cells grow to the appropriate size and receive a complete copy of the chromosome. Multiple proteins assemble to form the division machinery, or "divisome," at the middle of cells with segregated chromosomes. If the divisome forms at cell poles, septation results in minicells that do not contain chromosomes, and will not grow and divide (Adler et al., 1967). Additionally, if the divisome forms over chromosomes, septation can lead to chromosome guillotining and unequal distribution of the cell's genetic material into daughter cells (Niki et al., 1991). In the first step of divisome formation, FtsZ, an essential tubulin homolog, polymerizes into a ring (Z ring) at midcell (Bi & Lutkenhaus, 1991). Many proteins interact with FtsZ to modulate its assembly and regulate cytokinesis (Bi & Lutkenhaus, 1991).

1.1 Division site positioning

1.1.1 The *E. coli* Min system.

Defining the location at which cell division can occur is important to ensure that daughter cells are the same size. Two well-known systems that contribute to positioning the divisome at midcell are the Min system and nucleoid occlusion. The Min system is comprised of three proteins, MinC, MinD, and MinE that oscillate in *E. coli* cells (Monahan & Harry, 2013; Rowlett & Margolin, 2015a). MinC has two domains, an N-terminal domain (MinCn), and a C-terminal domain (MinCc),

and both domains synergistically inhibit polymerization of FtsZ. MinCn inhibits longitudinal interactions of subunits of FtsZ within a protofilament, whereas MinCc inhibits lateral interactions between protofilaments (Hu & Lutkenhaus, 2000; Shiomi & Margolin, 2007a; Shen & Lutkenhaus, 2009, 2010). MinD, a ParA-like ATPase (de Boer et al., 1991), contains a membrane targeting sequence (MTS) at its C-terminus (Szeto et al., 2003). MinD binds both the inner membrane and the C-terminus of MinC (de Boer et al., 1991; Hu & Lutkenhaus, 2000, 2003). When ATP-bound, MinD forms a dimer and associates with the membrane (Szeto et al., 2002; Hu & Lutkenhaus, 2003). Copolymers of alternating MinC and MinD dimers form, bind the membrane at a polar zone, and are removed from the membrane by MinE (Ghosal et al., 2014; Conti et al., 2015; Raskin & de Boer, 1997). In the absence of MinE, MinCD inhibits Z ring formation at all areas of the cell, resulting in filamentation and cell death (de Boer et al., 1989).

MinE maintains polar localization of MinCD by forming a ring at the edge of the MinCD zone and removing complexes of MinCD as the MinE ring moves poleward, causing the migration of MinCD to the opposite pole (Raskin & de Boer, 1997, 1999a, b; Hu et al., 2002). MinE contains an N-terminal amphipathic helix that serves as an MTS, and the ability to bind the membrane directly is important for MinE function (Ma et al., 2003; Hsieh et al., 2010). Disruption of the MinE MTS reduces the efficiency of MinD removal from the membrane, resulting in abnormal MinD localization outside of the polar zone and aberrant oscillation (Hsieh et al., 2010). Dimers of MinD are recognized by MinE, causing MinE to change conformation and displace MinC while binding MinD and stimulating its ATPase activity and removal from the membrane (Fig. 1-1; Raskin & de Boer, 1997; Hu et al., 2002; Suefuji et al., 2002; Lackner et al., 2003; Loose et al., 2011; Park et al., 2011). The interactions of MinD and MinE create an oscillating system that maintains the highest concentration of the passenger protein MinC at cell poles (Hu & Lutkenhaus, 1999; Raskin & de Boer, 1999a, b). As MinC directly interacts with FtsZ *in vitro* and inhibits its polymerization, the higher amounts of MinC located at cell poles prevent FtsZ from forming rings in these locations (Hu et al., 1999; Dajkovic et al., 2008; Shen & Lutkenhaus, 2009, 2010).

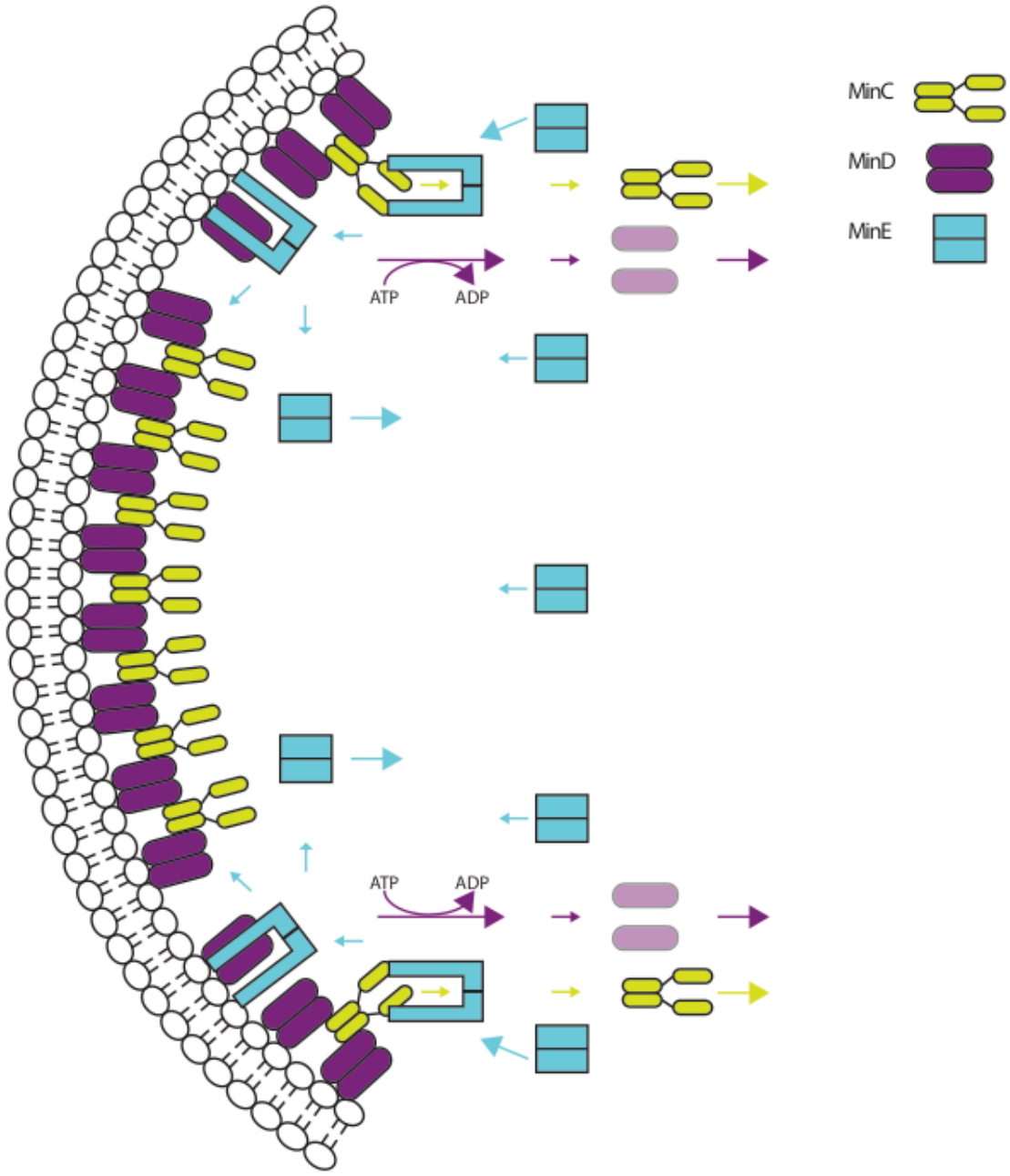

Figure 1-1. The mechanism of the Min system. Complexes of membrane-bound MinD (purple) and MinC (chartreuse) are targeted by MinE dimers (cyan). Dimers of MinE change conformation and bind to MinD and the membrane, stimulating the ATPase activity of MinD, displacing MinC and removing MinD from the membrane. MinD-ADP and MinC travel toward the opposite pole to start another oscillation cycle. MinE can remain membrane bound and remove more complexes of MinCD, or change conformation and travel toward the opposite pole following MinD. ***Adapted from***

"Rowlett, V.W., and Margolin, W. (2013) The bacterial Min system. Current Biology 23: R553-556." This figure is reprinted from, "Rowlett, V.W., and Margolin, W. (2015) The Min system and other nucleoid-independent regulators of Z ring positioning. Frontiers in Microbiology 6: 478," with permission from Frontiers in Microbiology (Copyright © 2015 Rowlett and Margolin doi: 10.3389/fmicb.2015.00478) and Elsevier (Copyright © 2013 Elsevier Ltd doi: 10.1016/j.cub.2013.05.024).

1.1.2 Conservation of the Min system.

Min proteins are found in the Gram-positive bacteria *Bacillus subtilis*. In this organism, the contribution of the Min system to divisome placement occurs by a distinct molecular mechanism. *B. subtilis* lacks MinE, and instead contains DivIVA, which localizes Min proteins to the poles of the cell (Cha & Stewart, 1997; Edwards & Errington, 1997). MinJ is an adapter protein that binds both DivIVA and MinD to recruit MinD and thus MinC to cell poles (Bramkamp et al., 2008; Patrick & Kearns, 2008). Although this Min system does not oscillate, it is not static, and Min proteins localize to midcell prior to septation, possibly to prevent more than one Z ring from forming at midcell and to establish a new gradient in daughter cells (Gregory et al., 2008; van Baarle & Bramkamp, 2010). Min proteins are found in many diverse species, including *Aquifex* spp., *Neisseria* spp., cyanobacteria, and in plastids of higher plants, but are absent in many bacteria, such as *Mycobacterium tuberculosis* (Rowlett & Margolin, 2013). Recent evidence suggests that Min proteins in *Helicobacter pylori* not only have roles in division site selection, but also cell shape, and nucleoid occlusion (Nishida et al., 2016).

1.1.3 Nucleoid occlusion.

Nucleoid occlusion prevents Z rings from forming over unsegregated nucleoids, which prevents closing the septum over the chromosome or chromosome guillotining (Männik & Bailey, 2015). In *E. coli*, nucleoid occlusion is mediated by SlmA, a protein that can bind both DNA and FtsZ (Bernhardt & de Boer, 2005; Cho et al., 2011; Tonthat et al., 2011), although there are conflicting models for the mechanism of SlmA inhibition of FtsZ (Bernhardt & de Boer, 2005; Tonthat et al., 2013; Cho & Bernhardt, 2013; Du & Lutkenhaus, 2014). Under fast growth conditions, deletion of *slmA* is synthetically lethal with deletion of *minCDE* (Bernhardt & de Boer, 2005), however, under slow growth conditions, cells not only survive, but also divide preferentially at midcell (Bailey el al., 2014). *E. coli* cells that lack all known systems still have a bias for Z ring positioning at midcell,

although midcell Z-ring positioning is less precise (Bailey et al., 2014). These data suggest that there are likely other proteins or factors that are involved in regulating Z ring placement.

1.1.4 Other positive and negative regulators of Z ring placement.

Positive regulators of Z ring placement have recently been identified in *E. coli* and other bacterial species. One example in *E. coli* involves connecting the chromosome to the divisome via interactions between MatP, the chromosomal Ter macrodomain to which it binds, and an early recruited divisome protein, ZapB (Espéli et al., 2012). This system helps both to position the Z ring and regulate ring constriction, which occurs faster when *matP* is deleted (Buss et al., 2015). The first example of a positive regulator of Z ring formation was found in *Streptomyces coelicolor*, a bacterium that lacks Min proteins and does not seem to use nucleoid occlusion. In *S. coelicolor*, a pair of proteins, SsgA and SsgB, localize to division sites independently of FtsZ and promote Z ring formation, a mechanism opposite that of Min and nucleoid occlusion systems (Willemse et al., 2011). SsgA recruits SsgB to midcell, where SsgB is suggested to promote FtsZ polymerization and serve as a membrane tether for Z rings (Willemse et al., 2011). Other positive regulators of Z ring positioning have also been found in *Myxococcus xanthus*, *Streptococcus pneumoniae*, and other species of bacteria, and the proteins involved are not well conserved (Treuner-Lange et al., 2013; Fleurie et al., 2014; Holečková et al., 2014).

Negative regulation also occurs by mechanisms other than Min and nucleoid occlusion. *Caulobacter crescentus* is an example of a bacterial species that lacks both Min and nucleoid occlusion systems, and instead contains MipZ, a ParA family ATPase protein that inhibits FtsZ polymerization directly (Thanbichler & Shapiro, 2006). MipZ binds the replication origin of the chromosome (*oriC*) and, prior to chromosome replication and segregation, is located at the cell pole opposite where FtsZ is localized (Thanbichler & Shapiro, 2006). Following replication, the duplicated *oriC* travels toward the opposite cell pole, forming a bipolar gradient of MipZ to localize Z rings to midcell (Thanbichler & Shapiro, 2006; Kiekebusch et al., 2012).

The variety of positive and negative regulators of Z ring positioning continues to expand as more bacterial species are studied, highlighting the diversity and complexity of bacteria (Monahan et al., 2014; Rowlett & Margolin, 2015a). Min and nucleoid occlusion systems have been the most well studied, and as a result are the best understood, but more studies are needed to identify factors involved in Z ring positioning that are currently unknown. Many Z ring positioning systems involve ParA-like proteins, that also play a role in chromosome segregation (Lutkenhaus et al., 2012), but positive regulators of Z ring positioning are not well conserved (Monahan et al., 2014), and the question of how these proteins localize to midcell remains.

1.1.5 Additional negative regulators of FtsZ assembly.

In addition to proteins that aid in positioning of the divisome, other negative regulators of FtsZ assembly are found in *E. coli* cells. Cell division is regulated by the availability of nutrients; in order to divide, cells must double in size and duplicate their chromosomes (Monahan & Harry, 2016). Moreover, many bacterial cells grown in high nutrients are significantly larger than those grown in low nutrients (Schaechter et al., 1958; Donachie & Begg, 1989). The first connection between nutrient availability and cell division was found in *B. subtilis* (Weart et al., 2007). The glycosyltransferase UgtP interacts with FtsZ in high nutrient conditions and inhibits FtsZ assembly; the resulting delay in cell division increases cell size (Weart et al., 2007). A similar size control mechanism has been identified in *E. coli*, which uses OpgH, a glycosyltransferase that shares no homology with UgtP and inhibits FtsZ by a different mechanism (Hill et al., 2013).

ClpXP and SulA also regulate FtsZ assembly in *E. coli*. ClpX is an ATPase that complexes with a serine protease ClpP to degrade proteins (Wojtkowiak et al., 1993). ClpXP negatively regulates FtsZ assembly by degrading monomers of FtsZ and disrupting polymers of FtsZ (Camberg et al., 2009). Under conditions of DNA damage, the SOS response is induced, resulting in the activation of SulA to delay cell division until chromosomes can be duplicated and partitioned (Huisman et al.,

1981). SulA inhibits FtsZ polymerization by sequestering monomers of FtsZ and functions to stop cell division until DNA is repaired (Chen et al., 2012).

1.2 Divisome assembly

1.2.1 Formation of a proto-ring.

When *E. coli* cells divide, they must coordinate constriction of the entire cell envelope, which consists of the inner membrane, a layer of peptidoglycan, and the outer membrane (Silhavy et al., 2010). The process of cell division first begins with proto-ring formation. As mentioned above, FtsZ, a eukaryotic tubulin homolog, polymerizes to form the Z ring after replication and segregation of nucleoids (Bi & Lutkenhaus, 1991; Margolin, 2005). FtsZ is a cytoplasmic protein that requires interactions with other proteins to associate with the inner membrane. FtsA and ZipA function to tether the Z ring to the inner membrane, and although either FtsA or ZipA can support Z ring formation, both are required for the recruitment of downstream divisome proteins (Fig. 1-2 A-B; Pichoff & Lutkenhaus, 2002, 2005). The mechanisms underlying this requirement are still unclear. The assembly of the Z ring tethered to the inner membrane by FtsA and ZipA is referred to as the proto-ring, and these are the first of several essential cell division proteins to localize to midcell (Vicente & Rico, 2006). If essential cell division proteins are disrupted, cells will continue to grow without dividing, resulting in cell filaments that eventually lyse (Ricard & Hirota, 1973).

1.2.2 Recruitment of downstream proteins.

Through the use of temperature sensitive mutants, depletion strains, and fluorescent protein fusions, the order in which divisome proteins are recruited to midcell has been established (Buddelmeijer & Beckwith, 2002). After a delay following the formation of the proto-ring, a number of essential (FtsK ➔ FtsQ ➔ FtsB ➔ FtsL ➔ FtsW ➔ FtsI ➔ FtsN) and non-essential proteins are recruited to midcell, with many arriving simultaneously (Aarsman et al., 2005; Goehring

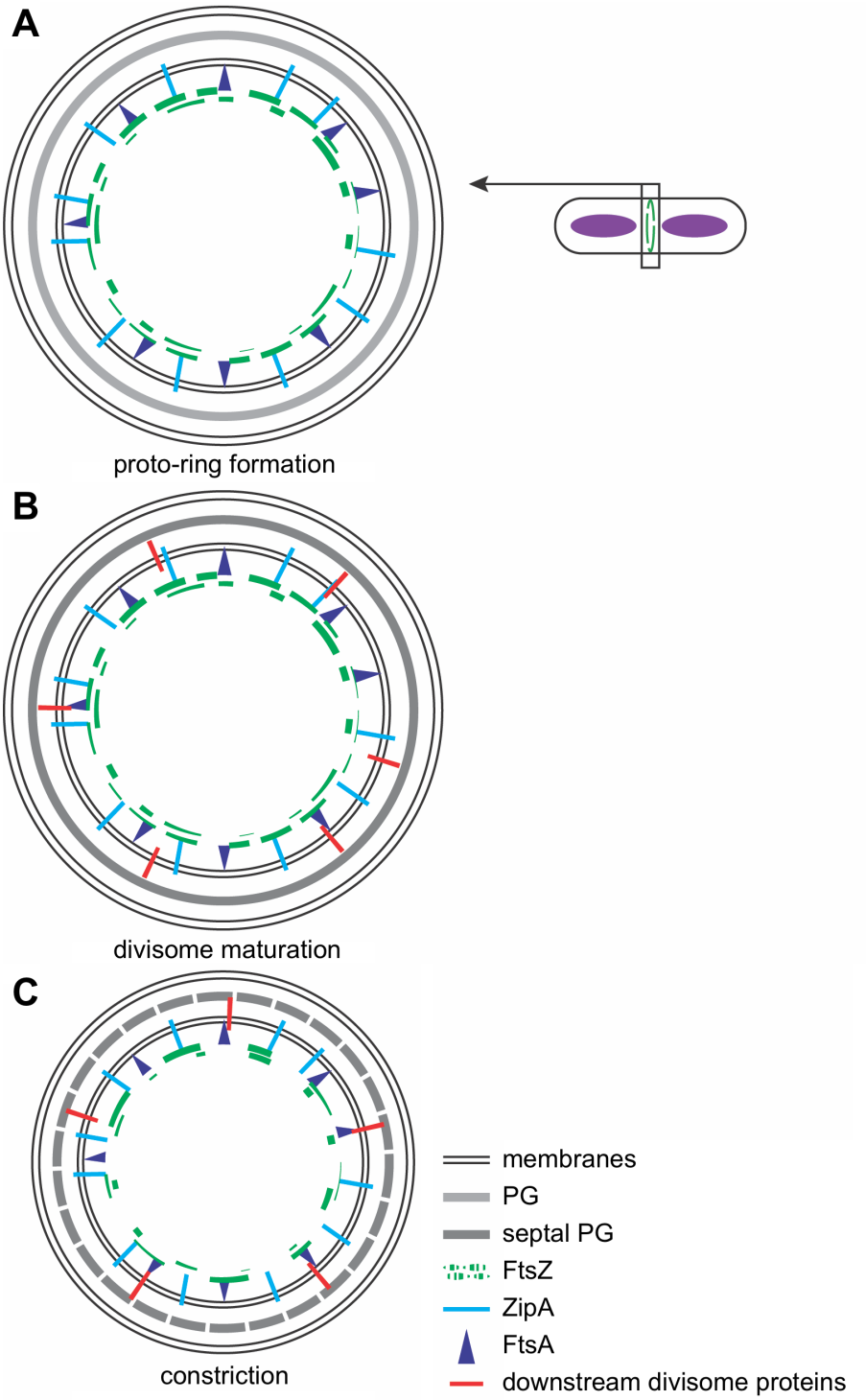

Figure 1-2. Roles of FtsA and ZipA during cell division. (A) FtsA and ZipA act as membrane tethers to stabilize the Z ring on the inner membrane and form the proto-ring. (B) FtsA and ZipA are both required to recruit downstream divisome proteins involved in septum synthesis. (C) FtsA is hypothesized to contribute to disassembly of the Z ring during later stages of cell division.

& Beckwith, 2005; Weiss, 2004). The arrival of these proteins completes divisome formation. Several downstream divisome proteins span the inner membrane, and are suggested to have roles in septal peptidoglycan (PG) synthesis, and communication with proteins located in the outer membrane to coordinate constriction of the entire cell envelope (Nanninga et al., 1991; Vicente et al., 2006).

1.2.3 Septum synthesis.

There are two types of PG synthesis that occur in *E. coli* cells (Szwedziak & Löwe, 2013). PG synthesis occurs along the long axis of the cell maintains the rod-shape of cells, and the machinery that governs this type of PG synthesis is termed the elongasome (den Blaauwen et al., 2008; Szwedziak & Löwe, 2013). Septal PG is synthesized by the divisome at midcell to form the cell poles of dividing daughter cells (Lutkenhaus et al., 2012). Both the divisome and elongasome interact with enzymes involved in the synthesis of Lipid II, a PG precursor (Mohammadi et al., 2007). Lipid II is synthesized in the cytoplasm, and translocated across the cytoplasmic membrane, although the proteins involved in translocation are the subject of debate (Ruiz, 2016). Once in the periplasm, penicillin-binding proteins (PBPs) polymerize and cross-link Lipid II to PG. The PBPs responsible for this function at the septum are PBP3 (FtsI) and PBP1B (Spratt, 1975, 1977; Bertsche et al., 2006). The Tol-Pal complex localizes to midcell during later stages of cell division to coordinate outer membrane constriction (Gerding et al., 2007). This complex has recently been suggested to coordinate with septal PG synthesis through interactions between PBP1B, CpoB, and the Tol protein TolA (Gray et al., 2015).

1.2.4 Interaction network of divisome proteins.

Divisome protein recruitment appears to occur in a linear manner, with the localization of downstream proteins dependent on the localization of all other upstream proteins. However, several protein-protein interaction studies have revealed a network of interactions that occur between divisome proteins. Bacterial two-hybrid assays have been used to identify a number of possible

interactions between divisome proteins (Karimova et al., 1998, 2005; Di Lallo et al., 2003; Maggi et al., 2008), however, since false-positives are common, other methods are used to confirm predicted interactions. FtsQ, FtsB, and FtsL have been shown to form a complex that is independent of localization to midcell (Buddelmeijer & Beckwith, 2004), and although the function of this complex is not known, it is predicted to be involved in repression and de-repression of PG synthesis mediated by FtsN, the last known essential protein to localize to the divisome (Liu et al., 2015). Interestingly, direct interaction of FtsN with the early recruited FtsA has recently been established (Busiek et al., 2012). Through this interaction a small amount of FtsN molecules are recruited early resulting in self-enhanced accumulation of FtsN at midcell (Gerding et al., 2009; Busiek & Margolin, 2014). Förster resonance energy transfer (FRET) has also been used to identify interacting partners of the *E. coli* divisome (Alexeeva et al., 2010). This FRET study identified interactions of FtsN with itself and later recruited proteins FtsW and FtsI, but also an interaction between FtsN and the early recruited ZapA protein (Alexeeva et al., 2010), and is another demonstration of early and late interactions. The interactions mentioned here are just a few examples from several studies to highlight the network of interactions that occur between divisome proteins. This picture is likely to become more complete as more studies confirm predicted interactions and identify novel interactions.

1.3 Proto-ring proteins

1.3.1 FtsZ as a scaffold and force generator.

Z ring formation is the first step of cell division, and FtsZ has been proposed to serve as a scaffold for the divisome, and may also provide a constrictive force during later stages of cell division (Erickson et al., 2010). FtsZ is highly conserved, and FtsZ or homologs of FtsZ are found in most bacteria, the euryarchaeal branch of Archaea, chloroplasts, some mitochondria, and higher plants (Margolin, 2005). Localization of FtsZ to midcell is required for the localization of all other downstream divisome proteins, suggesting that it functions as a scaffold for the divisome (Margolin,

2005). FtsZ has two globular domains separated by a core helix, followed by a variable linker region, and a conserved C-terminal domain to which many FtsZ regulating proteins bind, including ZipA and FtsA (Fig. 1-3; Adams & Errington, 2009; Busiek & Margolin, 2015). FtsZ binds to GTP and polymerizes in a head to tail fashion to form single protofilaments, bundles, sheets, and curved filaments under different conditions *in vitro*, unlike microtubules formed by tubulin (Mukherjee & Lutkenhaus, 1994; Erickson et al., 1996; Adams & Errington, 2009). Protofilament assembly of FtsZ is highly dynamic due to the intrinsic GTPase activity of FtsZ, which promotes protofilament curvature and/or disassembly (Lu et al., 2000; Romberg & Levin, 2003; Erickson et al., 2010; Li et al., 2013). During later stages of cell division, the reorganization of FtsZ protofilaments through GTP hydrolysis may generate force that contributes to constriction of the inner membrane (Erickson et al., 2010). Support for this hypothesis comes from the ability of FtsZ to generate a constriction force on liposomes when tethered to them by fusion to an artificial MTS or by the natural FtsA protein tether (Osawa et al., 2008; Osawa & Erickson, 2013).

1.3.2 Role(s) of ZipA.

ZipA is an integral membrane protein found in Gram-negative gamma-proteobacteria that directly interacts with FtsZ (Hale & de Boer, 1997; RayChaudhuri, 1999). The cytoplasmic C-terminal domain of ZipA is sufficient for interaction with the conserved C-terminal domain of FtsZ (Hale et al., 2000; Mosyak et al., 2000; Moy et al., 2000). The interaction of ZipA with FtsZ protects FtsZ from degradation by the ClpXP protease complex, whereas this protection is not conferred by FtsA (Pazos et al., 2013). *In vitro* studies have demonstrated the ability of ZipA to bundle protofilaments of FtsZ, suggesting a role for ZipA in promoting assembly of FtsZ in addition to serving as a membrane tether for the Z ring (RayChaudhuri, 1999; Hale et al., 2000; Kuchibhatla et al., 2011; Loose & Mitchison, 2014). Recently, several non-essential and unrelated FtsZ-associated proteins (Zaps) have been identified that have overlapping roles in promoting stability of the Z ring (Hale et al., 2011; Durand-Heredia et al., 2011, 2012; Schumacher et al., 2016). However, the

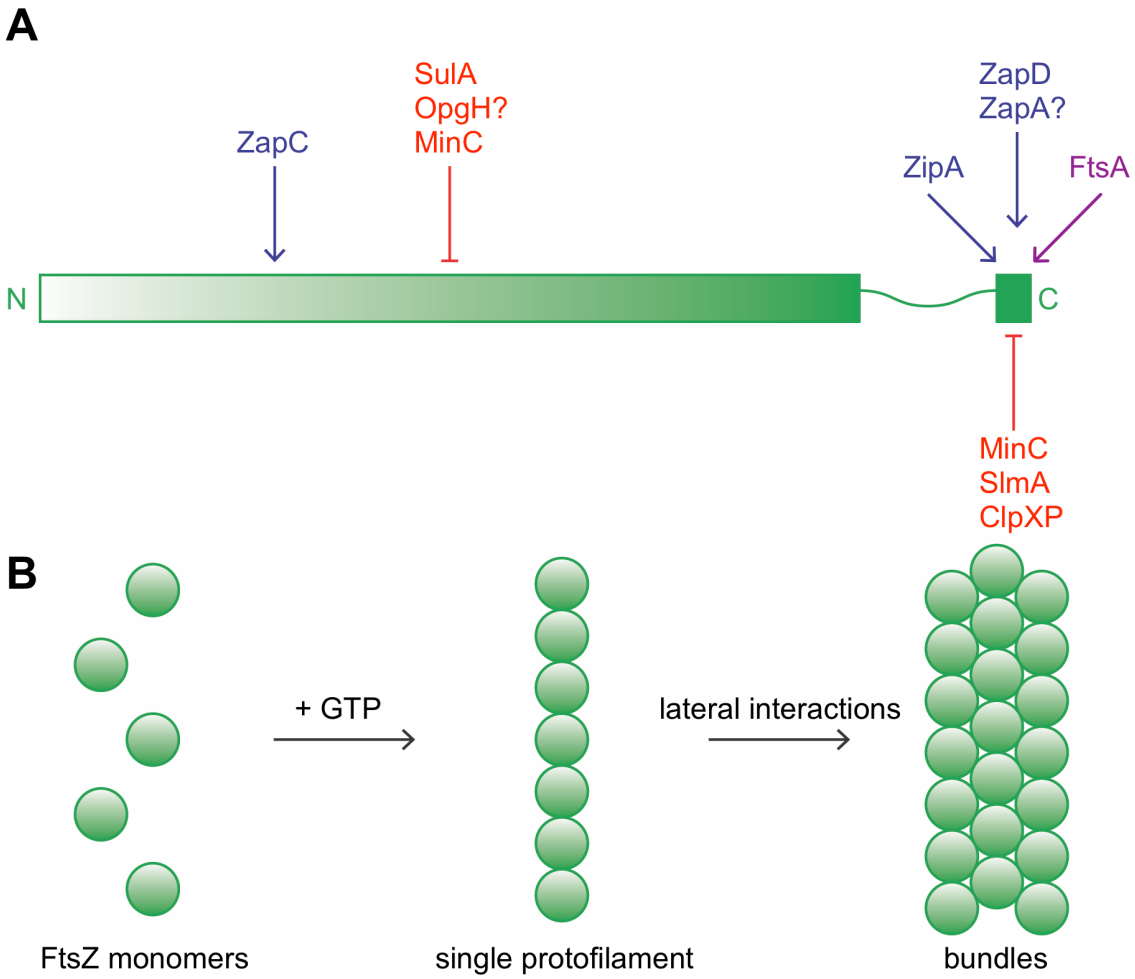

Figure 1-3. Domain organization and assembly of FtsZ. (A) Domain organization of FtsZ. The N-terminal and C-terminal globular domains comprising the core polymer-forming portion of FtsZ are shown as a single rectangle labeled with "N," followed by the variable linker and C-terminal protein-binding domain (labeled "C"). Negative regulators of assembly of *E. coli* FtsZ are colored red and positive regulators of assembly are colored blue, and the specific domains of FtsZ they target are shown. Separate domains of MinC target separate domains of FtsZ as shown. FtsA is colored purple, as it is hypothesized to both support Z ring formation and disassemble FtsZ at later stages of cell division. (B) Monomers of FtsZ assemble head to tail in a GTP dependent manner to form protofilaments, which can laterally interact to form bundles (Adams & Errington, 2009).

mechanisms by which Zap proteins and ZipA promote FtsZ assembly are likely distinct (Durand-Heredia et al., 2012; Huang et al., 2013). ZipA has also been suggested to have a role in early septal PG synthesis that is independent of FtsI (Potluri et al., 2012). This "preseptal" PG synthesis likely occurs as cells transition from elongation to division, but how ZipA contributes to septal PG synthesis is unknown, and likely does not occur through a direct interaction with ZipA and PG synthesis proteins (Potluri et al., 2012).

1.3.3 Role(s) of FtsA.

FtsA is a structural homolog of actin that contains a C-terminal amphipathic helix, which serves as an MTS to tether FtsA to the membrane (Bork et al., 1992; Pichoff & Lutkenhaus, 2005; van den Ent et al., 2001). A properly functioning MTS is essential for full FtsA function, as deletion of the MTS or certain point mutations that change its amphipathic properties result in an inability to bind the membrane and support division (Pichoff & Lutkenhaus, 2005). FtsA interacts with the conserved C-terminal domain of FtsZ, at a distinct site adjacent to where ZipA binds FtsZ, to tether the Z ring to the inner membrane (Ma & Margolin, 1999; Szwedziak et al., 2012). In addition to serving as a membrane tether, FtsA also recruits divisome proteins to midcell through its 1C subdomain (Rico et al., 2004; Corbin et al., 2004).

FtsA is found in many groups of bacteria, but is absent in actinobacteria and archaea (Margolin, 2000). In *B. subtilis*, FtsA is not strictly essential for cell division, although deletion of *ftsA* results in filamentous cells that divide less frequently (Beall & Lutkenhaus, 1992; Jensen et al., 2005; Ishikawa et al, 2006). These data suggest that another protein is involved in stabilizing Z rings in *B. subtilis* (Adams & Errington, 2009). SepF has been identified as an important divisome protein in *B. subtilis* (Hamoen et al., 2006; Ishikawa et al., 2006). Deletion of *sepF* is synthetically lethal with deletion of *ftsA*, and SepF overproduction can restore the defects of deletion of *ftsA*, suggesting that they have similar roles in Z ring stabilization (Ishikawa et al., 2006). Further support for SepF and FtsA having similar roles in cell division is that SepF is essential in *Synechococcus elongatus* and

Mycobacterium spp., which lack homologs of FtsA (Miyagishima et al., 2005; Gola et al., 2015; Gupta et al., 2015).

A gain-of-function allele of FtsA, $FtsA_{R286W}$ (FtsA*) is able to bypass the requirement for ZipA (Geissler et al., 2003), and FtsA is more well conserved than ZipA (Margolin, 2000), suggesting that FtsA has a more important role in cell division than ZipA. FtsA* has been suggested to have reduced self-interaction compared to wild-type FtsA, and can suppress the defect of a mutation in the MTS ($FtsA_{W408E}$) that reduces membrane binding (Pichoff et al., 2012; Shiomi & Margolin, 2008). These data suggest that monomeric FtsA has increased affinity for the membrane. Purified FtsA* can depolymerize FtsZ *in vitro* and promote constriction of Z rings in liposomes, suggesting that wild-type FtsA is also involved in disassembly of FtsZ during constriction of the cell septum (Fig. 1-2C; Beuria et al., 2009; Osawa & Erickson, 2013). FtsA binds ATP (Beuria et al., 2009; Loose & Mitchison, 2014) and our laboratory has shown that FtsA also hydrolyzes ATP, which may contribute to an oligomeric switch between a dimeric/oligomeric form and a monomeric form (Herricks et al., 2014). The oligomeric state of FtsA, its ability to bind and hydrolyze ATP, and its affinity for the membrane may be critical for FtsA function in divisome assembly and disassembly.

1.4 Gaps in knowledge and significance of research

Genetic and biochemical studies have shed light on the order of divisome protein recruitment to midcell, and some of the interactions that occur between them; however, many of their functions remain unsolved (Buddelmeijer & Beckwith, 2002; de Boer, 2010). How the proteins in this complex network communicate and coordinate to divide cells is unknown. Since the divisome of *E. coli* is likely overbuilt to ensure survival in a variety of conditions, these questions are difficult to address. Understanding the mechanisms that govern cell division is important, and by studying a simple model organism such as *E. coli*, we may be able to elucidate how an entire cell proliferates and divides. These studies can extend to other organisms with homologous proteins. Additionally, the high conservation of some bacterial cell division proteins make them attractive targets for the production

of novel antimicrobial therapies to combat the rise of antibiotic resistant bacterial species (den Blaauwen et al., 2014).

With higher resolution imaging techniques, we now have a more accurate view of the ultrastructure of the Z ring, but whether or not the Z ring is comprised of continuous or discontinuous filaments is still debated. There is evidence of FtsA involvement in the assembly of the divisome, as well as disassembly at later stages of cell division, but how FtsA switches between these functions remains unsolved.

For this study, the mechanism of how a fusion of MinCc to MinD resulted in asymmetrical cell division was investigated. We anticipated that this fusion would increase MinCc's inhibitory activity on FtsZ, however; instead it caused cells to jackknife at their division septa. Chapter III details the experiments used to uncover this mechanism, and I found that FtsA localized asymmetrically on the Z ring, likely contributing to asymmetrical constriction by recruiting downstream proteins to a single side of the Z ring.

The localization of the proto-ring proteins FtsZ, FtsA, and ZipA were investigated in wild-type cells using three-dimensional-structured illumination microscopy (3D-SIM). These results are detailed in Chapter IV. FtsZ localizes as a punctate ring, rather than a uniform and continuous ring, and FtsA and ZipA largely co-localize in similar structures. Localization of an FtsZ mutant with increased self-assembly, $FtsZ_{L169R}$ was also visualized and found to form punctate rings similar to wild-type FtsZ, as well as elaborate spirals and assemblies at cell poles, consistent with its increased self-assembly (Haeusser et al., 2015). Finally, Chapter V details the investigation of the assembly of purified FtsA and FtsA mutant proteins using transmission electron microscopy and their ability to bind membranes in liposome sedimentation assays. The results presented refine our view of the proto-ring proteins, as this was the first visualization of proto-ring proteins in *E. coli* using 3D-SIM. The importance for FtsA's activity in late cell division is supported, and the biochemical analysis of FtsA serves as a starting point for more in-depth studies of FtsA that will shed light on how FtsA functions.

Chapter II

Materials and Methods

This chapter is based in part upon, *"Rowlett, V.W., and Margolin, W. (2014) Asymmetric constriction of dividing Escherichia coli cells induced by expression of a fusion between two Min proteins. Journal of Bacteriology 196: 2089-2100" with permission from the American Society for Microbiology (Copyright © 2014, American Society for Microbiology doi:10.1128/JB.01425-13) and "Rowlett, V.W., and Margolin, W. (2014) 3D-SIM super-resolution of FtsZ and its membrane tethers in Escherichia coli cells. Biophysical Journal 107: L17-L20" with permission from Elsevier (Copyright © 2014 Biophysical Society. Published by Elsevier Inc. doi:10.1016/j.bpj.2014.08.024).*

2.1 Strains, plasmids, and growth conditions.

Strains and plasmids used in this study are shown in Table 2-1. *E. coli* strain XL1-blue was used to clone plasmids containing fusions that were then transformed into either wild-type (WT) WM1074, WM1032 (Δ*minCDE::kan*), other *min* deletion strains, or other background strains as indicated. Bacteria were grown to mid-logarithmic phase (optical density at 600 nm [OD_{600}] between 0.3 and 0.5) at 37˚C in Luria Bertani (LB) medium supplemented with 50 - 100 µg/ml ampicillin (Fisher Scientific), 25 - 50 µg/ml kanamycin (Sigma-Aldrich), or 10 - 20 µg/ml chloramphenicol (Acros Organics) as needed. Cells were induced with 0.01 to 1 mM isopropyl-β-D-galactopyranoside (IPTG) or 1 to 10 µM sodium salicylate for ~1 h prior to microscopic examination and fixation for immunofluorescence microscopy. For viability assays, cells in logarithmic phase were serially diluted in LB and spotted using a pronger onto LB plates containing appropriate antibiotics and 0, 0.1, or 1 mM IPTG and incubated overnight at 37˚C. For *ftsA12* complementation analysis, serial dilution plates were incubated at 30˚C and 42˚C.

MT78 was used to make a P1 phage lysate containing an *ftsA-null* allele linked to Tet resistance. This lysate was used to transduce cells containing pDSW210 with FtsA-FtsN, FtsA, FtsA*, and $FtsA_{K19M}$, and $FtsA^*_{K19M}$. Only FtsA, FtsA*, and $FtsA^*_{K19M}$ could be transduced with this lysate, and restriction digest with *Bgl*II (site is lost in *ftsA-null*) and sequencing were used to confirm that these strains had the *ftsA-null* allele in the chromosome.

Table 2-1. Strains and plasmids used in this study.

Strain or plasmid	Relevant genotype	Source / reference
Strains		
WM1074	MG1655 Δ*lacU169* (TX3772)	Laboratory collection
WM1032	WM1074 Δ*minCDE::kan*	(Sun & Margolin, 2001)
WM1115	WM1074 *ftsA12* temperature sensitive	Laboratory collection
WM2026	WM1074 with P_{lac}-*ftsZ-gfp*	(Geissler et al., 2007)
WM3486	Δ*minCDE::kan* with P_{lac}-*ftsZ-gfp* (P1 WM1032 × WM2026)	(Rowlett & Margolin, 2014a)
WM4475	Δ*minC::kan* (P1 WM3107 × WM1074)	(Rowlett & Margolin, 2014a)
WM2280	Δ*minD::kan* in WM1074	Laboratory collection
WM2738	WM1032 (Δ*minCDE*) with pWM2738	(Rowlett & Margolin, 2014a)
WM3107	Δ*minC::kan* in BW25113 (Keio collection)	(Baba et al., 2006)
WM3997	WM1032 (Δ*minCDE*) with pWM3563 (pBS58) + pWM2738	(Rowlett & Margolin, 2014a)
WM4082	pWM4066 (pKG116His_6-*minCc-minD*) in WM3486	(Rowlett & Margolin, 2014a)
XL1-Blue	Cloning strain	Stratagene
WM1659	*ftsA** (R286W) in chromosome	(Geissler et al., 2003)
WM4831	Δ*minCDE::kan* transduced into WM1659 + pWM2738	(Rowlett & Margolin, 2014a)
DPH642	(WM4915) WM1074 $ftsZ_{L169R}$ *leuO*::Tn*10*	(Haeusser et al., 2015)
C43(DE3)	F^- *ompT gal dcm* $hsdS_B$ (r_B^- m_B^-)(DE3)	(Miroux & Walker, 1996)
BL21(DE3)	F^- *ompT gal dcm lon* $hsdS_B$ (r_B^- m_B^-) λ(DE3)	Laboratory collection
MT78	TB28 (MG1655 Δ*lacIZYA::frt*) *zapA*-GFP *frt leu::Tn10 ftsA(0)*	(Tsang & Bernhardt, 2015)

Plasmids		
pKG116	Salicylate inducible *nahR* promoter	J. S. Parkinson
pDSW210	IPTG-inducible weakened *trc* promoter	(Weiss et al., 1999)
pWM2619	pDSW210 with His_6 tag	(Shiomi & Margolin, 2007a)
pWM2784	pDSW210 with *flag* tag	(Shiomi & Margolin, 2007b)
pWM2735	pDSW210His_6-*minC-gfp*	(Shiomi & Margolin, 2007a)
pWM2736	pDSW210His_6-*minCc-gfp*	(Shiomi & Margolin, 2007a)
pWM2737	pDSW210His_6-*minC-minD* fusion	(Rowlett & Margolin, 2014a)
pWM2738	pDSW210His_6-*minCc-minD* fusion	(Rowlett & Margolin, 2014a)
pWM3563	pBS58 (*E. coli ftsQAZ*)	(Wang & Lutkenhaus, 1993)
pWM4005	pDSW210His_6-*minCc-minD*ΔMTS	(Rowlett & Margolin, 2014a)
pWM4066	pKG116His_6-*minCc-minD*	(Rowlett & Margolin, 2014a)
pWM4070	pDSW210His_6-*minCc*(R172A)-*minD*	(Rowlett & Margolin, 2014a)
pWM4127	pDSW210His_6-*minCc-ftsN*	(Rowlett & Margolin, 2014a)
pWM4580	pDSW210His_6-*minCc*(R133A)-*minD*	(Rowlett & Margolin, 2014a)
pWM4581	pDSW210His_6-*minCc-minD*(G158R)	(Rowlett & Margolin, 2014a)
pWM1736	pBAD33-*sulA*	(Thanedar & Margolin, 2004)
PWM4679	pDSW210-*ftsA-gfp*	(Rowlett & Margolin, 2014b)
pET28a	IPTG-inducible PT7 promoter	Novagen
pWM1260	pET28aHis_6-*ftsA*	(Geissler et al., 2003)
pWM1609	pET28aHis_6-*ftsA** (R286W)	(Geissler et al., 2003)
pWM4678	pET28aHis_6-*ftsAK19M*	(Herricks, dissertation)
pWM4760	pET28aHis_6-*ftsAG50E*	(Herricks et al., 2014)
pWM4908	pET28aHis_6-*ftsA*Δ*C15*	This study
pWM971	pET11a-*ftsZ*	H. Erickson

pDH160	pET11a-*ftsZL169R*	(Haeusser et al., 2015)
pWM2785	pDSW210-*flag-ftsA*	(Shiomi & Margolin, 2007b)
pWM2787	pDSW210-*flag-ftsA**	(Shiomi & Margolin, 2007b)
pWM3157	pDSW210-*flag-FtsN*	(Busiek & Margolin, 2014)
pWM3158	pDSW210-*flag-ftsA-FtsN*	D. Shiomi
pWM3160	pDSW210-*flag-ftsAΔC15-ftsN*	D. Shiomi
pWM3169	pDSW210-*flag-ftsAW408E*	(Shiomi & Margolin, 2008)
pWM3170	pDSW210-*flag-ftsA*W408E*	(Shiomi & Margolin, 2008)
pWM4358	pDSW210-*flag-ftsAK19M*	(Herricks, dissertation)
pWM4817	pDSW210-*flag-ftsA*K19M*	J. Herricks

2.2 Plasmid construction.

Gene fusions used in this study were constructed using primers shown in Table 2-2. All plasmids used in Rowlett & Margolin 2014a were introduced into the Δ*minCDE* strain WM1032 unless otherwise indicated. Plasmids pWM2737 and pWM2738 were made by Daisuke Shiomi by amplifying the *minD* gene using primers 960 and 356 and inserting it as a *Sal*I-*Hind*III fragment into pWM2735 (pDSW210His$_6$-*minC-gfp*) and pWM2736 (pDSW210His$_6$-*minCc-gfp*), respectively. The His$_6$-tagged MinCc-MinD fusion was amplified using primers 864 and 356 and inserted between the *Sac*I and *Bam*HI sites of pKG116 to create pWM4066. Primers 960 and 1621 were used to amplify MinD lacking a membrane targeting sequence (MTS) to make pWM4005. To create the R172A lesion in the MinCc portion of MinCc-MinD, two sets of PCRs were used, the first amplifying MinCc using primers 864 and 926 (with the R172A lesion incorporated) and MinCc(R172A)-MinD using primers 927 (with the R172A lesion) and 356. The second reaction used primers 864 and 356 to amplify the MinCc(R172A)-MinD fusion, which was inserted between the *Sac*I and *Hind*III sites of pDSW210 His$_6$ (pWM2619) to create pWM4070. MinCc(R133A)-MinD and MinCc-MinD(G158R) were made by the same PCR method using primers 1686 and 1687 and inserting it into pWM2738 digested with *Sal*I and *Hind*III. Primers 2078 and 1081 were used by Kara M. Schoenemann to clone His$_6$-FtsAΔC15 into pET28a.

2.3 Live-cell microscopy.

Microscopy of cells grown in broth cultures was performed using an Olympus BX60 microscope with a 100X oil immersion differential interference contrast (DIC) objective. Cells were spotted either on 2% LB agarose pads or directly on glass slides mixed 1:1 with molten 2% low-melting-point LB agarose before addition of a coverslip. Images were processed using Pixelmator and ImageJ (Schneider et al., 2012) was used to determine angles of bent cells. For time-lapse microscopy of WM2738, cells were induced with 1 mM IPTG for 1 h prior to image capture, spotted on an agar pad, and grown at 37˚C under a microscope objective using a Tokai Hit temperature control system.

Table 2-2. Oligonucleotides used for plasmid construction.

Primer #	Sequence	Description
960	GCC GTC GAC GGA GGT GGC GGA GGC GCA CGC ATT ATT GTT GTT AC	Forward MinD
356	CCA AGC TTT ATC CTC CGA ACA AGC GTT TG	Reverse MinD
1621	GGA AGC TTT TAT TCT TCA ATG AAG CGG	Reverse MinD MTS
864	GCG AGC TCG TCA CAA AAA CGC GTT TAA TAG	Forward MinCc
927	CAT GAT GCG CGG TAC TAC GCT GGC AGG GG	Forward MinCcR172A
926	CCC CTG CCA GCG CAG CAC CGC GCA TCA TG	Reverse MinCcR172A
1686	GGG TCG ACG CAC AAC GAG AT	Forward FtsN
1687	TTA AGC TTT CAA CCC CCG GC	Reverse FtsN
1642	CAC CAT CAC CAT CAC CAT GTC ACA AAA ACG CGT TTA ATA G	Forward 116-H-Cc
1643	GGA TCC TTA TCC TCC GAA CAA GCG TTT GAG GAA GC	Reverse 116-H-D
2007	CGC TGA CCG GAA GCC ACC GGG GTA T	Reverse MinCR133A
2008	ATA CCC CGG TGG CTT CCG GTC AGC G	Forward MinCR133A
2009	GAC GCC AGA ATG CGT AAA ATA CGG T	Reverse MinDG158R
2010	ACC GTA TTT TAC GCA TTC TGG CGT C	Forward MinDG158R
2078	GGC CAT GGG CAG CAG CAT CAT CAT CAT CAT CAC ATC AAG GCGACG GA	Forward His_6 FtsA
1081	GCG AAT TCT TAA ACT GAT GCTGTA ACA CG	Reverse FtsAΔC15

Images were captured every 2 min with a Hamamatsu digital camera. Time-lapse microscopy of WM4082 cells grown *in situ* was performed using an Onix Cellasic system and a B04A bacterial microfluidic plate (EMD Millipore). Cells were diluted from overnight cultures in medium containing appropriate antibiotics and 10 μM IPTG to an OD_{600} of 0.1 to 0.2 and loaded into the plate. Medium with appropriate antibiotics was made to flow through at a flow pressure of 2 lb/in^2, and cultures were induced by switching to medium containing 10 μM sodium salicylate. An Olympus IX81 inverted microscope equipped with an Olympus IX2-UCN external power unit, a Lambda 10-3 filter wheel system, a 100X objective, a Lumen 200 (Prior) fluorescence illumination system, a ProScanII (Prior) motorized stage, and a high-resolution Hamamatsu C10600 camera were used for time-lapse imaging with the Cellasic system. Images were captured every 2 min.

2.4 Protein purification and analysis.

FtsZ and $FtsZ_{L169R}$ proteins were purified as described (Haeusser et al., 2014) by Daniel P. Haeusser. Briefly, untagged FtsZ and $FtsZ_{L169R}$ proteins were overproduced after inducing cultures of BL21(DE3) strains carrying pET11a-FtsZ plasmids with IPTG. The resulting cell pellets were thawed, resuspended in wash buffer with protease inhibitors, and lysed by tip sonication. Lysates were centrifuged to remove cell debris and FtsZ was purified from lysates by precipitation with 20% ammonium sulfate and further purified by another precipitation with 30% ammonium sulfate. Finally, protein was reuspended in polymerization buffer (50 mM MES pH 6.5, 50 mM KCl, 5 mM $MgCl_2$, 1 mM EGTA, 10% sucrose), flash frozen in liquid nitrogen, and stored at −80˚C (Haeusser et al., 2014).

FtsA and FtsA mutant proteins were purified as described (Herricks et al., 2014). Briefly, His_6-tagged proteins were overproduced from pET28a in C43 in 3-4 L cultures. Pelleted cells were resuspended in wash buffer with protease inhibitors added, homogenized, and lysed using a French Press at 1000 psi. Lysates were centrifuged to remove cell debris, and clarified lysates were incubated in a rotator at 4˚C with TALON Resin (Clontech, Takara Bio). The lysate resin mixture was then added to gravity flow columns, washed with buffers containing increasing amounts of imidazole, and

eluted in buffer with 150 mM imidazole. Eluted fractions containing protein were dialyzed at 4˚C with FtsA buffer A (20 mM Tris, pH 7.5, 100 mM KCl, 25 mM potassium glutamate, 5 mM $MgCl_2$, 20% glycerol, and 1 mM DTT), and stored at −20˚C (Herricks et al., 2014). FtsA, FtsA*, $FtsA_{G50E}$, $FtsA_{K19M}$, and FtsAΔC15 were purified by Veronica W. Rowlett and Kara M. Schoenemann with the following modifications. Tube-O-DIALYZER (G-Biosciences) tubes were used during dialysis. Protein samples of FtsA collected during purification steps (lysate, flow through, 5 mM, 20 mM, and 30 mM washes, and pooled protein) were mixed 1:1 with 5X SDS buffer, boiled, vortexed, electrophoresed on 12.5% SDS-PAGE gels and stained with Coomassie brilliant blue, prior to destaining.

Protein concentrations for FtsZ and FtsA proteins were determined using the CB-X protein estimation assay for uncomplicated and complicated samples, respectively (G-Biosciences). Mutated residues of *E. coli* FtsA were mapped onto the dimer crystal structure of *Thermotoga maritima* FtsA using UCSF Chimera (Pettersen et al., 2004; Szwedziak et al., 2012).

2.5 Transmission electron microscopy.

2.5.1 Thin sections of *E. coli* cells.

WM2738 cells were grown with or without 1 mM IPTG induction to mid-logarithmic phase, centrifuged to pellet cells, washed in Millonig's phosphate buffer (85 mM NaCl, 165 mM Na_2HPO_4, 15 mM NaH_2PO_4, pH7.4), and resuspended in 3% glutaraldehyde fixative. 80- and 120-nm thin sections were prepared and placed on copper grids, which were negatively stained for 1 min with 1% uranyl acetate and visualized using a JEM-1400 (JEOL) transmission electron microscope at 120 kV. Note: Thin sections were prepared by Steven Kolodziej.

2.5.2 Assembly of purified FtsZ and FtsA detected by electron microscopy.

$FtsZ_{WT}$ or $FtsZ_{L169R}$ were incubated in FtsZ polymerization buffer (50 mM MES pH 6.5, 50 mM KCl, 5 mM $MgCl_2$, 1 mM EGTA, 10% sucrose) with 2.5 mM $MgCl_2$ and 1 mM GDP or 1 mM GTP added at 30˚C for 10 min. Where noted, 10 mM $CaCl_2$ was added. After incubation, 10 µl of each sample was placed onto a glow-discharged formvar carbon coated nickel grid (Electron Microscopy Sciences) for 1 min. The liquid was wicked away with filter paper, and grids were washed with a 5 µl drop of 1% uranyl acetate, removed by filter paper, and followed by the addition of a second 5 µl drop of 1% uranyl acetate and incubation for 30 sec. Filter paper was used to wick off stain and grids were allowed to dry prior to visualization with a 120 kV JEOL 1400 Transmission Electron Microscope. Images were acquired at 120,000× magnification using a Gatan Orius CCD camera. For samples where GTP or GTP + $CaCl_2$ were added, 3 µM or 5 µM protein yielded similar results; EM images in Fig. 4-7B were from samples with 3 µM protein. For samples where GDP was added, 5 µM protein was used (Fig. 4-7B) to increase the chance of viewing FtsZ assembly.

FtsA and FtsA mutant proteins were diluted first to 2 µM in 25 µl FtsA buffer A (20 mM Tris, pH 7.5, 100 mM KCl, 25 mM potassium glutamate, 5 mM $MgCl_2$, 20% glycerol, and 1 mM DTT). Proteins were then diluted 1:1 in FtsA buffer B (20 mM Tris, pH 7.5, 100 mM KCl, 25 mM potassium glutamate, 5 mM $MgCl_2$) in a 50 µl final reaction volume either with or without 2 mM ATP (Sigma-Aldrich). Samples were incubated at 37˚C for 30 min prior to grid preparation. Grids were prepared as described for FtsZ, with a shortened staining period to 20 sec of the second 1% uranyl acetate drop.

2.6 Immunoblotting.

Pelleted cells were resuspended in 50 µl GTE buffer (50 mM glucose, 10 mM EDTA, 20 mM Tris pH, 7.5). Then 50 µl of SDS buffer was added and the samples were boiled for 5 min prior to separation by 12.5% SDS-PAGE. Proteins were transferred using a wet apparatus to a nitrocellulose membrane, which was stained with Swift membrane stain (G-Biosciences) to evaluate the amount of protein on the blot. A monoclonal anti-His_6 antibody (Sigma-Aldrich) was used at a concentration of

1:3000. A secondary anti-mouse antibody conjugated to horseradish peroxidase (HRP) was used at a concentration of 1:5000. A Western Lightning ECL Pro kit (PerkinElmer) was used for HRP detection.

2.7 Immunofluorescence microscopy (IFM).

Cells were fixed using 3 µl of 25% glutaraldehyde in 1 ml 16% paraformaldehyde and incubated with antibodies as described previously (Levin, 2002). Briefly, fixed cells were adhered to poly-L-lysine coated 15-well slides or coverslips, washed, and 2% BSA was used to block non-specific binding of antibodies. Antibodies against FtsZ, FtsA, ZipA, and His_6 were used to detect localization of FtsZ, FtsA, ZipA, and His_6-MinCc-MinD, respectively. Rabbit anti-FtsZ was used at a concentration 1:2000, rabbit anti-FtsA or anti-ZipA were used at a concentration of 1:500, and mouse anti- His_6 was used at 1:1000. A secondary antibody conjugated to Alexa Fluor 488 was used at 1:200 to detect FtsZ, FtsA, or ZipA; a secondary antibody conjugated to rhodamine was used at 1:50 to detect His_6-tagged proteins. Images were overlaid and colored using Pixelmator.

2.8 Quantitation of immunofluorescence localization patterns.

To quantitate the fluorescence intensities of MinCc-MinD with FtsZ, ZipA, or FtsA from dually labeled IFM Images, areas of cell bending were chosen that had not deeply constricted. The fluorescent images of MinCc-MinD (red channel) and FtsZ, ZipA, or FtsA (green channel) were merged and aligned with Pixelmator by aligning the cell outlines of a field of cells. The random distribution of cell orientations served as an internal control for proper registration of the images, as the proper registration aligned all cell outlines independent of their orientation. Cell bending areas were cropped from each image, boxes were drawn around the immediate area of septa ring at each bend, and fluorescence intensity plots were generated for each color channel using ImageJ. If a fluorescent band at the bend was slanted, which would skew intensity plots, the cropped images were

rotated to the same degree so that the band pattern of FtsZ would be horizontal. These plots were then merged, traced, and recolored in Pixelmator to analyze and generate the representative examples.

MinCc-MinD was scored for localization, and if either a larger peak of fluorescence or a directional shift in a fluorescence peak occurred on the inside of the cell bend, it was counted as localization to the inside of a bend. If the peak of fluorescence was in the center of the region scored, or a directional shift was observed on the opposite side of the bend, this was scored as localization to the center/outside of a bend. If a peak of MinCc-MinD localization co-localized with a peak of similar size of FtsZ, ZipA, or FtsA, this was counted as inclusion of localization. Conversely, if a peak of MinCc-MinD corresponded with a trough of FtsZ, ZipA, or FtsA fluorescence, this was counted as exclusion of localization (Fig. 2-1).

2.9 Three-dimensional-structured illumination microscopy (3D-SIM).

For 3D-SIM localization of proto-ring proteins, we used a DeltaVision OMX V4 Blaze microscope (Applied Precision, GE Healthcare, Issaquah, WA). Three-dimensional views were reconstructed using softWoRx software (Applied Precision).

2.10 Preparation of samples for 3D-SIM.

Cells producing FtsZ-GFP in strain WM2026 were grown to mid-logarithmic phase, fixed using glutaraldehyde and paraformaldehyde (Levin, 2002), adhered to poly-L-lysine (Sigma-Aldrich) coated coverslips and inverted onto a drop of either ProLong Gold (Life Technologies) or Vectashield mounting medium (Vector Laboratories). Strain WM2026 harbors the native *ftsZ* gene along with a *ftsZ-gfp* gene fusion located elsewhere in the chromosome under control of an IPTG-inducible *trc* promoter. To produce FtsZ-GFP as a dilute label less than the level of native FtsZ, 30 μM IPTG was added to cultures 3 h prior to fixation.

Wild-type cells (WM1074), a strain producing FtsA-GFP (WM4679), strains producing SulA (pWM1736), and cells with $ftsZ_{L169R}$ replacing native *ftsZ* in the chromosome (DPH642) were grown

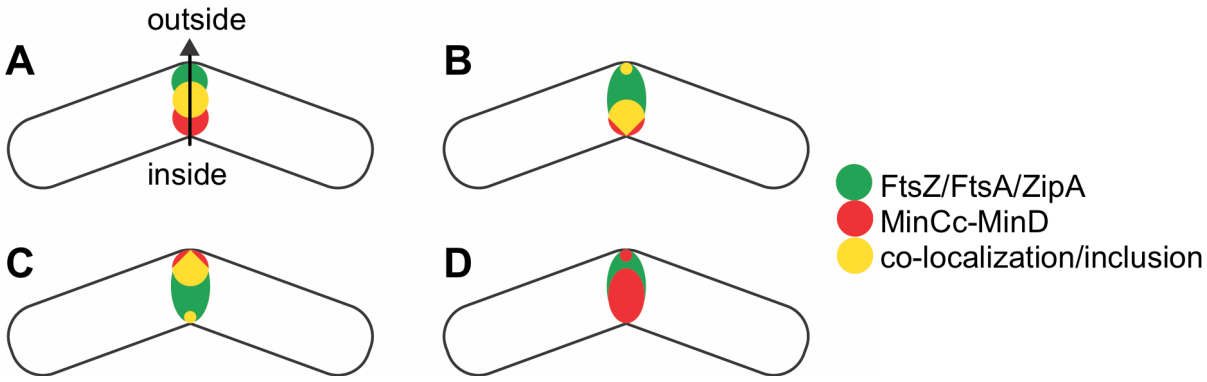

Figure 2-1. Quantitation of immunofluorescence localization patterns of *E. coli* cells overproducing MinCc-MinD. To quantitate the localization pattern at the site of cell bending, a line was drawn from the inside to the outside of the bend, and red/green fluorescence intensity profiles were compared. Examples of the four scored patterns are shown. (A) MinCc-MinD localizes primarily at the inside of the bend and FtsZ/FtsA/ZipA are excluded and localize primarily to the outside of the bend. (B) MinCc-MinD localizes primarily at the inside of the bend and co-localizes with FtsZ/FtsA/ZipA. (C) MinCc-MinD localizes primarily to the center/outside of the bend and co-localizes with FtsZ/FtsA/ZipA. (D) MinCc-MinD localizes primarily to the center/outside of the bend and FtsZ/FtsA/ZipA are excluded and localize primarily to the outside of the bend. A-D correspond to data shown in Fig. 3-8.

and fixed as described above, then treated with lysozyme followed by washes and incubation with affinity-purified anti-FtsZ, anti-FtsA, or anti-ZipA antibodies as described (Levin, 2002), with the following modifications. Fixed cells were adhered to poly-L-lysine coated coverslips instead of a 15-well slide. The coverslips were washed by immersion in a 1X phosphate-buffered saline (PBS) followed by soaking for 10 min in 1X PBS in a small container. Blocking buffer and diluted antibodies were spotted onto parafilm and coverslips were inverted onto the spots. To double label FtsA and ZipA, fixed and lysed WM4679 cells were incubated with 1:500 anti-ZipA antibody, and DyLight 550 (1:100) was used as a secondary antibody (Thermo Fisher Scientific, Waltham, MA).

2.11 ATP detection assay.

To detect ATP in purified protein samples, a BacTiter-Glo Microbial Cell Viability assay was used according to manufacturer instructions (Promega). Protein samples and an ATP standard curve were boiled for 5 min and allowed to cool to room temperature prior to addition of the substrate and luminescence detection in a BioTek (Winooski, VT) plate reader.

2.12 Preparation of liposomes.

Liposomes were prepared using 99% *E. coli* total lipids (Avanti Polar Lipids Inc., Alabaster, AL) and 1% rhodamine labeled phosphatidyl ethanolamine (Avanti). Chloroform was evaporated from lipids using a nitrogen gas stream. Lipids were placed in a speed vac for 30 min to make sure all chloroform was evaporated. Lipids were resuspended in FtsA buffer B (20 mM Tris, pH 7.5, 100 mM KCl, 25 mM potassium glutamate, 5 mM $MgCl_2$) using tip sonication for 20 sec. Resuspended lipids were passed through an extruder with a 400 nm pore size (Avanti).

2.13 Sedimentation assays.

FtsA proteins were diluted to 2 μM in FtsA buffer A, and then further diluted with the addition of either liposomes in FtsA buffer B, or FtsA buffer B without liposomes in a final reaction

volume of 100 µl. ATP was added where indicated and samples were incubated at 37˚C for 2 hours prior to ultracentrifugation at 60,000 rpm in a TLA 100.3 rotor (Beckman). Supernatants were removed and added to tubes with 20 µl 5X SDS buffer. Pellets were resuspended in 100 µl of buffer (50% buffer A and 50% buffer B) and 20 µl 5X SDS buffer was added. Samples were vortexed and boiled prior to separation by SDS-PAGE and Coomassie brilliant blue staining and destaining. Gels were scanned and analyzed using ImageJ to determine the amount of protein in the supernatant and pellet for each sample (Schneider et al., 2012).

2.14 Turbidity assay.

FtsA was diluted to 1 µM in FtsA buffer A and equilibrated to room temperature in a 96 well half area UV transmissible plate (Greiner Bio-One). The optical density at 320 nm was read every 30 sec for 3 min, prior to the addition of either 2 mM ATP, or FtsA buffer A, and samples were mixed with a multichannel pipette prior to reading OD_{320} every 30 sec for 90 min in a BioTek plate reader. Note: This assay was developed in collaboration with Veronica M. Garcia.

Chapter III

Asymmetric constriction of dividing *Escherichia coli* cells induced by expression of a fusion between two Min proteins

This chapter is based upon, "Rowlett, V.W., and Margolin, W. (2014) Asymmetric constriction of dividing Escherichia coli cells induced by expression of a fusion between two Min proteins. Journal of Bacteriology 196: 2089-2100" with permission from the American Society for Microbiology (Copyright © 2014, American Society for Microbiology doi:10.1128/JB.01425-13).

3.1 Introduction

Escherichia coli divides by binary fission using a machine, often called the divisome, comprised of several proteins that are recruited to midcell. In *E. coli*, two systems contribute to correct positioning of the divisome: nucleoid occlusion and the Min system (Margolin, 2000). Both systems spatially regulate the assembly of the Z ring, which serves to organize and recruit divisome proteins (Vicente et al., 2006; Adams & Errington, 2009). The Z ring consists of scattered protofilaments of FtsZ in a ring-shaped structure, which is tethered to the membrane by additional divisome proteins (Fu et al., 2010; Pichoff & Lutkenhaus, 2005). ZipA and FtsA tether FtsZ to the inner membrane, and Z rings can form in the absence of one or the other, but both are required for recruitment of downstream divisome proteins (Pichoff & Lutkenhaus, 2002). In the absence of the Min system, Z rings assemble not only at midcell between the two segregated daughter nucleoids, but at all nucleoid-free regions within the cell, including the cell poles (Yu & Margolin, 1999). Because only a subset of the many Z rings formed in a Δ*min* mutant are competent to form a division septum at any one time, Δ*min* cells are a mixture of cells of normal size, filaments of various lengths because of delayed cell division, and chromosome-free minicells formed by septation near the cell poles (de Boer et al., 1989).

The Min system consists of three proteins, MinC, MinD, and MinE (de Boer et al., 1989). MinC binds to FtsZ and inhibits FtsZ assembly (Hu et al., 1999). By itself, MinC cannot spatially restrict Z rings to midcell; MinC binds to MinD, an ATPase that coats a large portion of the cell membrane near the cell pole when in its ATP-bound state (Hu & Lutkenhaus, 2003; de Boer et al., 1991). MinE binds MinD and forms a ring at the edge of the MinD polar zone. MinE stimulates the

ATPase activity of MinD, which removes MinD from the membrane and causes the MinD zone to collapse in front of the poleward-migrating MinE ring (Raskin & de Boer, 1997; Hu et al., 2002). After the MinD polar zone is completely dislodged, MinD then rebinds ATP and moves toward the opposite cell pole, followed by MinE, and the pattern repeats (Raskin & de Boer, 1999b; Fu et al., 2001; Huang et al., 2003). The oscillation of this system near the cell poles and away from midcell keeps the concentration of the MinC inhibitor lowest at midcell and highest at cell poles over time (Raskin & de Boer, 1999b; Hu & Lutkenhaus, 1999). This has the effect of preventing FtsZ from assembling near cell poles, visualized by the oscillation of FtsZ-green fluorescent protein (GFP)/cyan fluorescent protein (CFP) fusions from pole to pole in response (Thanedar & Margolin, 2004; Tonthat et al., 2013; Bisicchia et al., 2013).

MinC consists of an N-terminal domain and a C-terminal domain separated by a short linker (Cordell et al., 2001; Hu & Lutkenhaus, 2000). The N terminus of MinC (MinCn) is sufficient for inhibition of FtsZ assembly, and the C terminus of MinC (MinCc) is both the binding interface for MinD and an inhibitor of FtsZ assembly (Hu & Lutkenhaus, 2000; Shiomi & Margolin, 2007a), although the inhibitory activity of MinCc requires the presence of MinD (Shiomi & Margolin, 2007a). MinCn binds to the conserved N-terminal domain of FtsZ, while MinCc binds to FtsZ's C-terminal core domain (Shen & Lutkenhaus, 2009, 2010). Their inhibition of FtsZ assembly is synergistic, with MinCn blocking FtsZ-FtsZ longitudinal interactions within a protofilament and MinCc inhibiting lateral interactions between FtsZ protofilaments (Dajkovic et al., 2008). When overproduced, MinCc also acts after FtsZ assembly by competing with ZipA and FtsA for FtsZ binding, dislodging FtsA from the Z ring preferentially, and eventually dislodging ZipA (Shen & Lutkenhaus, 2009).

As MinCc activity requires MinD, we originally sought to determine the effect on cells when MinCc and MinD are tethered together as a single fusion protein. Whereas overproduction of a MinC-MinD fusion induces cell filamentation as expected, overproduction of a MinCc-MinD fusion causes

many cells to jackknife at their division septa. This prompted further characterization of the phenotype and how the MinCc-MinD fusion induces it.

3.2 Results

3.2.1 Overproduction of a MinCc-MinD fusion induces frequent bending of *E. coli* cells at cell division septa.

Full-length MinC or the C-terminal half of MinC (MinCc) was fused translationally to the N terminus of full-length MinD in pDSW210 containing a weakened Ptrc promoter and His_6 tag to evaluate their effects on cell division. Constructs used in this study are shown in Fig. 3-1A. Cells of the WT strain (WM1074) were normal in the absence of IPTG induction of MinCc-MinD (Fig. 3-1D) but became extremely filamentous in the presence of inducer (Fig. 3-1E). This indicated that the MinCc-MinD fusion protein either is an active division inhibitor or can activate the native Min proteins present in these cells.

The effects of these fusions in a Δ*minCDE* background (WM1032) were then tested to determine if MinC-MinD or MinCc-MinD could inhibit FtsZ in the absence of endogenous Min proteins. Uninduced WM1032 control cells carrying the MinC-MinD fusion plasmid (Fig. 3-1B) displayed a mixture of cell lengths but were mostly filamentous. Uninduced WM1032 carrying the MinCc-MinD fusion plasmid (Fig. 3-1F) appeared as the expected mixture of filaments and minicells typical of a Δ*min* mutant. Upon induction of MinC-MinD production with 1 mM IPTG, cells filamented strongly (Fig. 3-1C). Full-length MinC inhibits cell division fairly well on its own but is a much more potent inhibitor in the presence of MinD, presumably because MinD concentrates MinC at the cytoplasmic membrane and enhances its affinity for the Z ring (Hu & Lutkenhaus, 1999; Raskin & de Boer, 1999a; Johnson et al., 2002). The absence of MinE likely enhances the division inhibition, as there is no removal of MinD from the membrane under these conditions.

The unexpected result came from the production of MinCc-MinD after a 1-hour induction with IPTG. Instead of straight filaments that appear after overproduction of MinC-MinD or when MinCc and MinD are overproduced separately (Shiomi & Margolin, 2007a), the majority of cells were observed to bend dramatically at the site of division (Fig. 3-1 G- I and Table 3-1). This was

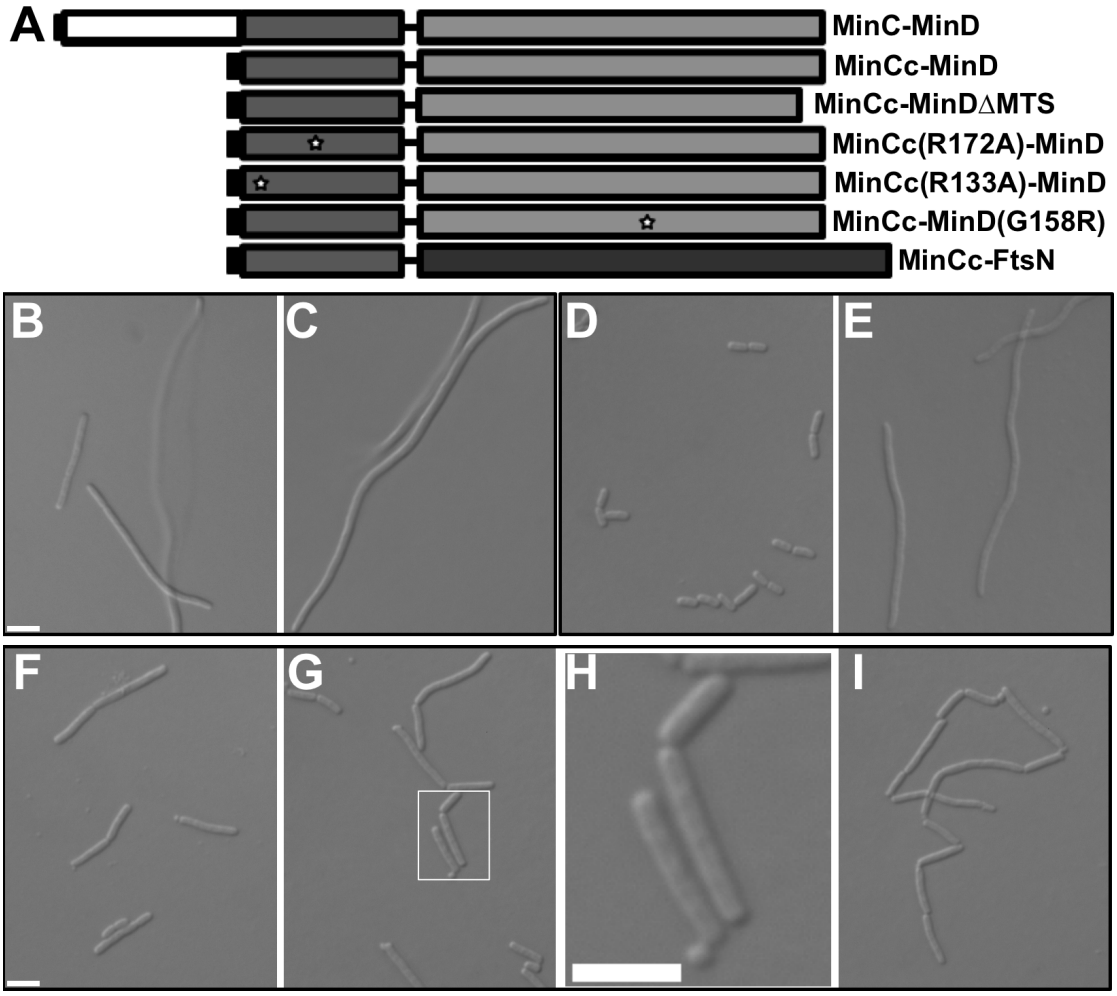

Figure 3-1. A MinCc-MinD fusion causes bending in Δ*minCDE E. coli* cells. (A) Fusion constructs used in this study. The black portion on the left represents the His_6 tag. The stars represent the positions of the R172A (MinC), R133A (MinC), and G158R (MinD) lesions, and ΔMTS represents the deletion of the membrane targeting sequence of MinD (MinDΔ259-270). The MinCc-MinD fusion consists of MinC122-231, a *Sal*I restriction site, pentaglycine linker, and MinD. (B-I) Full-length MinC-MinD fusion (pWM2737) uninduced (B) and induced (C) in a Δ*minCDE* background strain (WM1032); MinCc-MinD fusion (pWM2738) uninduced (D) and induced (E) in an isogenic *min*$^+$ background (WM1074); MinCc-MinD fusion uninduced (F) and induced (G) in a Δ*minCDE* background (WM1032); a bent cell from panel G (inset) is enlarged (H) and what appears to be a cell chain of the same strain as that in panel G with multiple bends is shown in panel I. All induced strains were induced with 1 mM IPTG. Bars, 4 μm.

Percentage of bent division septa

Plasmid or Strain[a]	Protein fusion	No. of septa	% of septa bent[b]
pWM2738	MinCc-MinD uninduced	100	7.0
	MinCc-MinD (10 μM IPTG)	84	40.5
	MinCc-MinD (0.1 mM IPTG)	93	76.3
	MinCc-MinD (1 mM IPTG)	100	82.0
pWM4005	MinCc-MinDΔMTS uninduced	91	2.2
	MinCc-MinDΔMTS (1 mM IPTG)	98	6.1
pWM4070	MinCc(R172A)-MinD uninduced	84	3.6
	MinCc(R172A)-MinD (1 mM IPTG)	100	8.0
pWM4127	MinCc-FtsN uninduced	44	9.1
	MinCc-FtsN (1 mM IPTG)	99	19.2
WM3997	MinCc-MinD uninduced + FtsQAZ	88	4.5
	MinCc-MinD (1 mM IPTG) + FtsQAZ	100	50.0
WM4831	MinCc-MinD uninduced, chromosomal *ftsA**	88	5.7
	MinCc-MinD (10 μM IPTG), chromosomal *ftsA**	76	22.4
	MinCc-MinD (0.1 mM IPTG), chromosomal *ftsA**	89	41.6
	MinCc-MinD (1 mM IPTG), chromosomal *ftsA**	98	49.0

[a] All strains were derivatives of WM1032 (Δ*minCDE::kan*).

[b] If straight daughter cells are defined as having an angle of ~180˚, then bent septa are defined as creating angles of <145˚ at the time of image capture.

obvious in many cells within the culture because cell separation was often delayed, resulting in crooked cell pairs or chains. The bends occurred in either direction (Fig. 3-1I). As expected, minicells were sometimes observed still attached to cell poles, but unlike minicells in normal Δ*min* strains, minicells of MinCc-MinD overproducers were often bent at a significant angle from the mother cell (Fig. 3-1H). These results are consistent with a defect in the normal symmetry of division septum formation.

When overproduced at moderate levels of induction (0.1 mM IPTG), which still induced bending cell divisions in over 75% of the cells, the MinCc-MinD fusion did not appreciably affect viability of Δ*minCDE* cells (Fig. 3-2, top panels; Table 3-1). This indicates that a majority of cells divide despite their asymmetric constrictions for multiple generations and is consistent with the ability of cells to grow and divide in time-lapse studies (see below). Lower (10 μM) IPTG concentrations also yielded normal viability, although the percentage of bends was a lower but still considerable 41% (Table 3-1). However, at the highest levels of induction (1 mM IPTG), overproduction of MinCc-MinD was lethal (Fig. 3-2).

3.2.2 Details of bending cell divisions are revealed by time-lapse and electron microscopic imaging.

To observe bending at the septum as it was occurring and to trace cell lineages more closely, WM2738 (Δ*minCDE*) cells overproducing MinCc-MinD were cultured and spotted 3 μl onto an agar pad to visualize growing cells by time-lapse imaging. These cells grew, bent at division sites, and often exhibited delays in septation like the cells in liquid culture (Fig. 3-3A). Most bends ultimately resulted in cell division at the site of the bend and ~80% of all cell division events resulted in a bend (Table 3-1). A closer look at the region of cell separation showed that the two separating cells appeared to crack off each other. This idea is supported by electron microscopic data (see below).

As MinCc interacts directly with FtsZ, I hypothesized that the MinCc-MinD fusion somehow affected morphology and/or constriction dynamics of the Z ring. I therefore repeated the MinCc-

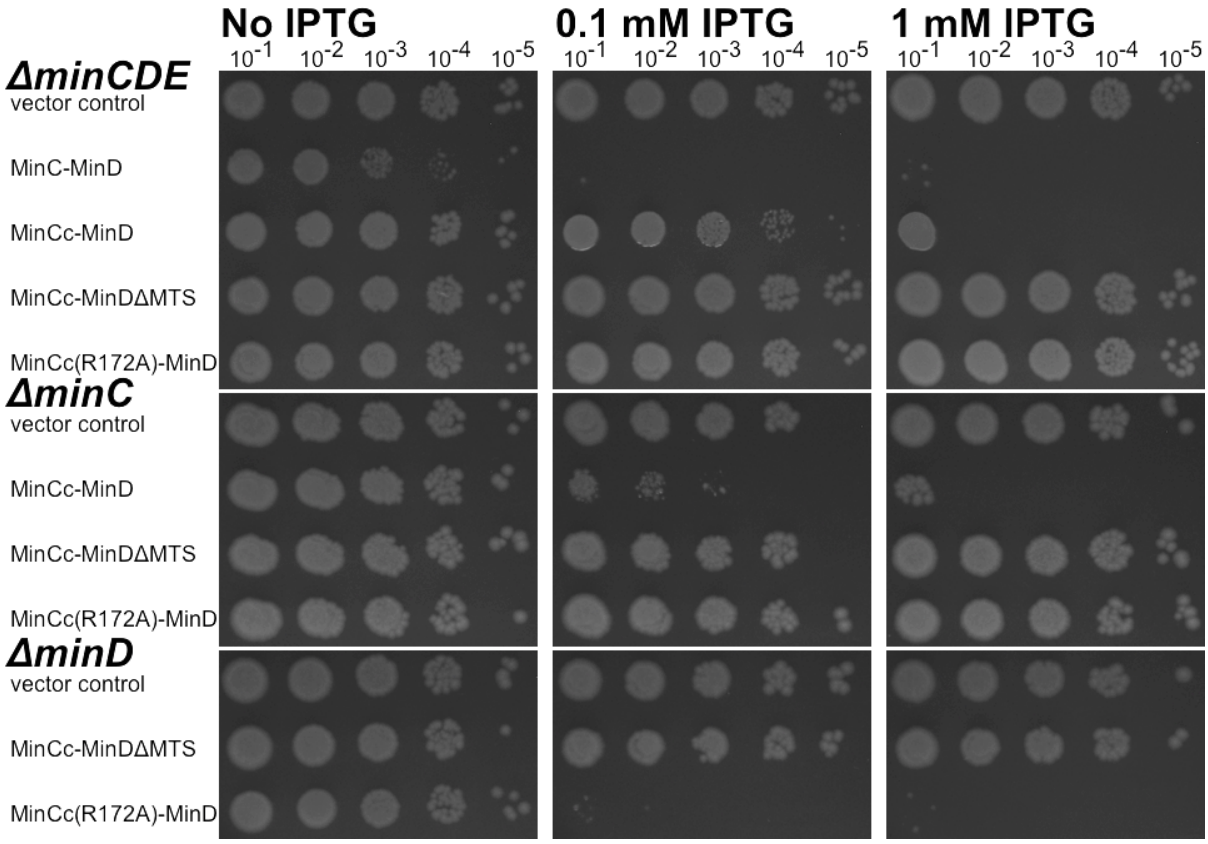

Figure 3-2. Viability of various fusion constructs. Strains shown were grown to logarithmic phase, serially diluted at the dilutions shown, spotted onto LB plates containing 0, 0.1, or 1 mM IPTG and grown overnight at 37˚C.

MinD overproduction time-lapse experiment, this time in cells expressing low levels of FtsZ-GFP as a dilute label so that the localization and dynamics of the Z ring could be traced (Sun & Margolin, 1998). This experiment was performed in a microfluidics chamber that immobilized cells and supplied nutrients for continuous growth. The growth and bending division of FtsZ-GFP-expressing cells (WM4082) were similar to those of cells not expressing FtsZ-GFP (Fig. 3-3). As FtsZ is required for cell division, we were not surprised to find that every bending division was associated with a fluorescent Z ring. Of cells that bent but did not show signs of septum formation during the time course, all bends were associated with Z rings. This is perhaps not surprising either, as Δ*min* cells form Z rings at most internucleoid spaces, although only a subset are active in septation (Yu & Margolin, 1999). This also explains the presence of Z rings at many sites that did not divide during the time course.

Careful observation of FtsZ-GFP localization patterns at the bending septa revealed that Z rings initially appeared normal, then constricted normally as well as could be detected (Fig. 3-3B, arrows). Once the aberrant asymmetric septa were formed and the cell poles started to crack away from each other at one end, FtsZ rapidly formed a new ring at one or both of the new poles (Fig. 3-3B). This is similar to what has been observed in *B. subtilis* cells lacking the Min system and led to the idea that the Min system is important for preventing new Z ring assembly adjacent to the currently active constricting ring (Gregory et al., 2008). Once a bending division was complete, the polar Z rings usually persisted in the daughter cells. We conclude that there is no obvious abnormal localization of FtsZ prior to a bending division versus a normal division, suggesting that the root cause of asymmetric constriction is not simply a preference for FtsZ to assemble more on one side of the cell than the other.

To visualize the bending sites in greater detail, we negatively stained thin sections of WM2738 cells with MinCc-MinD fusions either uninduced or induced and viewed them by electron microscopy (Fig. 3-4). When the MinCc-MinD fusion was not induced, typical symmetrical cell division septa that had similar constrictions on both sides of the cell were observed (Fig. 3-4A).

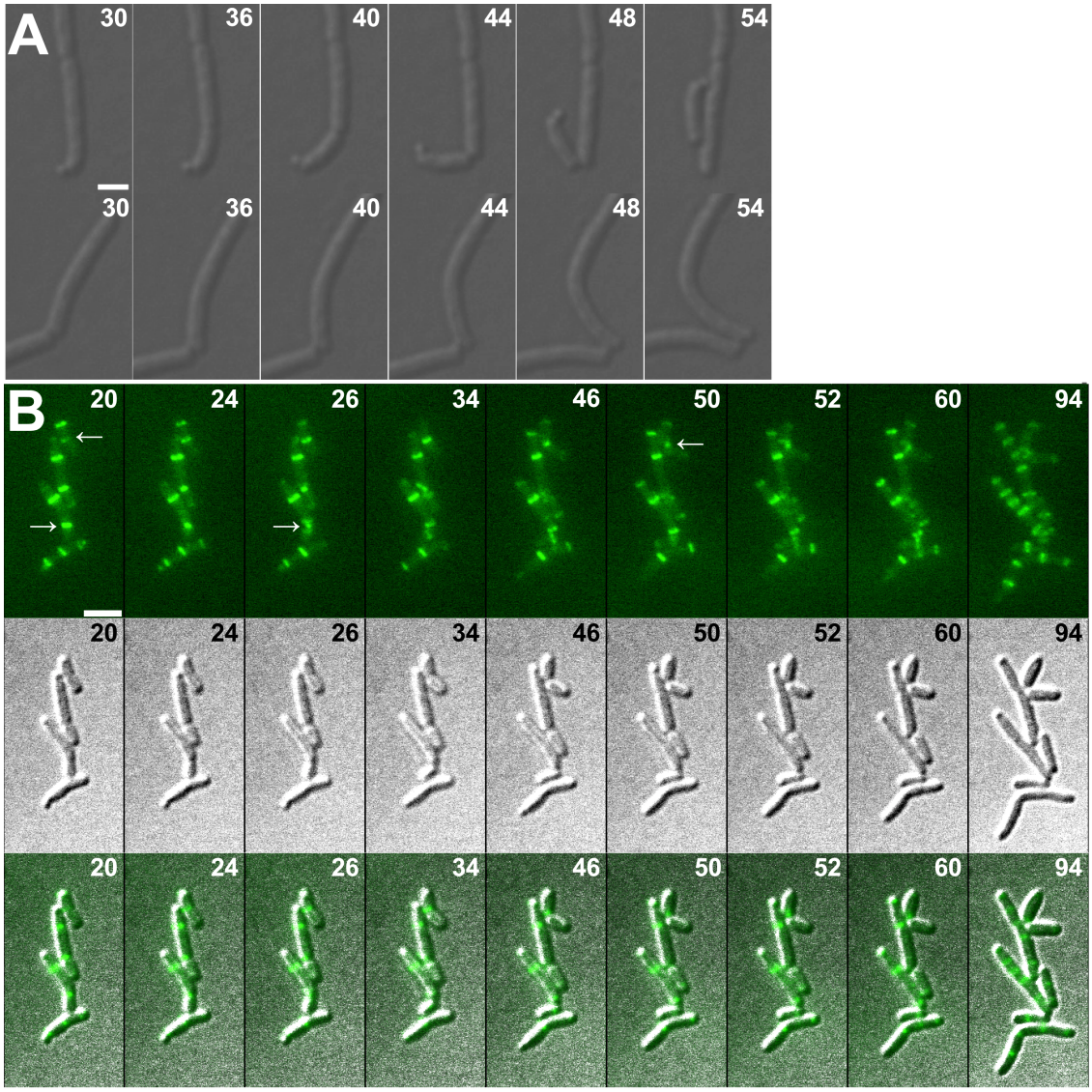

Figure 3-3. Growing and dividing cells overproducing MinCc-MinD in time-lapse images. (A) DIC images of two different fields of 1 mM IPTG-induced WM2738 cells, showing bending divisions. Time (min) elapsed from the start of the experiment is shown. (B) Time-lapse images of WM4082 cells producing FtsZ-GFP with 10 µM IPTG induction and MinCc-MinD induced with 10 µM sodium salicylate. Top row, FtsZ-GFP fluorescence; middle row, DIC; bottom row, overlay. Time (min) elapsed from the start of the experiment is shown. Leftmost arrows highlight Z rings prior to apparent cell bending; subsequent arrows reflect localization of FtsZ-GFP to foci at the constriction site and the rims of newly formed cell poles during a bending division event. Bars, 2 µm (A); 4 µm (B).

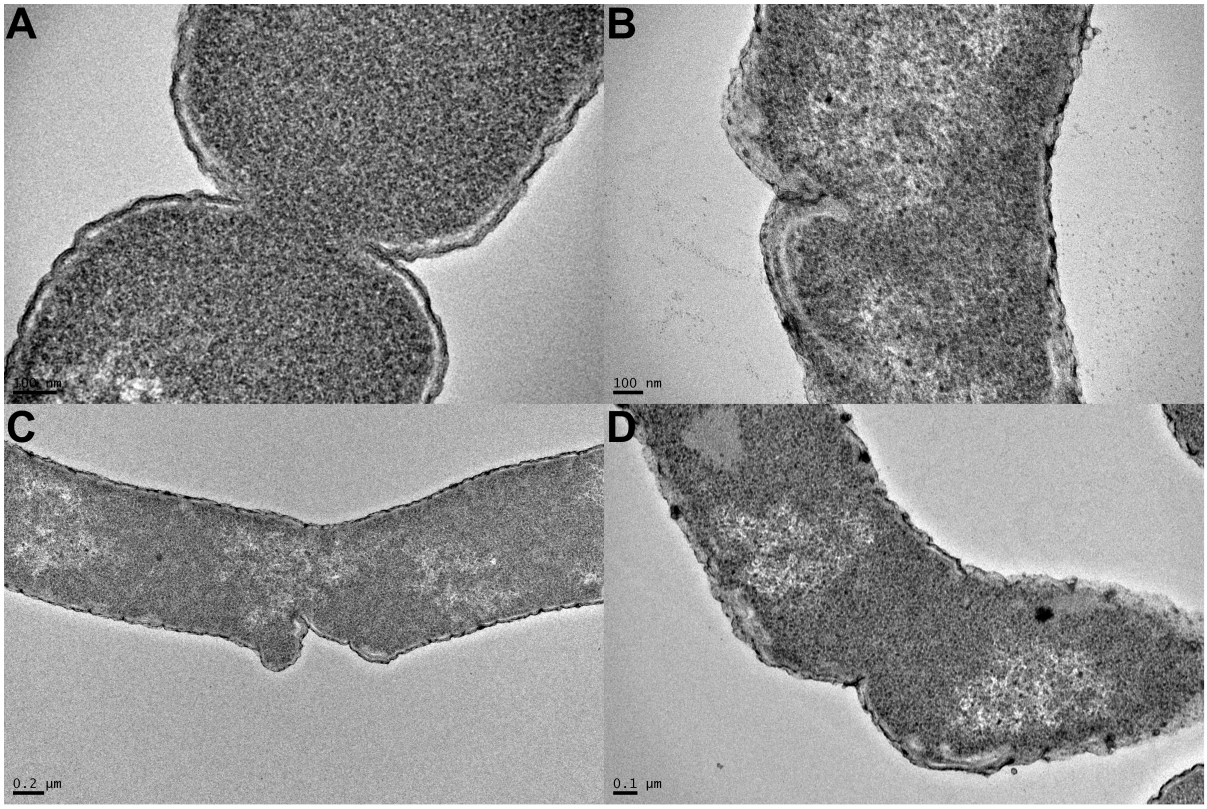

Figure 3-4. Transmission electron microscopy of thin sections of dividing WM2738 cells. WM2738 cells producing uninduced MinCc-MinD (A) or induced MinCc-MinD (1 mM IPTG) (B-D). Bars, 100 nm (A and B), 0.2 µm (C), and 0.1 µm (D).

However, upon induction of MinCc-MinD, I observed a number of bending division events that showed envelope invaginations mainly on one side of the cell, on the outside of the bend (Fig. 3-4 B-D). These observations are consistent with the idea that bending division is caused by a local disruption of septal wall growth and splitting on one side of the cell, despite the lack of any apparent asymmetry in FtsZ-GFP localization.

3.2.3 Localization of MinCc-MinD to cell division sites.

Although FtsZ-GFP localization seemed to be normal in Δ*minCDE* cells overproducing the MinCc-MinD fusion, I wanted to assess whether MinCc-MinD fusion proteins localized to Z rings or any other places in the cell. I constructed a GFP-MinCc-MinD fusion, but this fusion failed to induce cell bending in the Δ*minCDE* background and mostly localized uniformly around the cell and not at Z rings, suggesting that the three-way fusion was inactive. I also constructed C-terminal MinCc-GFP fusions and MinCc-yellow fluorescent protein (YFP)-MinD fusions, but these also failed to localize to meaningful patterns or provoke cell bending.

To circumvent these problems, I took advantage of the N-terminal His_6 tag on our original MinCc-MinD construct in Δ*minCDE* cells to localize the fusion protein by immunofluorescence microscopy (IFM) using anti-His_6 tag monoclonal antibodies. The same cells were probed with polyclonal anti-FtsZ, and the signals were overlaid. A Δ*minCDE* strain containing an empty vector plasmid showed no localization with the anti-His_6 tag antibody (data not shown). In uninduced Δ*minCDE* cells with the His_6-MinCc-MinD plasmid, weakly fluorescent bands were observed in a subset of cells, and these bands usually colocalized with Z rings (data now shown). Upon overproduction of His_6-MinCc-MinD with IPTG, fluorescent foci were usually visible instead of bands. These foci were more intense than the bands in the uninduced cells, and they were present in most cells (Fig. 3-5A). The foci were distributed fairly sparsely throughout the cell length, but the majority of these foci (~80%) roughly colocalized with FtsZ staining.

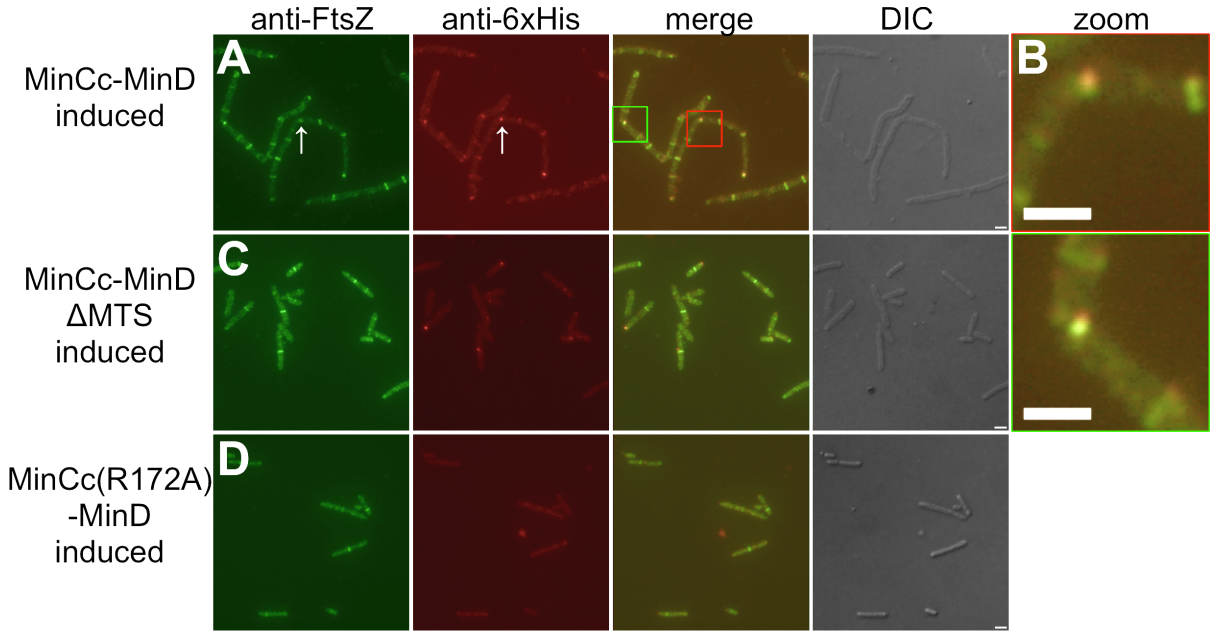

Figure 3-5. Localization of His_6-MinCc-MinD fusions in Δ*minCDE* (WM1032) cells. (A) Native FtsZ (green) and His_6-MinCc-MinD from pWM2738 (red), the latter induced with 1 mM IPTG. (B) Magnified view of red and green insets from panel A. (C) Localization of native FtsZ, along with MinCc-MinDΔMTS induced with 1 mM IPTG. (D) Localization of native FtsZ, along with MinCc(R172A)-MinD induced with 1 mM IPTG. Arrows in panel A highlight a bend with colocalized FtsZ and MinCc-MinD. Camera exposure times were identical for all anti-His_6 or all anti-FtsZ fields. Bars, 2 μm.

3.2.4 The bending division phenotype depends on self-interaction and membrane and septal targeting of MinCc-MinD.

An R172A lesion in MinCc has been shown to disrupt its interaction with the septum, and presumably FtsZ itself (Zhou & Lutkenhaus, 2005). I engineered this mutation into the MinCc-MinD fusion to test whether the likely interaction between MinCc and FtsZ contributes to the bending phenotype. As expected, when fusions containing the R172A lesion were expressed, bending cell divisions were severely attenuated, down from ~80% to 8% of total cell division events (Table 3-1 and Fig. 3-6 C and D). The R172A-containing protein fusion also failed to localize efficiently (Fig. 3-5D), supporting the idea that the MinCc portion of the MinCc-MinD fusion likely interacts with FtsZ in order to cause a cell to divide asymmetrically. To rule out the possibility that the fusion proteins were not being overproduced in these cells, Western blot was used to detect their N-terminal His_6 tags using anti-His_6 antibodies (Fig. 3-6I). The bands for MinCc-MinD were only slightly more intense than those for MinCc(R172A)-MinD, indicating that they were produced at roughly equivalent levels upon IPTG induction. Production of MinCc-MinD was reduced in a WT (WM1074) background (Fig. 3-7), probably because MinCc-MinD is a potent division inhibitor in a Min^+ strain as described above and makes cells sick. Full-length MinC-MinD was barely detectable in a Δ*minCDE* background (Fig. 3-7), likely for similar reasons.

MinD is targeted to the membrane by an 8- to 12-residue membrane targeting sequence (MTS) on its C terminus (Hu & Lutkenhaus 2003; Szeto et al., 2002). I deleted the MTS in the MinD portion of the MinCc-MinD fusion (MinCc-MinDΔMTS) to test whether membrane targeting of the fusion was required for the bending division phenotype. After IPTG induction of the truncated MinCc-MinD fusion in Δ*minCDE* cells, the percentage of cells with asymmetric septa was dramatically reduced to ~6% (Table 3-1 and Fig. 3-6 A and B), despite the overproduction of this protein to nearly the level of the normal fusion protein (Fig. 3-6I). Without IPTG induction, the truncated MinCc-MinD fusion weakly colocalized with FtsZ staining in IFM experiments (data not shown). Higher levels of the truncated fusion protein after IPTG induction localized to multiple foci

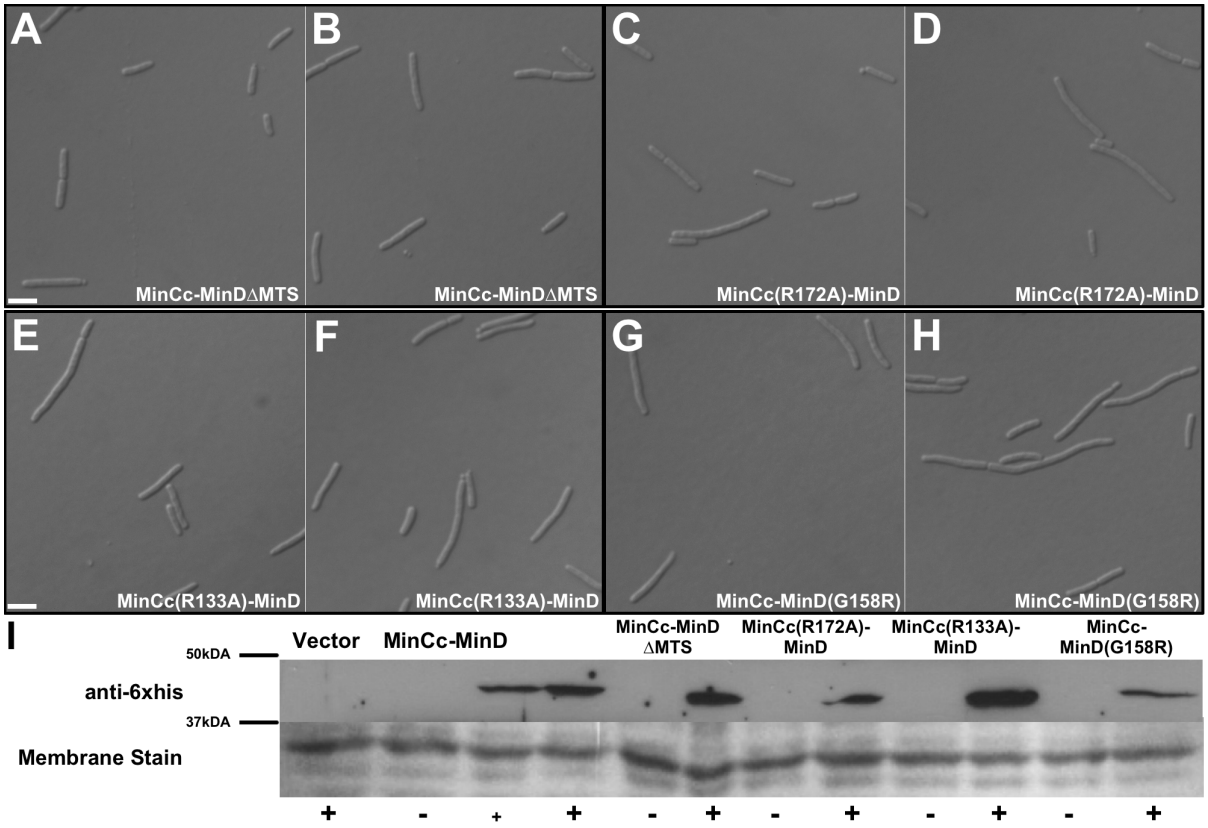

Figure 3-6. Membrane targeting, septal interaction, and self-interaction contribute to the effects of MinCc-MinD on cell bending. (A-H) DIC microscopy images are shown for WM1032 (Δ*minCDE*) cells producing the MinCc-MinDΔMTS fusion from pWM4005 uninduced (A) and induced (B) with 1 mM IPTG, MinCc(R172A)-MinD from pWM4070 uninduced (C) and induced (D) with 1 mM IPTG, MinCc(R133A)-MinD uninduced (E) and induced (F) with 1 mM IPTG, or MinCc-MinD(G158R) uninduced (G) and induced (H) with 1 mM IPTG. Bars, 2 μm. (I) Western blot and corresponding membrane stain of uninduced (-) and induced (+) pDSW210His$_6$ vector control and various fusions produced from the pDSW210His$_6$ derivatives. The small plus sign below lane 3 represents induction of MinCc-MinD with 0.1 mM IPTG.

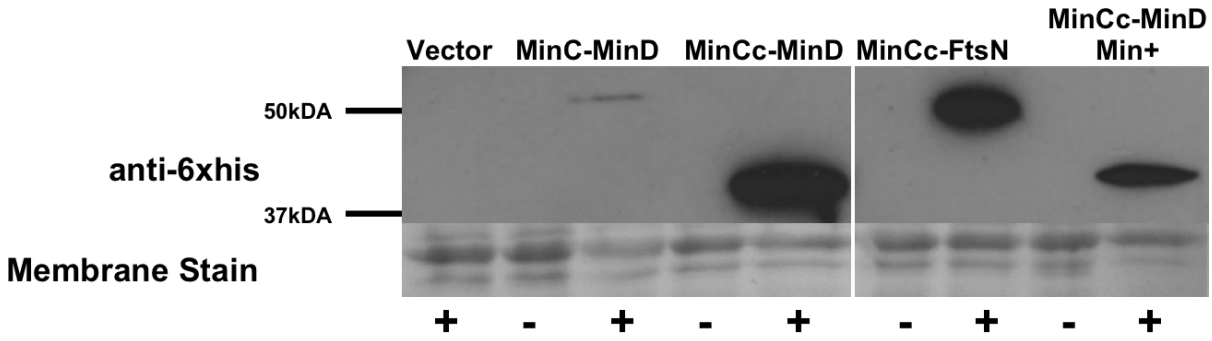

Figure 3-7. Western blot of fusions. Western blot and corresponding membrane staining of uninduced (-) and 1 mM IPTG-induced (+) pDSW210His$_6$ vector control and various fusions produced from the pDSW210His$_6$ derivatives. All strains are Δ*minCDE* except for the last two lanes, which are in a Min$^+$ background.

that were not obviously colocalized with FtsZ (Fig. 3-5C). Although it is difficult to explain the localization results, the lack of a cell bending phenotype despite strong overproduction of the truncated fusion suggests that membrane localization is important for MinCc-MinD to induce cell bending.

To determine if MinCc-MinD fusions need to interact with other fusions to cause cells to bend, I constructed two point mutants. An R133A lesion in the MinCc portion of MinC has been shown to disrupt its interactions with MinD but not MinC (Zhou & Lutkenhaus, 2005). A G158R lesion in MinD results in loss of interaction with MinC without affecting interactions with MinD or MinE (Ma et al., 2004). When R133A was introduced into the MinCc portion of the MinCc-MinD fusion, cell bending was suppressed (Fig. 3-6 E and F). Likewise, when G158R was introduced into the MinD portion of the MinCc-MinD fusion, MinCc-MinD(G158R) also suppressed the bending phenotype (Fig. 3-6 G and H). These mutant fusions were clearly overproduced as shown by Western blotting (Fig. 3-6I), although G158R levels were lower than R133A levels. These data suggest that interaction between the fusion proteins is required for the bending phenotype.

To test whether MinD itself is specifically required for the effect or whether targeting MinCc to the membrane by another means would be sufficient, I fused MinCc to the N terminus of FtsN, a cell division protein that contains a single transmembrane and periplasmic domain. This produced a MinCc fusion to full-length FtsN. Overproduction of MinCc-FtsN (WM4127) induced 19% of septa to have bends, more than the mutant MinCc-MinD constructs, but still much less than the normal construct (Table 3-1). MinCc-FtsN was stably overproduced (Fig. 3-7) and should localize to the cytoplasmic membrane. These data suggest that although membrane targeting plays a role, other determinants of MinD, including residues at the MinCc-MinD fusion junction, may be important for full activity.

To investigate the activities of the MinCc and MinD portions of the MinCc-MinD fusion further, I characterized the effects of the fusions in cells lacking either MinC or MinD (Fig. 3-2 and Table 3-2). In cells lacking only MinC, production of the MinCc-MinD fusion cased cells to bend and

Table 3-2 Phenotypes of protein fusions in different Min deletion backgrounds[a]

	Phenotype by background:			
Protein	Min$^+$	Δ*minCDE*	Δ*minC*	Δ*minD*
Vector control	WT	Min$^-$	Min$^-$	Min$^-$
MinCc-MinD	Filamentous	Bent	Bent	Uninduced lethal
MinCc-MinDΔMTS	−	Min$^-$	Min$^-$	Min$^-$
MinCc(R172A)-MinD	−	Min$^-$	Min$^-$	Filamentous
MinC-MinD	−	Filamentous	−	−

[a]All were overproduced with 1 mM IPTG in LB broth during logarithmic growth except as noted. −, not determined.

filament, as in the Δ*minCDE* background. Producing MinCc(R172A)-MinD and MinCc-MinDΔMTS in the Δ*minC* strain yielded a typical minicell phenotype indistinguishable from that of Min^- cells. In contrast, repeated attempts to introduce the plasmid carrying the MinCc-MinD fusion into a Δ*minD* strain failed. This suggests that the native full-length MinC in the Δ*minD* strain can interact with the MinD portion of the MinCc-MinD fusion, even when present at low uninduced levels, to suppress assembly of FtsZ efficiently throughout the cell. It is not clear why MinCc-MinD is more toxic in a Δ*minD* strain than in a WT strain, although one explanation is that the Δ*minD* construct is polar on *minE*, which would reduce *minE* expression and increase the ability of MinC to bind to MinD at many sites on the cytoplasmic membrane. The MinCn portion of the native MinC is likely required for this inhibition. In support of this idea, production of the MinCc(R172A)-MinD fusion, which normally has little effect in a strain lacking MinC, causes filamentation and ultimately cell death in the $minC^+$ Δ*minD* strain as cellular levels of the fusion are increased (Fig. 3-2).

3.2.5 MinCc-MinD localizes to the inside of most developing bends and preferentially excludes FtsA.

Now that the need for the fusion protein to bind to FtsZ and interact with other fusion proteins was established, and FtsZ localization itself did not seem to be perturbed significantly by the fusion, we wanted to investigate whether any downstream cell division proteins were forced to localize asymmetrically. As we did for MinCc-MinD and FtsZ, we used IFM to examine the localization of His_6-tagged MinCc-MinD in greater detail and whether the localization of FtsA or ZipA was perturbed by the fusion protein. Anti-His_6 antibody was used for His_6-MinCc-MinD in conjunction with either anti-FtsA or anti-ZipA antibodies in double-labeling IFM experiments on bending induced WM2738 cells or nonbending WM1032 parental cells. As before, we observed only faint background staining for His_6 in the WM1032 controls and strong His_6-MinCc-MinD foci in the induced WM2738 cells. When I examined cells at an early stage of bending division, prior to deep constriction, quantitating fluorescence intensities across isolated rings at developing cell bends

revealed that 82 to 84% of the His_6-MinCc-MinD foci were found mainly at the inside of the bends (Fig. 3-8 A and B and addition of columns A and B in Fig. 3-8E).

Localization of FtsZ, FtsA, or ZipA was then measured in these same His_6-MinCc-MinD-overproducing cells and I quantitated fluorescence intensities across isolated rings at developing cell bends. I found that 45% of these bends exhibited FtsZ or ZipA staining that overlapped the peak His_6-MinCc-MinD staining (34% + 11% for FtsZ; 33% + 12% for ZipA), whereas 55% of the bends had FtsZ or ZipA staining that was largely distinct from the peak of His_6-MinCc-MinD staining (50% + 5% for FtsZ; 49% + 6% for ZipA). This is outlined in Fig. 3- 8 A and D versus 3-8 B and C and in Fig. 3-8E columns A and D versus columns B and C. Strikingly, however, 90% of bends (74% + 16%) displayed a peak of FtsA staining intensity that was distinct from the peak of His_6-MinCc-MinD staining (Fig. 3-8 A and D and addition of columns A and D in Fig. 3-8E). This suggested that FtsA localization was specifically antagonized by MinCc-MinD and thus significantly biased toward the outside of the developing cell bend, which is where most of the constriction occurs. In support of this, 74% of the bends had His_6-MinCc-MinD at the inside of the bend and FtsA localized away from His_6-MinCc-MinD toward the outside of the bend (Fig. 3-8 A and E, column A). Although ZipA was localized more symmetrically at the bending septa and should be able to tether FtsZ to the membrane throughout the circumference of the ring, both ZipA and FtsA are required for recruitment of downstream divisome proteins (Pichoff & Lutkenhaus, 2002). This supports the idea that the asymmetry of FtsA localization leads to asymmetric septation.

3.2.6 FtsA* or excess FtsQ, FtsA, and FtsZ partially suppress the bending phenotype.

Cell division genes *ftsQ*, *ftsA*, and *ftsZ* are located adjacent to each other on the *E. coli* chromosome (Robinson et al., 1984, 1986; Yi et al., 1985). Multicopy *ftsQAZ* has been shown to suppress the lethality of overproduction of MinC with MinD (Pichoff & Lutkenhaus, 2001) and suppress the filamentation of Δ*minCDE* strains (Begg et al., 1998). To determine if increased expression of *ftsQAZ* could also suppress the bending division phenotype, I introduced a multicopy

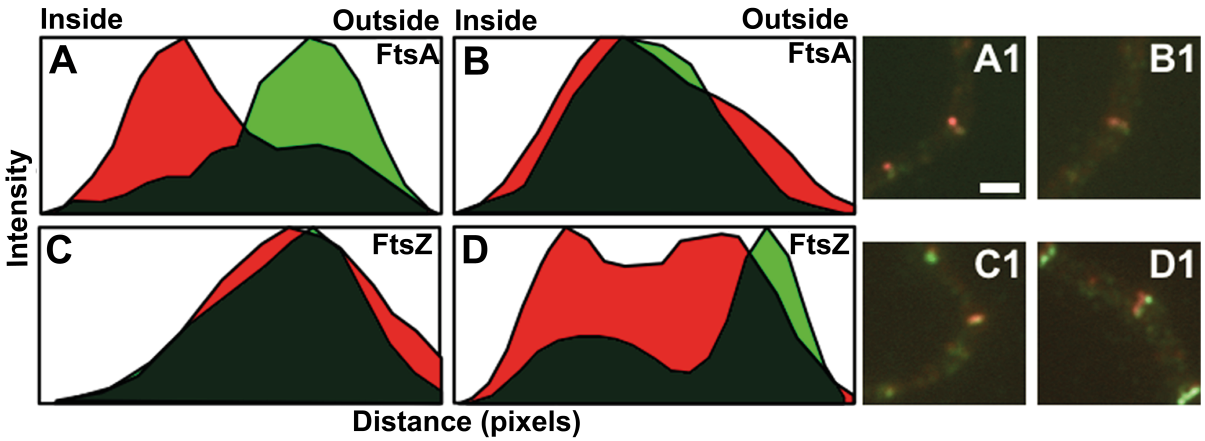

E

MinCc-MinD localization relative to localization of:	(A) MinCc-MinD toward inside of bend excluding FtsZ/ ZipA/FtsA	(B) MinCc-MinD toward inside of bend including FtsZ/ ZipA/FtsA	(C) MinCc-MinD toward center/ outside of bend including FtsZ/ ZipA/FtsA	(D) MinCc-MinD toward center/ outside of bend excluding FtsZ/ ZipA/FtsA	# counted
FtsZ	50%	34%	11%	5%	44
ZipA	49%	33%	12%	6%	33
FtsA	74%	10%	0%	16%	31

F

Figure 3-8. Aggregated His_6-MinCc-MinD fusion proteins preferentially displace FtsA from the Z ring. Immunofluorescent staining of WM2738 cells induced with 1 mM IPTG and stained with anti-FtsZ, and anti-His_6, anti-ZipA and anti-His_6, or anti-FtsA and anti-His_6 at developing bending cell division septa was quantitated as described in Materials and Methods (Fig. 2-1). Representative plots are shown above for anti-FtsA (green) and anti-His_6 (red) (A and B) and anti-FtsZ (green) and anti-His_6 (red) (C and D). (A-D) Four classes of common localization patterns are shown. (A) Representative intensity plot of His_6-MinCc-MinD localization toward the inside of a bend and displacement (or lower-intensity peak) of FtsZ, ZipA, or FtsA as represented in column A of the table in panel E. (B) Representative intensity plot of His_6-MinCc-MinD localization toward the inside of a

bend and colocalization with a peak of FtsZ, ZipA, or FtsA as represented in column B of the table in panel E. (C) Representative intensity plot of His_6-MinCc-MinD localization at the center/outside of a bend with a colocalized peak of FtsZ or ZipA (none observed for FtsA), as represented in column C of the table in panel E. (D) Representative intensity plot of His_6-MinCc-MinD localization at the center/outside of a bend corresponding with displaced FtsZ, ZipA, or FtsA as represented in column D of the table in panel E. Panels A1-D1 show representative micrographs of each example shown in panels A-D; bar, 2 μm. (E) Table of quantitations of the four observed classes of patterns. (F) Model of asymmetric constriction.

plasmid containing these genes under their native transcriptional controls (pBS58) (Bi & Lutkenhaus, 1990) into our Δ*minCDE* strain that overproduces MinCc-MinD (WM3997). While the percentage of bending septa was lower with the *ftsQAZ* plasmid than without it (Table 3-1), bending was still observed at ~50% of septa, and overall viability was normal, even at the highest induction levels (Fig. 3-9 and Fig. 3-10). As increased *ftsQAZ* stimulates cytokinesis and thus decreases cell length in Δ*minCDE* strains, the observed lower bending frequency could be explained by more efficient cytokinesis of these cells, which would cause us to not count cells that were bent but ultimately separated. However, the increased levels of FtsA in these cells may also help to compete with the MinCc moiety of the MinCc-MinD fusion.

This led us to ask whether a stronger FtsA-FtsZ interaction might suppress the cell bending phenotype by overcoming the effects of MinCc-MinD. Overproducing FtsA was not an option, as increasing levels of FtsA inhibit cell division (Dai & Lutkenhaus, 1992). However, there is evidence from yeast two-hybrid assays that the gain-of-function allele of FtsA, FtsA* (R286W), interacts more strongly with FtsZ than does WT FtsA (Geissler et al., 2007; Pichoff et al., 2012). To test whether FtsA* might compete more effectively with MinCc-MinD and perhaps suppress the asymmetric constriction phenotype, I overproduced MinCc-MinD in Δ*min* cells in which *ftsA** replaced WT *ftsA* in the chromosome. Similar to the cells expressing *ftsQAZ* in multicopy, ~50% of septa in cells with FtsA* exhibited asymmetric constrictions upon the induction of MinCc-MinD with 1 mM IPTG, a significant decrease from the ~80% rate with WT FtsA (Table 3-1; Fig. 3-10). MinCc-MinD levels were similar in the two strains (data not shown). Moreover, these cells were completely viable at levels of MinCc-MinD (1 mM IPTG) that were toxic to $ftsA^+$ cells (see Fig. 3-2). Finally, induction of MinCc-MinD at lower levels of IPTG resulted in proportionately lower bending frequencies in the *ftsA** background than in the $ftsA^+$ background (Table 3-1; Fig. 3-10). These results are consistent with the idea that stronger FtsA-FtsZ binding suppresses asymmetric constrictions.

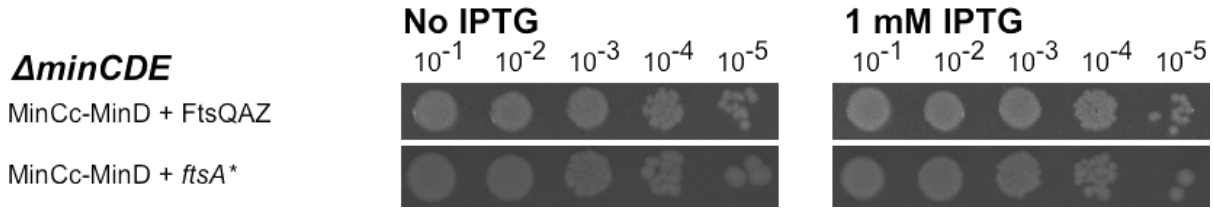

Figure 3-9. Colony viability assays. Colony viability of *E. coli* cells overproducing FtsQAZ or containing chromosomal *ftsA** in a strain with MinCc-MinD uninduced or induced.

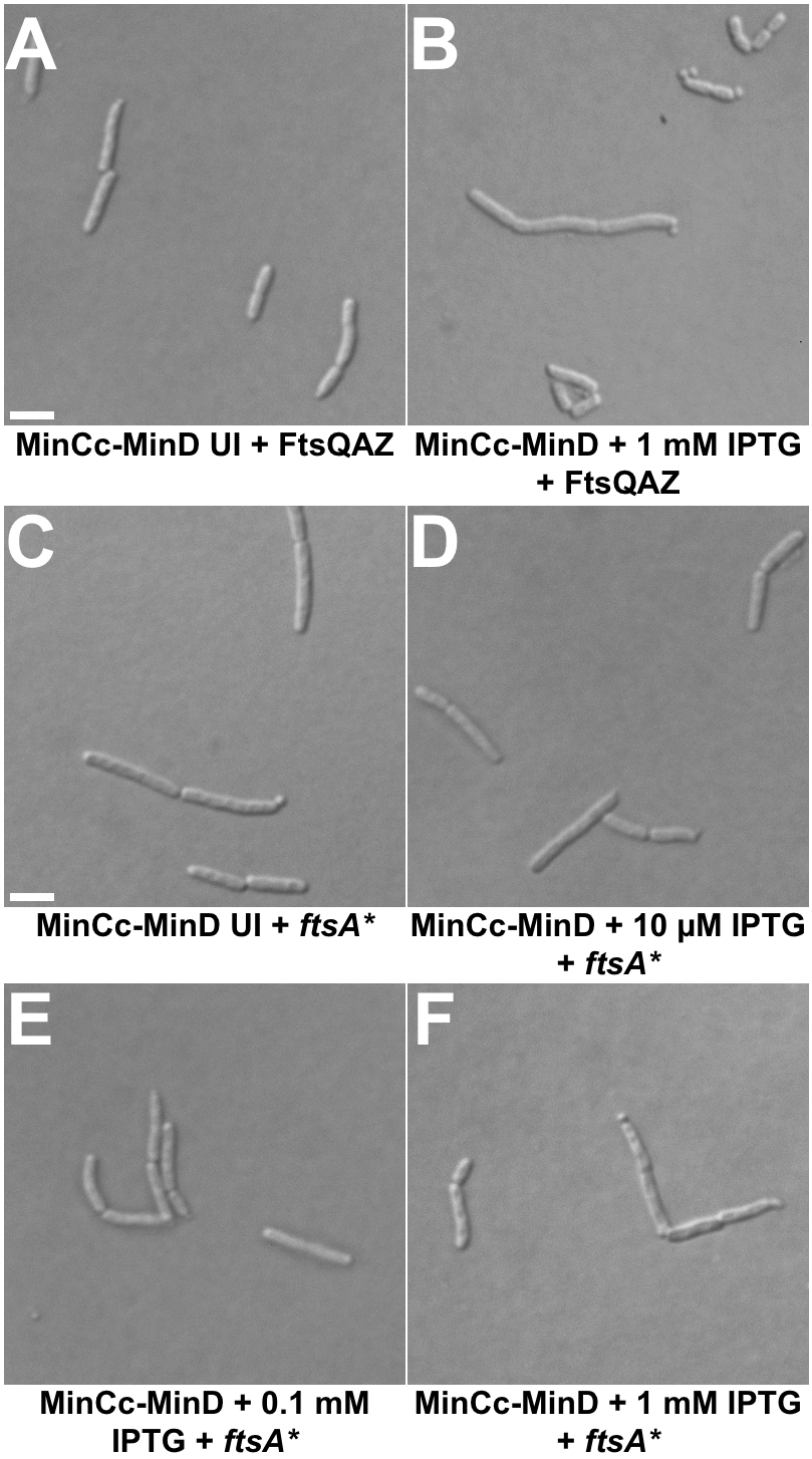

Figure 3-10. Morphologies of MinCc-MinD cells overproducing FtsQAZ or carrying chromosomal *ftsA*.* Representative morphologies of cells overproducing FtsQAZ (A-B) or carrying chromosomal *ftsA** (C-F), with MinCc-MinD from pWM2738 either uninduced (UI) or induced (I) with IPTG levels as indicated. DIC micrographs are shown; bar, 2 µm.

3.3 Discussion

When *E. coli* and other bacilli such as *Bacillus subtilis* divide, the daughter cells generally remain in line. On solid medium, the result is that two separated *E. coli* daughter cells are roughly parallel to each other, as are their progeny. In the case of *B. subtilis*, fairly straight cell chains are produced. The symmetry of these typical cell division events also indicates that the divisome normally acts symmetrically, with septal murein synthesized evenly around the cell circumference at midcell and amidases cleaving bonds symmetrically as well. However, some rod-shaped bacteria that divide by binary fission form a sharp bend at their septum, dividing more on one side than the other. Many actinobacteria, such as mycobacteria, divide by a snapping division mechanism (Thanky et al., 2007). Magnetotactic bacteria, such as *Magnetospirillum gryphiswaldense*, also divide this way and feature arc-like Z-ring structures at sides of division (Katzmann et al., 2011). Similar Z arcs have been observed in *E. coli* cells deficient in RodA or MreB, which grow and divide as spheres. These spherical cells also divide asymmetrically, with an invaginating septum mainly on one side of the cell corresponding to the Z arc (Addinall et al., 1996; Corbin et al., 2002; Bendezú & de Boer, 2008). The difference with cells overproducing MinCc-MinD is that we do not observe obvious asymmetric localization of the Z ring prior to or during the early stage of a bent septum. Later stages of bending division feature a V-shaped FtsZ staining pattern at the new cell poles developing on the other side of the septum, because the Min proteins are absent and cannot inhibit Z ring assembly at the new poles.

Why might MinCc-MinD, in particular, cause the bending division phenotype? When produced at high levels, the fusion protein becomes toxic, and cells producing it are unable to form colonies on plates. However, bending divisions are not lethal to the population, because lower levels of induction allow normal viability even though the majority of these cells still divide by bending (Fig. 3-2; Table 3-1). Also, Δ*min* cells producing MinCc-MinD fusions do not inhibit septum formation as readily as do cells producing MinC-MinD, probably because the MinCc portion has a more limited ability to disrupt FtsZ polymers than does the full-length protein containing MinCn. It is plausible that the MinD portion of the MinCc-MinD fusion is fully active, given that MinD can

oscillate from cell pole to cell pole even with a large GFP protein fused to its N terminus (Raskin & de Boer, 1999b). Moreover, MinCc-MinD can inhibit cell division effectively in Min^+ cells. This is likely because of the presence of native MinC protein, as MinCc-MinD inhibits growth at least as efficiently in cells lacking only MinD. We speculate that upon overproduction, MinCc-MinD fusions form polymers or an array. This could occur if the MinCc portion of one MinCc-MinD fusion protein interacts with the MinD portion of another fusion protein. Consistent with this idea, mutations that should prevent this interaction abolished bending cell divisions. Presumably, a subset of MinCc domains in the MinCc-MinD polymers/array remains capable of targeting the C-terminal tail of FtsZ.

As Z rings in normal cells and in cells overproducing MinCc-MinD appear similar, it is unlikely that the MinCc-MinD aggregate induces asymmetric constriction by forcing FtsZ to localize asymmetrically. Instead, we favor a model in which the Z ring assembles circumferentially, but a MinCc-MinD aggregate bound to a portion of the Z ring blocks the normal ability of those FtsZ C-terminal domains to recruit other divisome proteins. The strong tendency of FtsA in particular to avoid the region occupied by MinCc-MinD supports the idea that FtsA is specifically occluded from the Z ring by the MinCc-MinD aggregates, which would then prevent further maturation of the ring at the site of these aggregates. In support of this idea, MinCc has been reported to compete with FtsA for binding to the FtsZ C terminus (Shen & Lutkenhaus, 2009). MinCc-MinD may displace FtsA more readily than ZipA because the latter binds to FtsZ with higher affinity.

Electron microscopic analysis of bending cells demonstrates that most of the constriction activity occurs on the outside of the developing bend, suggesting that this is the main cause of the bending phenotype. My model predicts that MinCc-MinD should localize preferentially to the inside of a developing bend and FtsA to the outside, where additional divisome proteins such as FtsN, which has been shown to interact with FtsA directly (Busiek et al., 2012), are preferentially recruited to induce constriction (Fig. 3-8F). In support of the model, I found that a significant majority of MinCc-MinD aggregates localize to the inside of a developing septal bend, and FtsA localizes primarily toward the outside. Replacing FtsA with FtsA* partially suppressed bending, consistent with the idea

that FtsA* can compete somewhat with MinCc-MinD for binding to FtsZ and hence reduce the frequency of MinCc-MinD-induced asymmetric constrictions. Given the strong effects of the Z-ring-targeted aggregates formed by MinCc-MinD, we speculate that other proteins that target the Z ring may, if they are not fully functional, also perturb symmetrical activity of the Z ring, causing a similar bending division phenotype. Related future questions to address include how the Z ring and complete divisome maintain a mostly symmetrical circumferential shape in species such as *E. coli* and if there are advantages in dividing symmetrically.

Chapter IV

3D-SIM super-resolution of FtsZ and its membrane tethers in *Escherichia coli* cells

This chapter is based upon, "Rowlett, V.W., and Margolin, W. (2014) 3D-SIM super-resolution of FtsZ and its membrane tethers in Escherichia coli cells. Biophysical Journal 107: L17-L20" with permission from Elsevier (Copyright © 2014 Biophysical Society. Published by Elsevier Inc. doi:10.1016/j.bpj.2014.08.024).

4.1 Introduction

The assembly of the bacterial tubulin FtsZ has been well studied *in vitro*, but the fine structure of the cytokinetic Z ring it forms *in vivo* is not well defined. Super-resolution microscopy methods including photoactivated localization microscopy (PALM) and three-dimensional-structured illumination microscopy (3D-SIM), among others, have recently provided a more detailed view of Z-ring structures (Fig. 4-1; Rowlett & Margolin, 2015b). The first super-resolution views of Z rings were immunofluorescence of *Bacillus subtilis* FtsZ viewed by stimulated emission depletion (STED) (Jennings et al., 2011). Two-dimensional PALM studies showed that Z rings in *Escherichia coli* are likely composed of loosely-bundled dynamic protofilaments (Fu et al., 2010; Buss et al., 2013). Three-dimensional PALM studies of *Caulobacter crescentus* initially showed that Z rings were comprised of loosely bundled protofilaments forming a continuous but dynamic ring (Fu et al., 2010; Buss et al., 2013; Biteen et al., 2012), and recent cryo-electron tomography (cryo-ET) studies suggest that FtsZ forms continuous long polymers. However, a recent high-throughput study showed that the Z rings of this bacterium are patchy or discontinuous (Holden et al., 2014), similar to Z rings of *B. subtilis* and *Staphylococcus aureus* viewed using 3D-SIM (Strauss et al., 2012). Strauss et al. also demonstrated that the patches in *B. subtilis* Z rings are highly dynamic (Strauss et al., 2012). Therefore, a consensus has not yet been reached on the structure of the Z ring, and more studies are needed to explain these conflicting results.

Assembly of the Z ring is modulated by several proteins that interact directly with FtsZ and enhance assembly or disassembly (Romberg & Levin, 2003). For example, FtsA and ZipA promote ring assembly in *E. coli* by tethering it to the cytoplasmic membrane (Pichoff & Lutkenhaus, 2002,

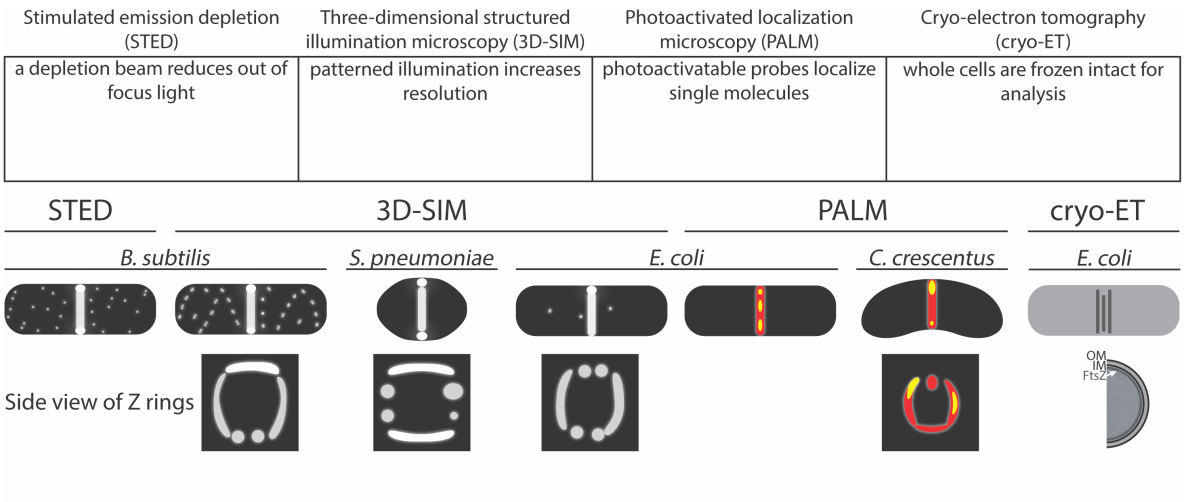

Figure 4-1. Examples of Z ring localization using different methods of super-resolution microscopy. The main principle of each method is listed in the table. The side views of Z rings represent a rotated image of the cell above them. For the PALM images, yellow areas represent areas of higher signal intensity. Cartoons from left to right were drawn based on Z-ring localization reported in (Jennings et al., 2011; Strauss et al., 2012; Tsui et al., 2014; Rowlett & Margolin, 2014b; Fu et al., 2010; Holden et al., 2014; Szwedziak et al., 2014). ***This figure has been reprinted from, "Rowlett, V.W., and Margolin, W. (2015b) The bacterial divisome: ready for its close-up. 370(1679): 20150028" with permission by The Royal Society.***

2005). SulA is an inhibitor of FtsZ assembly, induced only after DNA damage, which sequesters monomers of FtsZ to prevent its assembly into a Z ring (Chen et al., 2012). Our initial goals were to visualize Z rings in *E. coli* using 3D-SIM, and then examine whether any FtsZ polymeric structures remain after SulA induction. FtsA and ZipA were also observed to determine if they localized in patchy patterns similar to those of FtsZ.

4.2 Results

4.2.1 3D-SIM localization of proto-ring proteins.

3D-SIM was used to view the high-resolution localization patterns of FtsZ in *E. coli* cells producing FtsZ-GFP (Fig. 4-2). To rule out GFP artifacts, I also visualized native FtsZ from a wild-type strain (WM1074) by immunofluorescence (IF). Both FtsZ-GFP (Fig. 4-2 A, B, and B1) and IF staining for FtsZ (Fig. 4-2 C, D, and D1) consistently localized to patches around the ring circumference, similar to the *B. subtilis* and *C. crescentus* FtsZ patterns (Holden et al., 2014; Strauss et al., 2012). Analysis of fluorescence intensities (Fig. 4-3 A and B) revealed that the majority of Z rings contain one or more gaps in which intensity decreases to background levels (82% for FtsZ-GFP and 69% for IF). Most rings had 3-5 areas of lower intensity, but only a small percentage of these areas had fluorescence below background intensity (34% for FtsZ-GFP and 21% for IF), indicating that the majority of areas with lower intensity contain at least some amount of FtsZ.

To elucidate how FtsZ transitions from a disassembled ring to a new ring, I imaged a few dividing daughter cells before they were able to form new Z rings (Fig. 4-2E). Previous conventional microscopy had revealed dynamic FtsZ helical structures (Thanedar & Margolin, 2004), but the resolution had been insufficient to see further details. Here, FtsZ visualized in dividing cells by 3D-SIM localized throughout as a mixture of patches and randomly-oriented short filaments (asterisk and dashed oval in Fig. 4-2, respectively). These structures may represent oligomeric precursors of Z ring assembly.

To visualize FtsZ after Z-ring disassembly another way, SulA, a protein that blocks FtsZ assembly, was overproduced. *E. coli* cells producing FtsZ-GFP were observed after induction of *sulA* expression from a pBAD33-*sulA* plasmid (pWM1736) with 0.2% arabinose. After 30 min of *sulA* induction, Z rings remained intact in most cells (Fig. 4-4A and data not shown). The proportion of cellular FtsZ-GFP in the ring with and without induction of *sulA* was consistent with previous data (data not shown) (Fu et al., 2010; Anderson et al., 2004). Notably, after 45 min of *sulA* induction, Z

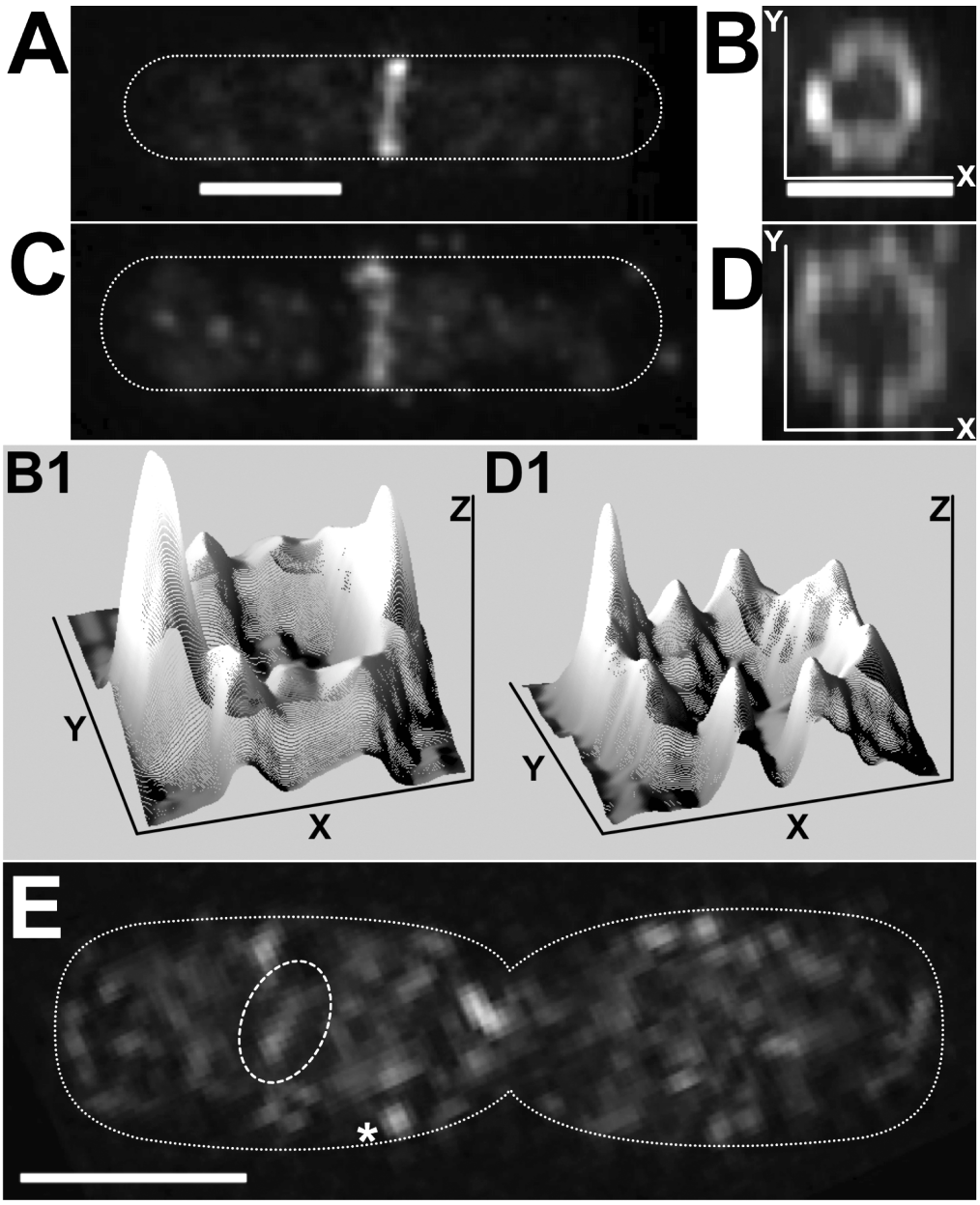

Figure 4-2. 3D-SIM localization of FtsZ in *E. coli*. (A) Cell with a Z ring labeled with FtsZ-GFP. (B) Rotated view of Z ring in panel A. (C) Cell with a Z ring labeled with DyLight 550 (Thermo Fisher Scientific, Waltham, MA). (D) Rotated view of Z ring in panel C. (B1 and D1) Three-dimensional surface intensity plots of Z rings in panels B and D, respectively. (E) A dividing cell producing FtsZ-GFP. The cell outline is shown in the schematic. (Asterisk) Focus of FtsZ localization; (open dashed ovals) filamentous structures of FtsZ. Three-dimensional surface intensity plots were created using ImageJ (Schneider et al., 2012). Scale bars, 1 μm.

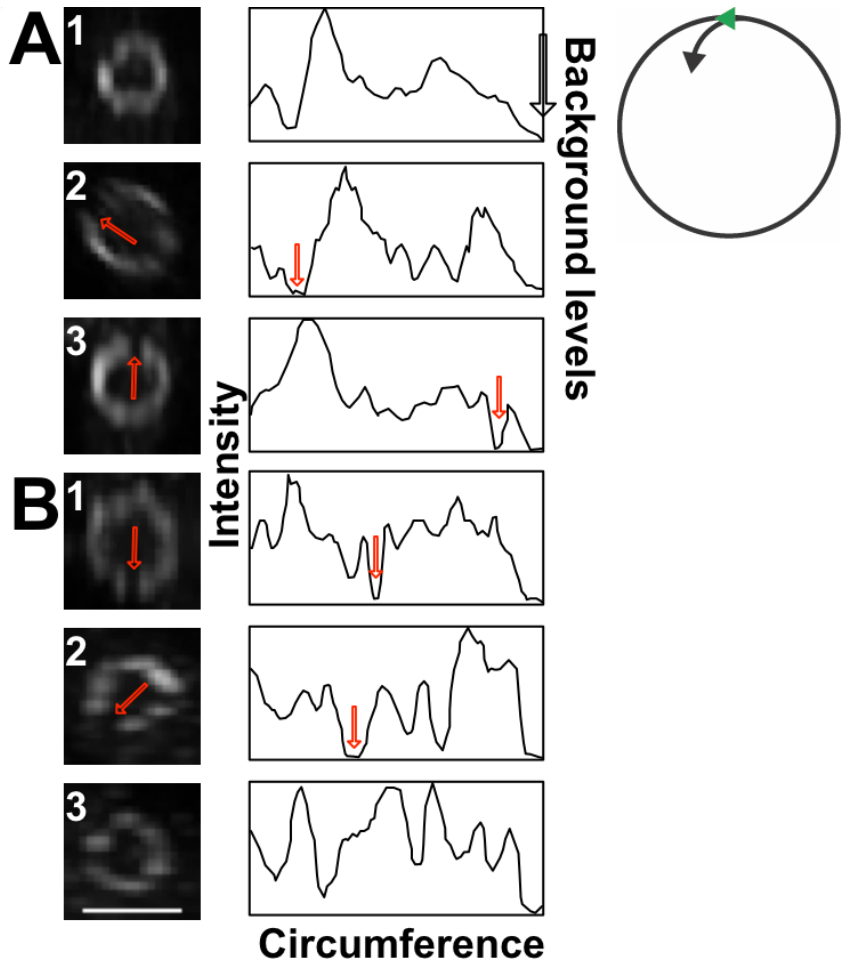

Figure 4-3. Quantitation of fluorescence intensities around the circumference of Z rings. (A) Three representative examples of FtsZ-GFP ring cross-sections and their fluorescence intensities. The plots on the right represent fluoresce intensities along a line originating at the top of the ring drawn counterclockwise around the entire circumference of the Z ring (see far right example-line originates from green arrow and ends at black arrow), with a final extension of the line into the lumen of the ring to define the background fluorescence intensity, shown at the far right of the intensity plots (denoted by large open arrow). Red arrows indicate areas of fluorescence intensity that are at or below background levels; areas of the ring corresponding to these areas are shown with arrows in the images on the left. (B) Three representative examples of the intensity of Z rings detected by immunofluorescence. Plots and arrows are as described above. Intensity measurements were generated using ImageJ (Schneider et al., 2012) and traced in Pixelmator. Scale bar, 1 μm.

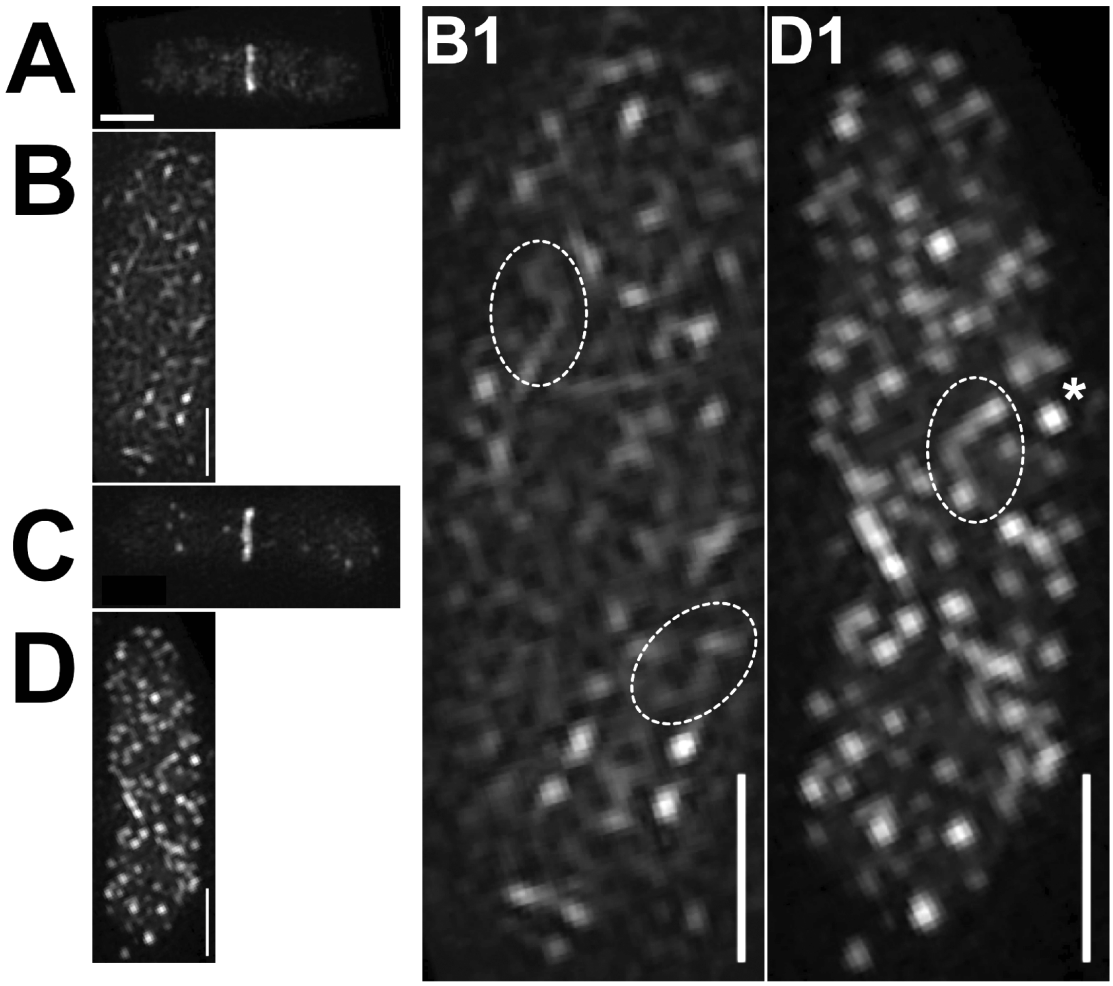

Figure 4-4. 3D-SIM localization of FtsZ after overproduction of SulA. (A) Cell producing FtsZ-GFP after 0.2% arabinose induction of SulA for 30 min. (B) After 45 min. (B1) Magnified cell shown in panel B. (C) Cell producing native FtsZ labeled with AlexaFluor 488 (Life Technologies, Carlsbad, CA) 30 min after induction; (D) 45 min after induction. (D1) Magnified cell shown in panel D. Scale bar, 1 μm. (Asterisk) Focus of FtsZ localization; (open dashed ovals) filamentous structures of FtsZ.

rings were gone (Fig. 4-4 B and B1), replaced by numerous patches and randomly-oriented short filaments (asterisk and dashed ovals in Fig. 4-4), similar to those observed in a dividing cell. FtsZ normally rapidly recycles from free monomers to ring-bound polymers (Anderson et al., 2004), but SulA binds to FtsZ monomers and sequesters them, reducing the pool of FtsZ monomers available for assembly into FtsZ protofilaments. This prevention of continued FtsZ protofilament assembly results in the breakdown of the Z ring once SulA concentration is sufficiently high (Chen et al., 2012). The observed FtsZ-GFP patches and filaments are likely FtsZ polymers that disassemble before they can organize into a ring.

This result was confirmed by detecting FtsZ localization by IF after overproducing SulA in wild-type cells (Fig. 4-4 C, D, and D1). The overall fluorescence patterns in cells producing FtsZ-GFP versus cells producing only native FtsZ were similar (Fig. 4-4 B1 and D1), although we observed fewer filaments with IF, perhaps because FtsZ-GFP confers slight resistance to SulA, or because the increased amount of FtsZ in the FtsZ-GFP producing cells might titrate the SulA more effectively.

Additionally, we wanted to observe the localization patterns of the membrane tethers FtsA and ZipA. Since both proteins bind to the same C-terminal conserved tail of FtsZ (Ma & Margolin, 1999; Szwedziak et al., 2012; Mosyak et al., 2000), they would be expected to colocalize with the circumferential FtsZ patches in the Z ring. I visualized FtsA using protein fusions to mCherry and GFP (data not shown) as well as IF using a wild-type strain (WM1074) (Fig. 4-5A). The patchy ring pattern of FtsA localization was similar to the FtsZ pattern. ZipA also displayed a similar patchy localization in WM1074 by IF (Fig. 4-5B).

To determine whether FtsA and ZipA colocalized to these patches, I used a strain producing FtsA-GFP (WM4679) for IF staining of ZipA using a red secondary antibody. FtsA-GFP (Fig. 4-5C) and ZipA (Fig. 4-5D) had similar patterns of fluorescence, although the three-dimensional intensity profiles (Fig. 4-5 C1 and D1) reveal slight differences in intensity that are also visible in a merged image (Fig. 4-5E). Quantitation of fluorescence intensities around the circumference of the rings

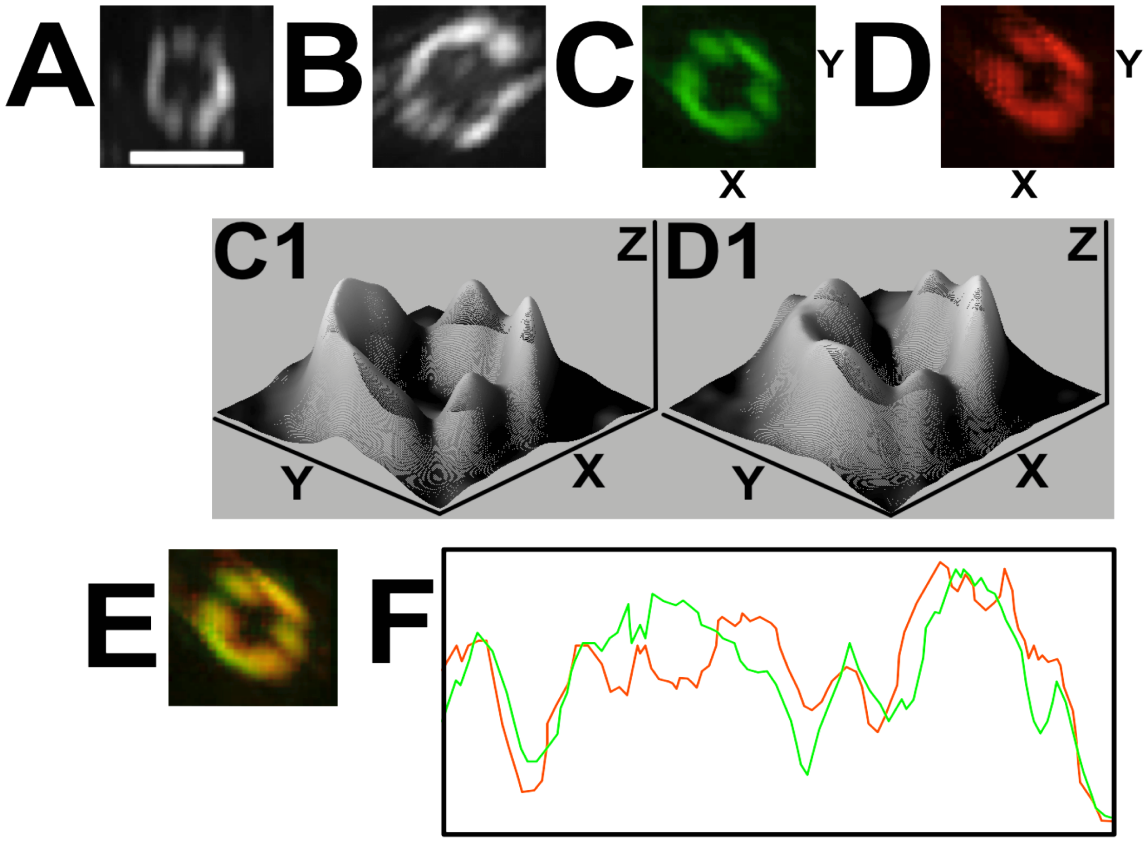

Figure 4-5. 3D-SIM localization of FtsA and ZipA. Localization of FtsA (A) and ZipA (B) by IF using AlexaFluor 488. (C) FtsA-GFP ring. (D) Same cell shown in panel C with ZipA labeled with DyLight 550. (C1 and D1) Three-dimensional surface intensity plots of FtsA ring from panel C or ZipA ring from panel D, respectively. (E) Merged image of FtsA (green) and ZipA (red) from the ring shown in panels C and D. (F) Intensity plot of FtsA (green) and ZipA (red) of ring shown in panel E. The plot represents intensity across a line drawn counterclockwise from the top of the ring around the circumference, then into its lumen. Red/green intensity plot and three-dimensional surface intensity plots were created using ImageJ (Schneider et al., 2012). Scale bar, 1 µm.

revealed that FtsA and ZipA colocalized almost completely in approximately half of the rings analyzed (Fig. 4-5F, and Fig. 4-6A), whereas in the other rings there were significant differences in localization in one or more areas (Fig. 4-6B). FtsA and ZipA bind to the same C-terminal peptide of FtsZ and may compete for binding. Cooperative self-assembly of FtsA or ZipA might result in large-scale differential localization visible by 3D-SIM.

4.2.2 3D-SIM localization and transmission electron microscopy of a gain-of-function allele of *ftsZ*.

A gain-of-function allele of *ftsZ*, $ftsZ_{L169R}$, allows *E. coli* cells to be viable in the absence of the normally essential ZipA protein (Haeusser et al., 2015). Upon initial examination by conventional IF of cells expressing $ftsZ_{L169R}$ replacing *ftsZ* at its native locus, a number of normal Z rings were observed, but there was a noticeable increase in polarly localized Z rings, and apparent doublets or spirals (Haeusser et al., 2015). 3D-SIM was used to visualize localization patterns of $FtsZ_{L169R}$ with greater resolution (Fig. 4-7A). With this level of resolution we were able to see similar normal Z rings and aberrant structures, but found that what looked like doublets of Z rings by conventional IF, were instead single connected spirals (Fig. 4-7A). The spirals and polar assemblies of $FtsZ_{L169R}$ suggested that this mutation in FtsZ results in greater self-assembly.

ZipA bundles purified FtsZ *in vitro*, implying a role for FtsZ assembly *in vivo* (RayChaudhuri, 1999; Hale et al., 2000; Loose & Mitchison, 2014). To investigate self-assembly of $FtsZ_{L169R}$ *in vitro*, purified FtsZ and $FtsZ_{L169R}$ proteins incubated with GDP, GTP, or GTP and calcium chloride were viewed by transmission electron microscopy (Fig. 4-7B). Neither $FtsZ_{WT}$ or $FtsZ_{L169R}$ form filaments when GDP is added, but although GTP addition results in single protofilaments of $FtsZ_{WT}$, filaments of double width (~10 nm) were observed with $FtsZ_{L169R}$ (Fig. 4-7B). The addition of calcium chloride induced bundles of filaments for both $FtsZ_{WT}$ and $FtsZ_{L169R}$ (Fig. 4-7B). These data along with data that $FtsZ_{L169R}$ sediments without the addition of calcium

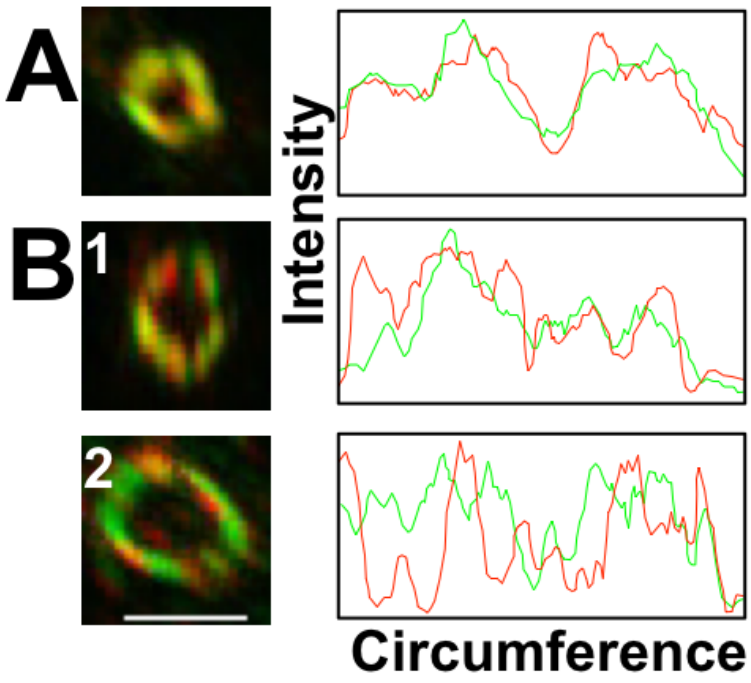

Figure 4-6. Quantitation of FtsA and ZipA colocalization. WM4769 cells producing FtsA-GFP were fixed and stained to detect ZipA localization using a red secondary antibody. (A) An example of FtsA and ZipA colocalization (another is shown in Fig. 4-5 E-F), measured by plotting RGB intensities along a line originating at the top of the ring drawn counterclockwise around the entire circumference of the ring, with a final extension of the line into the lumen of the ring to define background intensity (far right of plot). See Fig. 4-2 for more details. The green line represents FtsA localization and the red line represents ZipA localization. (B) Two representative examples of colocalization patterns that have one (B1) or more (B2) significant differences in localization. RGB plots are as described above. RGB plots were generated using ImageJ (Schneider et al., 2012) and traced in Pixelmator. Scale bar, 1 μm.

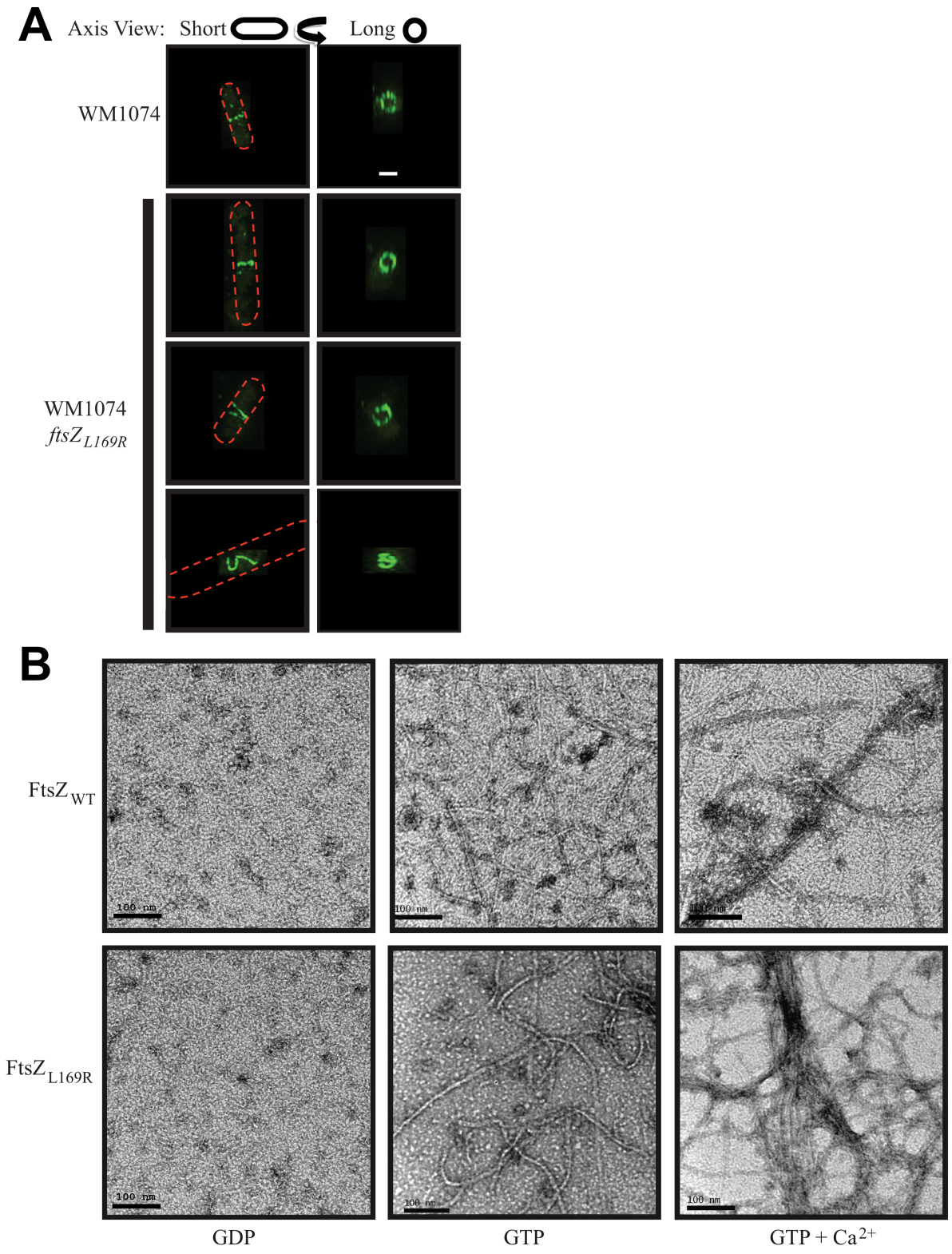

Figure 4-7. 3D-SIM localization and transmission electron micrographs of FtsZ and $FtsZ_{L169R}$.

(A) Representative IF 3D-SIM images of $FtsZ_{WT}$ and $FtsZ_{L169R}$ viewed along the short axis of the

cells and 90˚ rotated views along the long axis. General cell outlines are represented by red dashes. Scale bar, 1 μm. (B) Electron micrographs of negatively stained $FtsZ_{WT}$ or $FtsZ_{L169R}$ after incubation with 1 mM GDP, GTP, or GTP and 10 mM calcium chloride. Scale bars, 100 nm. **Note: DPH642 (chromosomal *$ftsZ_{L169R}$*) was constructed by Daniel P. Haeusser and FtsZ and $FtsZ_{L169R}$ proteins were purified by Daniel P. Haeusser.** ***This figure was adapted from panels of Figures 1 and 6 in, "Haeusser, D.P., Rowlett, V.W., and Margolin, W. (2015) A mutation in Escherichia coli ftsZ bypasses the requirement for the essential division gene zipA and confers resistance to FtsZ assembly inhibitors by stabilizing protofilament bundling. Mol Microbiol 97: 988-1005," and is reprinted with permission from John Wiley and Sons (© 2015 John Wiley & Sons Ltd doi: 10.1111/mmi.13081).***

chloride, whereas $FtsZ_{WT}$ does not, and has reduced GTPase activity, strongly support the idea that this mutation results in increased lateral interaction of FtsZ protofilaments (Haeusser et al., 2015).

4.3 Discussion

In conclusion, our 3D-SIM analysis shows that the patchy localization of FtsZ is conserved in *E. coli* and suggests that it may be widespread among bacteria. After disassembly of the Z ring either in dividing cells or by excess levels of the cell division inhibitor SulA, FtsZ persisted as patches and short filamentous structures. This is consistent with a highly dynamic population of FtsZ monomers and oligomers outside the ring, originally observed as mobile helices in *E. coli* by conventional fluorescence microscopy (Thanedar & Margolin, 2004) and by photoactivation single-molecule tracking (Niu & Yu, 2008). FtsA and ZipA, which bind to the same segment of FtsZ and tether it to the cytoplasmic membrane, usually display a similar localization pattern to FtsZ and each other, although in addition to the differences we detect by 3D-SIM, there are also likely differences that are beyond its ~100-nm resolution limit in the *X*,*Y* plane.

As proposed previously (Lan et al., 2009), gaps between FtsZ patches may be needed to accommodate a switch from a sparse Z ring to a more condensed ring, which would provide force to drive ring constriction (Osawa & Erickson, 2011). If this model is correct, the gaps should close upon ring constriction, although this may be beyond the resolution of 3D-SIM in constricted rings. Another role for patches could be to force molecular crowding of low-abundance septum synthesis proteins such as FtsI, which depend on FtsZ/FtsA/ZipA for their recruitment, into a few mobile supercomplexes.

How are FtsZ polymers organized within the Z-ring patches? Recent polarized fluorescence data suggest that FtsZ polymers are oriented both axially and circumferentially within the Z ring *in E. coli* (Si et al., 2013). The seemingly random orientation of the non-ring FtsZ polymeric structures we observe here supports the idea that there is no strong constraint requiring FtsZ oligomers to follow a circumferential path around the cell cylinder. The patches of FtsZ in the unperturbed *E. coli* Z ring likely represent randomly oriented clusters of FtsZ filaments that are associated with ZipA, FtsA, and essential septum synthesis proteins.

The advantage of the three-dimensional information that 3D-SIM provides is evidenced by the ability to distinguish between distinct assemblies of proteins that are not readily apparent with conventional microscopy. One example is the ability to distinguish spirals from double rings observed with $FtsZ_{L169R}$ (Haeusser et al., 2015). Additionally, 3D-SIM has been able to resolve rings of peptidoglycan synthesis proteins Pbp1a and Pbp2x, which localize outside of the Z ring in *Streptococcus pneumoniae* (Tsui et al., 2014). During later stages of cell division, Pbp2x, which is involved in production of septal peptidoglycan, has distinct localization from other proteins involved in side-wall synthesis, including Pbp1a (Land et al., 2013). New super-resolution microscopy methods should continue to shed light on the *in vivo* organization of these protein assemblies.

Chapter V

In vitro biochemical analysis of FtsA

5.1 Introduction

During the early stages of *E. coli* cell division FtsZ recruits FtsA to midcell (Addinall & Lutkenhaus, 1996). FtsA is a structural homolog of eukaryotic actin, although it contains a unique 1C subdomain that replaces subdomain 1B (Bork et al., 1992; van den Ent & Löwe, 2000). FtsA contains a C-terminal MTS, which allows it to bind to the inner membrane and serve as a tether for the Z ring (Pichoff & Lutkenhaus, 2005), and deletion of residues from the C-terminus of FtsA results in loss of function (Yim et al., 2000). In addition to tethering the Z ring to the membrane, FtsA has also been shown to recruit downstream proteins to midcell through its 1C subdomain (Rico et al., 2004; Corbin et al., 2004), and is suggested to have a role in disassembly of the Z ring at later stages of cell division (Beuria et al., 2009; Osawa & Erickson, 2013). How FtsA switches from functioning in assembly of the Z ring to disassembly is unclear.

The ability for FtsA to bind ATP seems to be important for its function, as mutations that map to the ATP-binding site render the protein temperature-sensitive, or non-functional (Sanchez et al., 1994; Herricks et al., 2014). These mutations allow cells to grow and divide at 30˚C, but cells are unable to divide when shifted to 42˚C. As expected, intragenic suppressors of these mutations map to the ATP binding site, and presumably alter the mutant binding pocket to restore favorable ATP binding and/or hydrolysis. Interestingly, however, some suppressors map to the predicted FtsA dimer interface, suggesting that more monomeric FtsA may be able to overcome ATP binding defects (Herricks et al., 2014). $FtsA_{G50E}$ is one such intragenic suppressor of $FtsA_{S195P}$, a temperature sensitive allele (*ftsA27*) that is defective in ATP hydrolysis and perhaps binding (Herricks et al., 2014). $FtsA_{R286W}$ (FtsA*), which can also suppress $FtsA_{S195P}$, also restores partial function to $FtsA_{W408E}$, a membrane binding defective allele of FtsA (Shiomi & Margolin, 2008). Both $FtsA_{G50E}$ and FtsA* can support division in the absence of normally essential ZipA, and are thought to be more monomeric than wild-type FtsA (Herricks et al., 2014; Geissler et al., 2003; Pichoff et al., 2012). The locations of these residues are mapped onto the dimer crystal structure of FtsA from *Thermotoga maritima* in Figure 5-1.

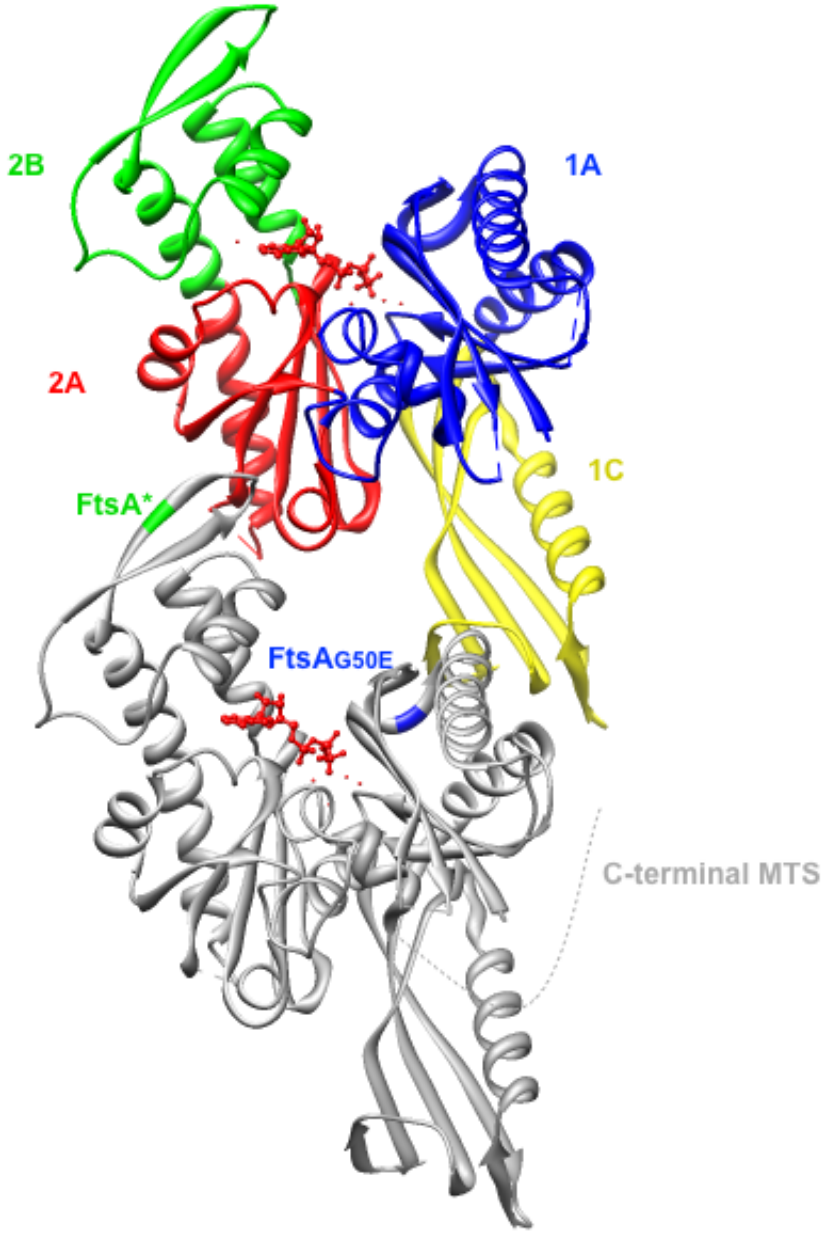

Figure 5-1. Dimer crystal structure of *Thermotoga maritima* FtsA. Top: Monomer with labeled subdomains. Subdomain 2B (green) is involved in FtsA-FtsZ interaction, subdomain 1C (yellow) is involved in downstream protein recruitment, and all subdomains contribute to self-interaction. Bottom: Gray monomer with *E. coli* FtsA mutations highlighted: FtsA* (green) and $FtsA_{G50E}$ (blue). The C-terminal MTS is not shown in the structure and is drawn by the gray dashed line. ATP is shown in red. Structure: Szwedziak et al., 2012; colored using UCSF Chimera (Pettersen et al., 2004).

FtsA from *Streptococcus pneumoniae* has been shown to form polymers dependent on ATP addition *in vitro* (Lara et al., 2005). In contrast, FtsA from *T. maritima* can form filaments on a lipid monolayer without the addition of ATP (Szwedziak et al., 2012), possibly because ATP is already bound to the purified protein; it should be noted that the crystal structure of *T. maritima* FtsA was purified with bound ATP (Szwedziak et al., 2012). The presence of ATP or ADP is important for the ability of purified *E. coli* FtsA* to shorten *E. coli* FtsZ polymers (Beuria et al., 2009). FtsZ-YFP and FtsA* from *E. coli* incorporated into liposomes and incubated with GTP and ATP allows assembly of Z rings that can generate a constrictive force (Osawa & Erickson, 2013). Furthermore, on lipid bilayers, FtsA was found to cause dynamic rearrangements of ring structures of FtsZ in the presence of ATP/ADP and GTP (Loose & Mitchison, 2014). These data suggest the importance of ATP/ADP binding for FtsA function, although no ATPase activity was detected in the 2014 study. Therefore, although ATPase activity was detected in another study and correlated with the FtsA activity in cell division (Herricks et al., 2014), the role of ATP hydrolysis in FtsA function remains unclear.

To address the role of ATP in FtsA activities *in vitro* and to correlate these activities with *in vivo* activities, I investigated the assembly of purified FtsA and FtsA mutant proteins using transmission electron microscopy (TEM), and assessed their ability to bind liposomes using sedimentation analysis. I also confirmed that purified FtsA is ATP bound using a luminescent assay to detect ATP in protein preparations of FtsA and FtsA mutant proteins.

5.2 Results

5.2.1 FtsA forms short filaments and rings.

To analyze structures made by FtsA protein *in vitro*, FtsA, FtsA*, $FtsA_{G50E}$, and FtsA with a deletion of the last 15 C-terminal residues (FtsAΔC15) were purified from *E. coli* cells overproducing His_6-tagged proteins from T7 promoter constructs (Fig. 5-2). Protein concentrations were measured and proteins were diluted to 1 μM in FtsA buffer and incubated at 37˚C for 30 minutes prior to negative staining and viewing by TEM. Wild-type FtsA formed rings of various diameters (~10 – 75 nm) as well as short filaments (Fig. 5-3), suggesting a wide range of filament curvatures. Most short filaments and the curved filaments comprising the rings were ~5-10 nm in diameter, consistent with protofilaments 1-2 subunits thick. FtsA mutants predicted to have less self-interaction, FtsA* and $FtsA_{G50E}$, formed similar rings and filaments as wild-type FtsA, as did FtsAΔC15, suggesting that the MTS is not involved in self-interaction. Surprisingly, the addition of ATP had no effect on the structures observed, indicating that the addition of ATP did not result in increased polymerization, decreased polymerization, or gross structural alteration of the proteins.

5.2.2 Purified FtsA and some FtsA mutants are ATP bound.

The observation that added ATP had no effect on FtsA polymers does not rule out a role for ATP in polymer assembly, as purified FtsA may be ATP bound as suggested by Szwedziak et al., 2012. To test for the presence of ATP in the different purified proteins, I used an assay with a luminescence readout (Fig. 5-4). Proteins and the ATP standard curve were boiled for 5 minutes to denature the protein and release bound ATP before equilibrating and measuring luminescence at room temperature. This assay cannot be used as an exact quantitation of the amount of ATP present, since there is no way to determine whether the protein is fully denatured using this assay, but it does indicate that ATP is bound to purified wild-type FtsA and some FtsA mutant proteins. There was no ATP detected in a protein preparation of $FtsA_{K19M}$, which was used as a negative control because it is

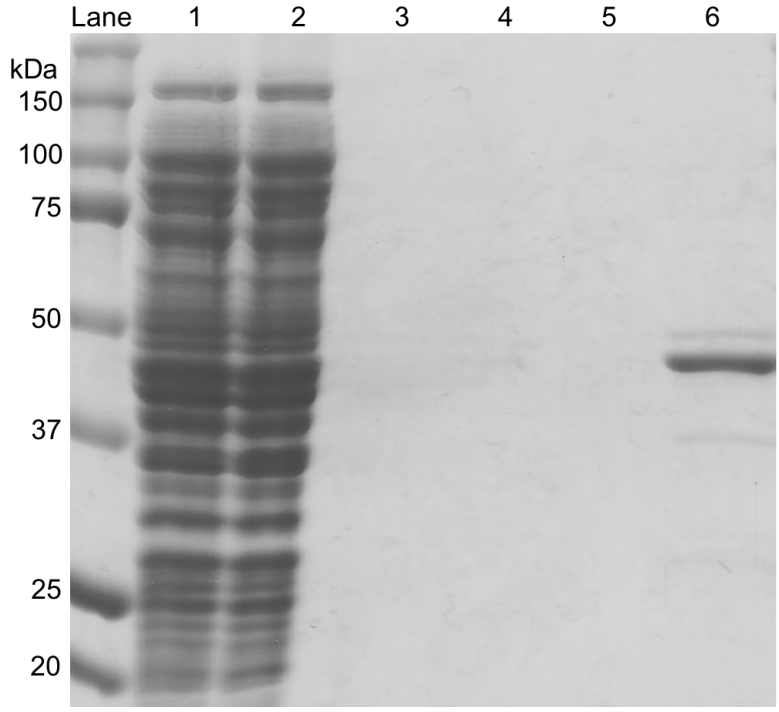

Figure 5-2. Purification of His_6-FtsA from *E. coli* cells. Coomassie stained SDS-PAGE gel of samples from purification of FtsA. Lane 1 is cell lysate, Lane 2 is the flow through of the column after incubation of lysate with Talon resin, Lanes 3-5 are samples taken after 5 mM, 20 mM, and 30 mM washes, respectively. Lane 6 is purified His_6-FtsA. Proteins of similar purity were used in the assays described below. His_6-FtsA is predicted to be 46 kDa.

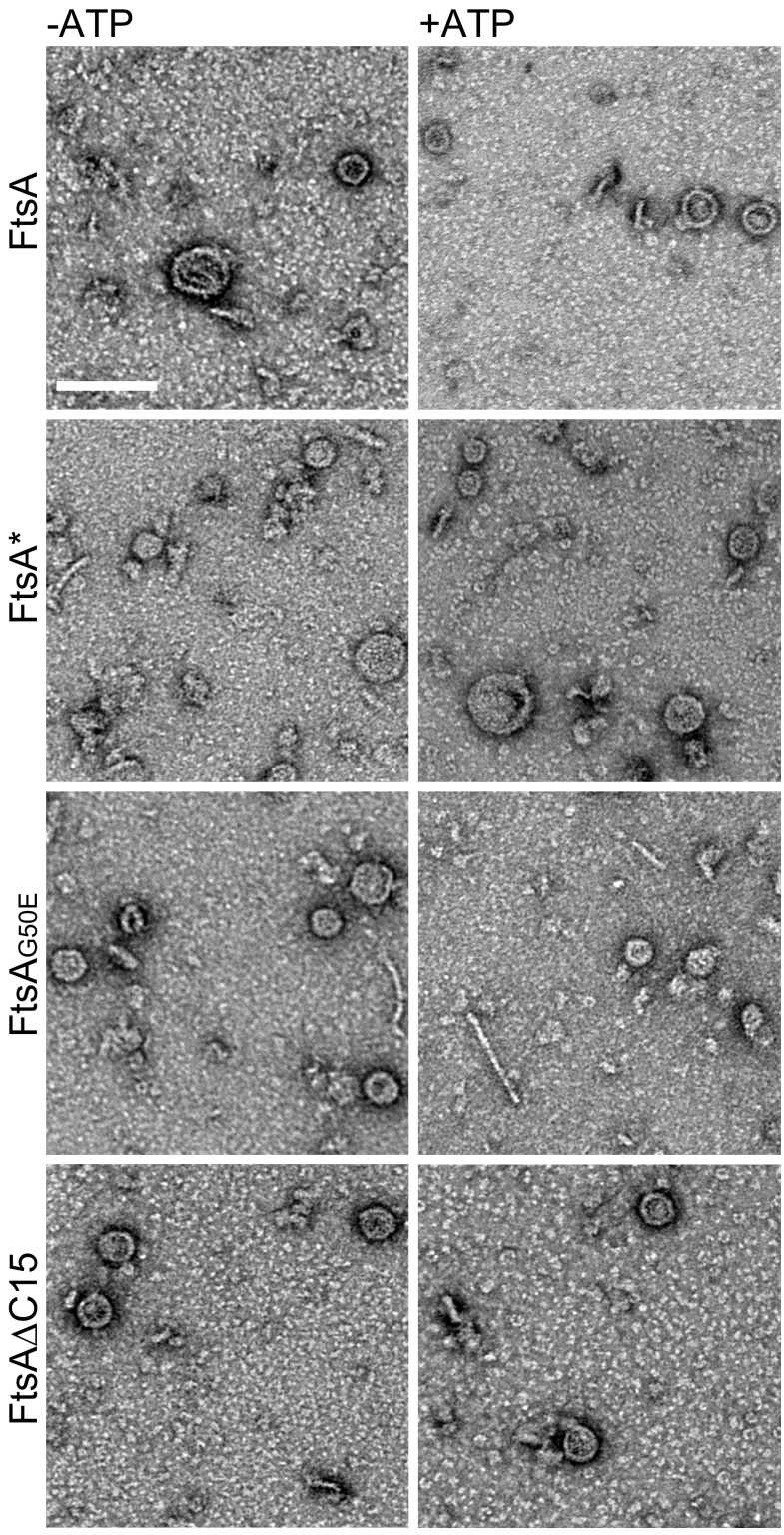

Figure 5-3. Transmission electron micrographs of FtsA and FtsA mutant proteins stained with uranyl acetate. Left panels: micrographs of proteins without ATP added; right panels: micrographs of proteins incubated with 2 mM ATP prior to grid preparation. Scale bar, 100 nm.

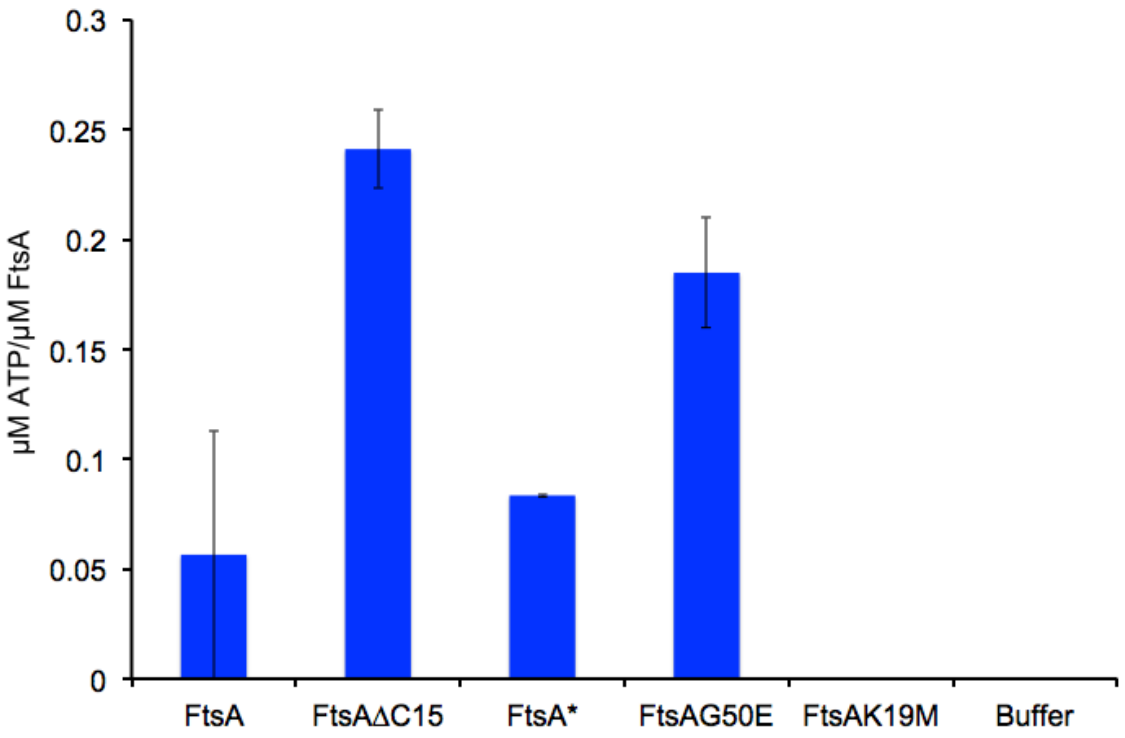

Figure 5-4. FtsA purifies with ATP bound to the nucleotide-binding site. ATP detected in purified FtsA proteins graphed as µM ATP per µM FtsA. Error bars show standard deviation. Three independent triplicate experiments are shown for FtsA, other proteins were measured in triplicate assays.

severely defective for cell division and ATP binding/hydrolysis (Herricks, dissertation). These data confirm that some FtsA proteins purify with ATP bound to the nucleotide-binding site, and suggest that using this purification scheme, we are purifying FtsA that is likely already polymerized.

5.2.3 FtsA binds liposomes.

To test the ability of FtsA and FtsA mutant proteins to bind liposomes, I used a sedimentation assay to isolate liposome bound proteins. When incubated without the addition of liposomes, some FtsA pelleted with or without ATP added, and this likely represents polymers and/or aggregates of FtsA (Fig. 5-5, blue bars). When liposomes were added with or without ATP added, there was a dramatic increase of the amount of protein pelleted for FtsA (blue bars), FtsA* (gray bars), and $FtsA_{G50E}$ (black bars), indicating that they are binding to and sedimenting with liposomes (Fig. 5-5). FtsAΔC15 was tested as a negative control, since it lacks an MTS and should not be able to bind liposomes (Shiomi & Margolin, 2008) although it can form polymers (see previous section). As expected, the amount of FtsAΔC15 (light blue bars) that pellets is unaffected by the addition of liposomes (Fig. 5-5). Since a significant proportion of FtsA seems to purify with ATP bound, we cannot conclude from the ATP-independence of liposome binding whether or not ATP binding is important for membrane association.

5.2.4 Reversibility of membrane binding may be important for FtsA function.

FtsA's C-terminal MTS can interact strongly with the cytoplasmic surface of the membrane, but because it is not a transmembrane helix, it can also be dislodged from the membrane; MinD is an excellent example of this reversibility. To determine if reversible binding of FtsA is important for function in cell division, we fused FtsA to a single-pass transmembrane protein, FtsN. FtsA and FtsN have been shown to interact directly (Busiek et al., 2012), and the fusion of FtsA to FtsN should tether FtsA to the membrane irreversibly. The FtsA-FtsN fusion was stably expressed and able to support growth at 42˚C of a strain with a temperature sensitive allele of *ftsA*, *ftsA12* (Table 5-1; data

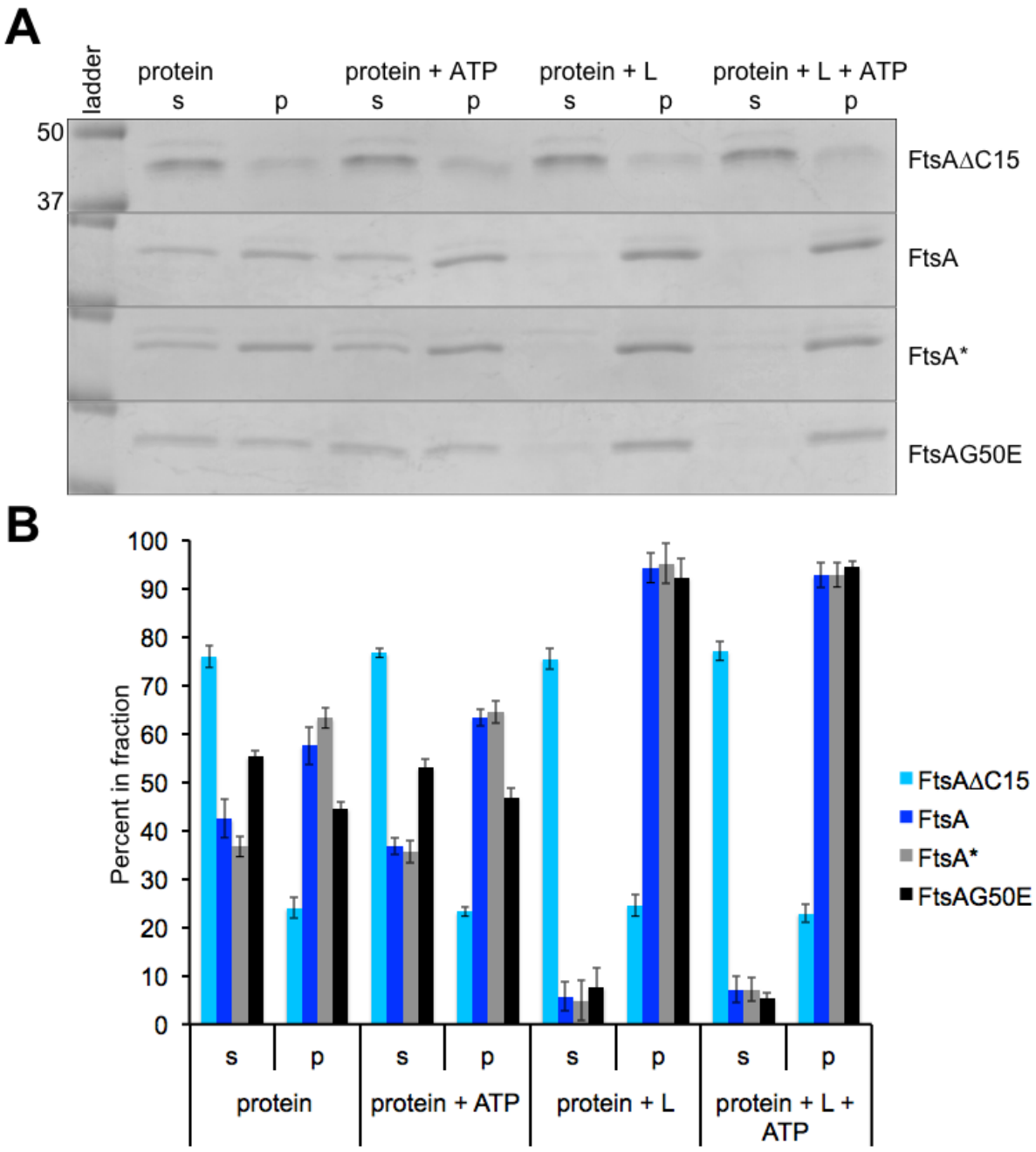

Figure 5-5. Sedimentation analysis of liposome bound FtsA proteins. (A) Representative Coomassie stained SDS-PAGE gels of supernatant (s) and pellet (p) fractions of protein incubated alone (protein), protein incubated with ATP (protein + ATP), protein incubated with liposomes (protein + L), and protein incubated with liposomes and ATP (protein + L + ATP). (B) Quantitation of percent of FtsA protein in the supernatant (s) and pellet (p) fractions from the Coomassie stained

gels. FtsAΔC15 (light blue), FtsA (blue), FtsA* (gray), and $FtsA_{G50E}$ (black) are shown. Error bars represent standard deviation of three independent experiments. ImageJ was used to quantitate band density (Schneider et al., 2012).

Table 5-1. Growth of FtsA mutants in an *ftsA12* background[a] and with *ftsA-null* transduction[b].

WM1115 *ftsA12*	**30˚C**	**42˚C 0 mM IPTG**	**42˚C 0.1 mM IPTG**	***ftsA-null* TD**
empty vector	+	-	-	no
FtsA*	+	+	+	yes
$FtsA_{W408E}$	+	-	-	n.d.
$FtsA^*_{W408E}$	+	-	+	no
$FtsA^*_{K19M}$	+	+	+	yes
$FtsA_{K19M}$	+	+	-	no
FtsA-FtsN	+	+	+	no
FtsAΔC15-FtsN	+	-	+	no
FtsA	+	+	+	yes
FtsN	+	-	-	n.d.

[a] Growth is indicated by (+) no growth is indicated by (-)

[b] no/yes indicates the inability/ability to transduce *ftsA-null* into these strains, respectively. n.d. is not determined.

Note: This is a summary of data from William Margolin, Jennifer Herricks, Daisuke Shiomi, Kim Busiek, Kara Schoenemann, and Veronica Rowlett. The *ftsA12* results from FtsA*, $FtsA_{W408E}$, and $FtsA^*_{W408E}$ are published (Shiomi & Margolin, 2008). The *ftsA12* results from $FtsA_{K19M}$ are published (Herricks, dissertation).

not shown). Although this result suggested that reversible membrane binding is not essential, we wanted to rule out the possibility that any residual activity from FtsA12 might help the fusion protein to function even at the non-permissive temperature. To do this, we attempted to replace the wild-type chromosomal copy of *ftsA* with an *ftsA* null allele (a frameshift mutation at the *Bgl*II site near the 5' end of *ftsA*). This was done by P1 transduction of this *ftsA* null allele, which is ~50% linked to a nearby tetracycline-resistance (Tet^R) marker in *leuO*. After selection for Tet^R transductants, ~50% of cells carrying control *ftsA* constructs that can support division as the sole copy of *ftsA* in the cell lost the *Bgl*II site and were confirmed to have the chromosomal frameshift by sequencing the chromosomal copy of *ftsA*. However, 100% of Tet^R transductants harboring *ftsA-ftsN* or *ftsA*Δ*C15-ftsN* fusions retained the *Bgl*II site, indicating that the frameshift mutation could not be introduced into these strains.

These results suggest that FtsA12 still retains some activity even at the non-permissive temperature that allows function of the fusion (Table 5-1). As FtsA12 has an intact MTS, it may still be able to bind the membrane at the non-permissive temperature, although its putative residual activity is unclear. Nevertheless, contrary to our initial conclusions from the complementation of the *ftsA12* mutant, the inability of the fusions to function on their own in cell division suggests that a permanently membrane-tethered FtsA cannot support division.

5.2.5 FtsA* suppresses defects of $FtsA_{K19M}$ and $FtsA_{W408E}$ *in vivo*.

FtsA* is able to suppress the defects of $FtsA_{W408E}$, which contains a mutation in the MTS changing a critical hydrophobic residue to a charged residue. This weakens the amphipathic nature of the helix, resulting in reduced membrane binding and failure to function in cell division (Shiomi & Margolin, 2008). When comparing growth in the *ftsA12* strain at 42˚C, $FtsA_{W08E}$ fails to complement FtsA12, FtsA* is able to complement without induction, and the $FtsA^*_{W408E}$ double mutant requires induction with 0.1 mM IPTG (Shiomi & Margolin, 2008; Table 5-1). Therefore, as R286W (FtsA*

mutation) is distal from the MTS on the FtsA molecule, the results suggest that FtsA* is able to restore membrane binding by a defective MTS through an allosteric mechanism.

$FtsA_{K19M}$, containing a mutation near the ATP binding pocket, exhibits reduced ATP binding and hydrolysis (Herricks, dissertation). $FtsA_{K19M}$ is able to complement *ftsA12*, however, growth of these cells is poor compared to complementation with wild-type FtsA (Herricks, dissertation). Moreover, using the same procedure described in the previous section, we were unable to transduce the *ftsA-null* allele into a strain with $FtsA_{K19M}$ expressed from a plasmid (Table 5-1), suggesting that $FtsA_{K19M}$ cannot support growth as the only copy of *ftsA* in cells. Surprisingly, combining FtsA* with $FtsA_{K19M}$ in *cis* suppresses this defect (Table 5-1). How FtsA* overcomes the defects of $FtsA_{W408E}$ and $FtsA_{K19M}$ is unclear, but the mechanism may be complex as this single point mutation is suggested to have several distinct properties from wild-type FtsA including stronger binding to FtsZ, increased ATP binding and hydrolysis, decreased toxicity when overexpressed, and decreased self-interaction (Shen & Lutkenhaus, 2009; Rowlett & Margolin, 2014a; Herricks et al., 2014; Geissler et al., 2007; Pichoff et al., 2012).

5.2.6 ATP addition has no effect on FtsA polymerization measured by optical density.

The formation of rings and short filaments of FtsA visible in TEM prompted us to test whether we could detect protein assembly by light scattering and whether added ATP had any effect. To do this, FtsA protein was equilibrated to room temperature in a 96 well plate and optical density at 320 nm was measured for protein with and without ATP added every 30 seconds for 90 minutes. Turbidity increased gradually over time, but there was no significant difference between protein with or without ATP added (Fig. 5-6). Also, turbidity increased much more slowly with FtsA than with FtsZ, which polymerizes upon addition of GTP followed by depolymerization due to its intrinsic GTPase activity (Król & Scheffers, 2013; Garcia et al., submitted). It remains unclear if the slow increase in turbidity reflects ordered polymerization or protein aggregation. Additionally, in this assay

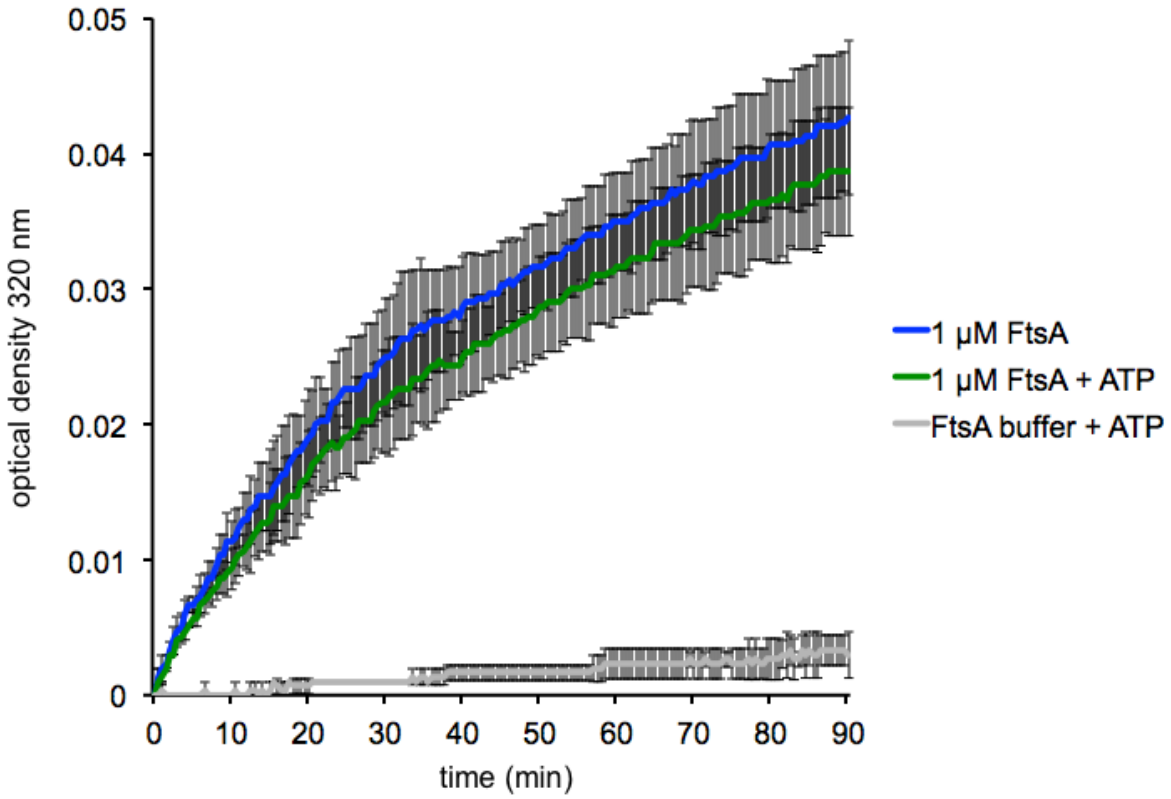

Figure 5-6. Turbidity assay of FtsA. FtsA was equilibrated to room temperature and diluted to 1 µM in a 96 well plate. Optical density at 320 nm was read in a BioTek plate reader every 30 sec for 90 min. FtsA without (blue) and with 2 mM ATP added (green); FtsA buffer with ATP (gray) is read as a negative control. Error bars represent the standard deviations of three independent experiments.

a low concentration of FtsA was used, and higher FtsA concentrations may be needed to observe relevant protein dynamics.

5.3 Discussion

FtsA is involved throughout the process of cell division. FtsZ recruits FtsA to midcell early in the cell division cycle, and it serves as a membrane tether for the Z ring with ZipA (Addinall & Lutkenhaus, 1996; Pichoff & Lutkenhaus, 2005). Following formation of the proto-ring, a number of downstream proteins are recruited to midcell to form a complete divisome (Margolin, 2005). Although FtsA has been shown to interact with only FtsN directly (Busiek et al., 2012), FtsA has been suggested to interact with FtsQ and FtsI based on bacterial two-hybrid assays (Karimova et al., 2005), and the interaction between FtsA and FtsI is also supported by DivIVA polar recruitment assays (Corbin et al., 2004). When divisome formation is complete, FtsA is predicted to have a role in disassembly of the Z ring based on the ability of purified FtsA* to shorten polymers of FtsZ (Beuria et al., 2009), and to constrict Z rings around liposomes *in vitro* (Osawa & Erickson, 2013). How does FtsA switch from a divisome assembly mode to disassembly mode? It is likely that the oligomeric state of FtsA influences its function, and this may be regulated by ATP binding and hydrolysis.

Wild-type FtsA and FtsA mutant proteins all form similar structures as judged *in vitro* by electron microscopy. I was unable to distinguish differences in assembly of FtsA mutants. However, these conditions may not be optimal for FtsA organization, and it is possible that differences in oligomerization would be seen on lipid monolayers. The ring-like assemblies of FtsA protein are reminiscent of protein rings formed by SepF, a protein found in many Gram-positive species. In *Bacillus subtilis*, SepF contains a membrane-binding MTS and interacts with FtsZ, and can thus serve as a membrane tether for the Z ring (Hamoen et al., 2006; Król et al., 2012; Gündoğdu et al., 2011; Duman et al., 2013). SepF also interacts with FtsZ and is essential for cell division in *Mycobacteria* spp. (Gupta et al., 2015). Notably, inactivation of FtsA in *B. subtilis* causes a severe division defect, but overproduction of SepF corrects this defect (Beall & Lutkenhaus, 1992; Ishikawa et al., 2006), indicating that FtsA and SepF have overlapping functions. As SepF forms oligomeric rings *in vitro* and can align and bundle FtsZ protofilaments, it suggests that FtsA may have a similar role, at least in Gram-positives.

The MTS of FtsA may also contribute to an artificial self-interaction in our *in vitro* conditions, as purified FtsA and FtsA mutant proteins containing an MTS sediment more readily than FtsAΔC15. Nevertheless, FtsAΔC15 is able to polymerize into rings and short filaments as readily as wild-type FtsA. FtsA* is suggested to be more monomeric than wild-type FtsA by *in vivo* assays (Pichoff & Lutkenhaus, 2005; Pichoff et al., 2012), however this does not appear to be the case *in vitro*, as FtsA* forms structures similar to wild-type FtsA and a similar amount pellets in sedimentation assays. $FtsA_{G50E}$ is also predicted to be more monomeric (Herricks et al., 2014), and our assays have not ruled this out, as less $FtsA_{G50E}$ pellets when sedimented without liposomes (Fig. 5-5 black bars). However, this difference in pelleting is not reflected by the TEM experiments, where $FtsA_{G50E}$ qualitatively assembled into the same type of polymers as wild-type FtsA.

Even if FtsA, FtsA*, and $FtsA_{G50E}$ have differences in oligomerization too subtle to detect by TEM, they all seem to bind liposomes, and the addition of ATP has no effect on liposome binding. It is possible that there is enough ATP bound to the purified protein to allow liposome binding, as is the case for *T. maritima* FtsA and its ability to bind a lipid monolayer without added ATP (Szwedziak et al., 2012). FtsA from *S. pneumoniae* has been shown to bind giant unilamellar vesicles in an ATP-dependent manner (Krupka et al., 2014); however, it is also possible that ADP may be sufficient for membrane binding. In support of this idea, *E. coli* FtsA purified from inclusion bodies and equilibrated in buffer contining ADP does not require the addition of ADP or ATP to bind giant unilamellar vesicles or lipid coated microbeads (Jimènez et al., 2011; Martos et al., 2012). Loose and Mitchison also added ADP to their preparation of purified FtsA, and the addition ADP or ATP was required for FtsA to dynamically organize FtsZ on supported lipid bilayers (Loose & Mitchison, 2014). We do not add ADP in our dialysis buffer, and we have not yet analyzed the amounts of ADP in purified proteins or the effect of added ADP in our assays

The inability to transduce an *ftsA-null* allele into a strain producing a fusion of FtsA-FtsN suggests that the ability of the MTS to bind the membrane reversibly is important for function. This is different from the conclusion reached by Shiomi and Margolin, where a fusion of FtsAΔC15 to MalF

allowed partial complementation of the conditional *ftsA12* allele at 42˚C (Shiomi & Margolin, 2008), as well as my data showing that FtsAΔC15-FtsN can complement *ftsA12* (Table 5-1). However, like FtsA-FtsN, these fusions were also unable to be transduced by an *ftsA-null* allele. Therefore, I conclude that reversible binding of FtsA to the membrane may be important for its function, perhaps because FtsA subunits need to turn over rapidly to function properly in cell division. In support of this idea, FRAP experiments suggest that GFP-FtsA turns over as rapidly as FtsZ-GFP, with a recovery half time between 11-16 seconds (Geissler et al., 2007). As FtsN seems to interact with itself *in vivo* (Karimova et al., 2005; Alexeeva et al., 2010), it is also possible that the FtsA-FtsN transmembrane fusion alters the oligomeric state of FtsA in a way that artificially hinders its function. However, the fact that it is stably produced as a fusion protein and able to complement *ftsA12* suggests that it does retain some key FtsA functions.

In Figure 5-2 there is a faint protein band slightly above that of FtsA. Our lab and others have identified this contaminant by mass spectrometry (data not shown) as Rho protein, an ATP-dependent helicase involved in termination of transcription (Holmes et al., 1983; Robichon et al., 2011). Although this appears to be a significant contaminant, it does not seem to be a factor in our assays. For example, even though all of our purified wild-type and mutant proteins contain a similar amount of Rho, there is no detectable ATP in purified $FtsA_{K19M}$, which is defective for ATP binding *in vitro* (Fig. 5-4; Herricks, dissertation), indicating that any ATP bound to Rho in our preparation is likely not present in detectable amounts.

In conclusion, FtsA may require other cellular factors for full function that are absent in these reductionist assays. For example, the ATPase activity of purified FtsA is quite low, approximately 1 ATP hydrolyzed per FtsA molecule per minute (Herricks et al., 2014). It is plausible that FtsA ATPase activity may be stimulated by another protein, and this activity may regulate the oligomeric state of FtsA *in vivo*. More analysis is required to better understand how FtsA functions.

Chapter VI

Discussion and Future Directions

Cell division in *E. coli* is regulated by many proteins that govern where and when the divisome can form. The Min system and nucleoid occlusion aid in centering the Z ring at midcell, where it is further stabilized by FtsA and ZipA to form the proto-ring (Margolin, 2005; Vicente & Rico, 2006). ZipA or FtsA can support formation of Z rings, and both are required for recruitment of downstream proteins (Pichoff & Lutkenhaus, 2002). ZipA is easily bypassed by a single point mutation in FtsA, and FtsA is more conserved than ZipA, suggesting that it has a more important role in cell division (Margolin, 2000; Geissler et al., 2003). A model for the activities of ZipA and FtsA during cell division is shown in Figure 6-1. During initiation of cell division ZipA and FtsA tether the Z ring to the inner membrane, and ZipA likely bundles FtsZ protofilaments (Pichoff & Lutkenhaus, 2002; RayChaudhuri, 1999; Hale et al., 2000; Kuchibhatla et al., 2011; Loose & Mitchison, 2014; Haeusser et al., 2015). Following proto-ring formation several downstream proteins are recruited to form a complete divisome, and we hypothesize that this switches FtsA from promoting Z ring formation to disassembly of the Z ring (Corbin et al., 2004; Beuria et al., 2009; Busiek et al., 2012). Only the interaction between FtsA and the late cell division protein FtsN has been shown directly (Busiek et al., 2012), but others are hypothesized. Interactions between ZipA and downstream divisome proteins have not been observed. Finally, ZipA, FtsA, and other downstream proteins remain localized until daughter cells separate, while FtsZ moves to new sites of cell division in daughter cells (Söderström et al., 2014). FtsA forms polymers *in vitro*, but the role and dynamics of FtsA polymers during cell division remain unknown.

6.1 An FtsA ring is essential for symmetrical septum constriction.

A fusion of the C-terminus of MinC (MinCc) to MinD localized as a focus to a portion of the Z ring when overproduced in an otherwise Min$^-$ strain (Chapter III) (Rowlett & Margolin 2014a). This focus had no visible effect on Z rings, but displaced FtsA localization likely by physically blocking FtsA from accessing its binding site on FtsZ near the MinCc-MinD focus. Interactions between the MinCc and MinD moieties of the fusions likely caused aggregation of MinCc-MinD

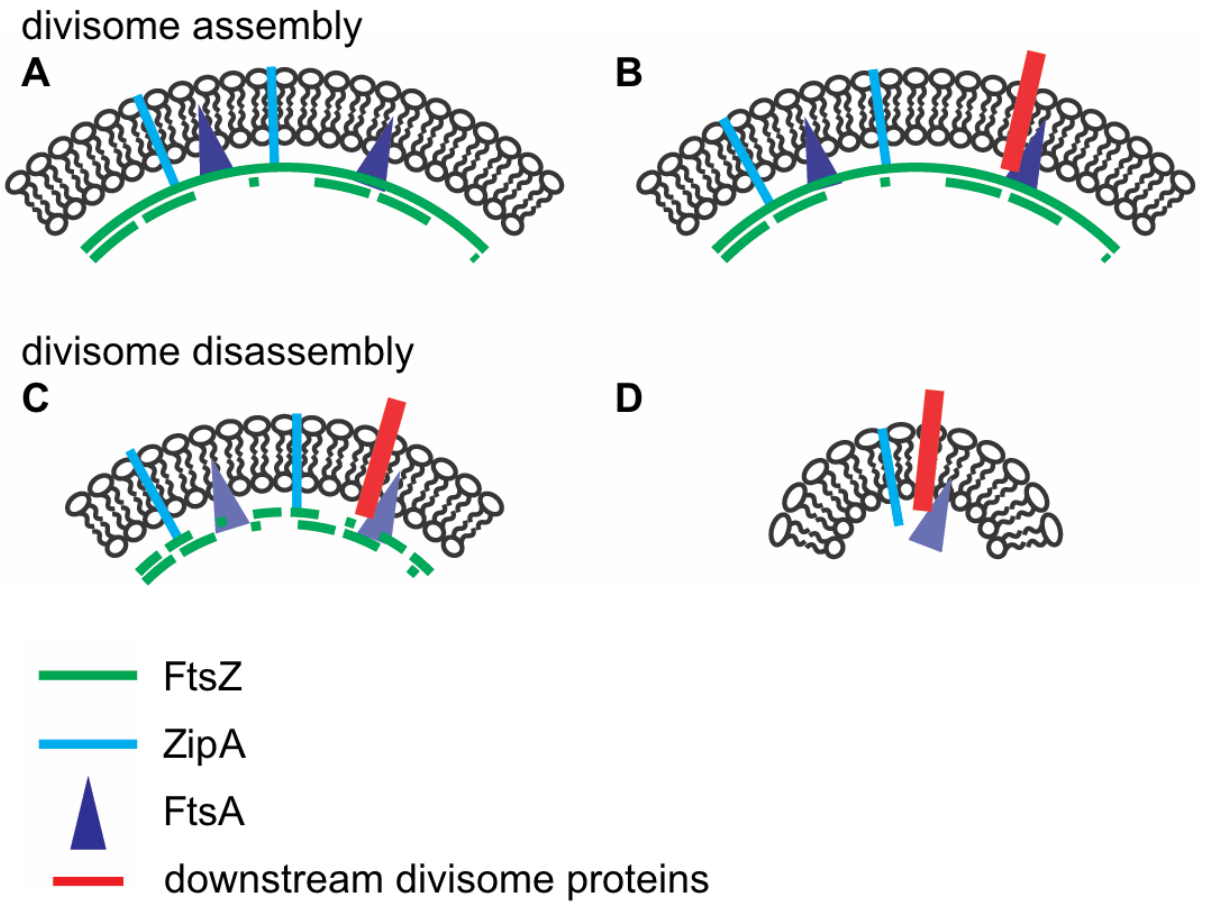

Figure 6-1. Model of ZipA and FtsA activity during cell division. (A) FtsA and ZipA serve as membrane tethers for the Z ring (Pichoff & Lutkenhaus, 2002), and ZipA has been proposed to bundle FtsZ protofilaments (RayChaudhuri, 1999; Hale et al., 2000; Kuchibhatla et al., 2011; Loose & Mitchison, 2014; Haeusser et al., 2015). (B) Downstream divisome proteins are recruited to form a complete divisome. (C) Interaction with a late component of the divisome may cause FtsA to switch from an assembly mode to a disassembly mode to shorten FtsZ protofilaments during constriction (Beuria et al., 2009). (D) FtsZ eventually leaves, while ZipA and FtsA remain at midcell until compartmentalization of daughter cell cytoplasms (Söderström et al., 2014).

fusions to create this block. The result was that FtsA did not form a normal ring congruent with the Z ring, but instead only an arc on the side of the Z ring opposite from the MinCc-MinD block. The division septum only formed on the side of the cell where FtsA localized, ultimately causing cells to divide by jack-knifing. The other membrane tether ZipA was likely unaffected because of its higher affinity binding to FtsZ (Shen & Lutkehnhaus, 2009; Kuchibhatla et al., 2011). These results support the idea that FtsA is required for local recruitment of downstream divisome proteins and/or for direct contributions to the process of divisome constriction.

This type of asymmetric cell division illustrates one example of the robustness of *E. coli* cell division. Even when cells are only able to complete the divisome on a restricted area of the septum, they are still able to continue growth and division. The start of constriction on one side that is able to eventually complete division is similar to septal formation in round shaped *E. coli* cells (Iwaya et al., 1978), but under our conditions Z rings were not affected. Mutants that cause cell rounding have arc-like FtsZ localization, and constriction can begin before a complete Z ring is formed (Addinall & Lutkenhaus, 1996). As further support for the robustness of cell division, several mutants of FtsZ form spirals that lead to twisted septa, yet many cells can successfully divide through these spirals (Addinall & Lutkenhaus, 1996; Stricker & Erickson, 2003; Haeusser et al., 2015). *E. coli* cells can even be squeezed into ~0.25 μm channels where they form irregular shapes and still divide with accuracy comparable to normal cells (Männik et al., 2012)!

6.2 FtsZ, FtsA, and ZipA localize into punctate rings.

3D-SIM localization of FtsZ revealed that FtsZ in Z rings localized in a patchy bead-like pattern instead of a continuous ring (Chapter IV) (Rowlett & Margolin, 2014b). These data were consistent with super-resolution imaging of FtsZ in other bacteria and suggest that the patchy localization of Z rings is widespread among bacteria. FtsA and ZipA largely co-localized, although there were some differences in localization likely because they compete for binding to the C-terminal domain of FtsZ. What is the reason for discontinuous localization of FtsZ? Condensation of gaps

between FtsZ patches may provide force during ring constriction (Lan et al., 2009; Osawa & Erickson, 2011). Alternatively, patches of FtsZ localization could be important to localize low-abundance divisome proteins into a few mobile supercomplexes around the ring. 3D-SIM was useful to distinguish the structure of $FtsZ_{L169R}$, which self-interacts more readily than wild-type FtsZ (Haeusser et al., 2015). When viewed by conventional immunofluorescence microscopy, $FtsZ_{L169R}$ localized in a variety of patterns that included both normal and polar Z rings and aberrant rings that appeared to be doublets (Haeusser et al., 2015). With increased resolution, we found that what looked like doublets by conventional fluorescence microscopy were connected spirals (Haeusser et al., 2015).

The first super-resolution images of FtsZ were immunofluorescence localization of FtsZ in *Bacillus subtilis* visualized by stimulated emission depletion (STED) microscopy (Jennings et al., 2011). Our conclusions that FtsZ has a patchy localization around the circumference of the ring are in agreement with other 3D-SIM studies of FtsZ localization in *B. subtilis* and *Staphylococcus aureus* (Strauss et al., 2012). Our use of both FtsZ-GFP and immunofluorescence of the native protein was important to rule out any artifacts of the GFP tag (Margolin, 2012). Higher resolution than 3D-SIM and STED imaging has been achieved through the use of photoswitchable fluorescent probes combined with photoactivated localization microscopy (PALM) or stochastic optical reconstruction microscopy (STORM) imaging. Jie Xiao's laboratory has used PALM to view FtsZ localization in *E. coli* cells and these studies also support the patchy localization of Z rings (Fu et al., 2010; Buss et al., 2013, 2015).

6.3 Debate over the ultrastructure and force generation of the Z ring.

Cryo-electron tomography (cryo-ET) has recently been used to visualize structures that are likely FtsZ (Li et al., 2007; Szwedziak et al., 2014) One of the major advantages to cryo-ET is that samples are plunge frozen and do not require staining, preserving their structure (Rowlett and Margolin, 2015b). As large cells are unsuitable for cryo-ET analysis due to their density, the first images of FtsZ came from *Caulobacter crescentus*, which forms a thin constriction between dividing

daughter cells (Li et al., 2007). Z rings in these cells consist of short (~100 nm) filaments of FtsZ arranged around the ring, instead of long continuous filaments. These data support the patchy model of FtsZ localized within Z rings. However, more recent cryo-ET evidence suggests that FtsZ forms long polymers that overlap to form continuous Z rings (Szwedziak et al., 2014). These data are from *C. crescentus* cells, and an *E. coli* strain with cells that are thinner than other wild-type strains (Woldringh, 1976). These two groups used the same strain of *C. crescentus*, grown in similar conditions, and it remains unclear why there are conflicting results on the continuity of Z rings (Li et al., 2007; Szwedziak et al., 2014). It is logical that a thinner *E. coli* strain might result in FtsZ forming more continuous protofilaments, but this does not appear to be the case, as this same *E. coli* strain recently imaged with single-molecule localization microscopy (SMLM) has patchy Z rings (Vendyaykin et al., 2016). It is alternatively possible that fixation of cells viewed by super-resolution results in artifacts of patchy localization, however, this is unlikely as *B. subtilis* cells have been viewed live by 3D-SIM and localization remained patchy (Strauss et al., 2012). While the density of antibody labeling may affect the accurate quantitation of how many Z rings have gaps, it is unlikely that the observed gaps are due to inefficient labeling, as patchy Z rings are observed in *B. subtilis* cells producing FtsZ-GFP as the only copy of FtsZ in the cell (Strauss et al., 2012). Further studies are needed to resolve these conflicting models of Z ring organization.

Another difference between *C. crescentus* Z rings and those in *E. coli* cells is the alignment of FtsZ polymers within the ring. While short polymers of FtsZ are aligned circumferentially in *C. crescentus* cells, short polymers of FtsZ in *E. coli* cells are positioned at various angles with some aligning parallel to the long axis of the cell (Fu et al., 2010; Holden et al., 2014; Si et al., 2013). These differences in FtsZ polymer arrangement may reflect different modes of cytokinesis: *C. crescentus* cells divide solely by membrane constriction and may need their Z rings to exert more force than in *E. coli*, which divides by coordinated constriction and septum ingrowth (Judd et al., 2005). Perhaps the FtsZ filaments parallel to the *E. coli* cell's long axis are more involved in

organizing septum synthesis complexes, while the circumferential polymers are more involved in exerting a constriction force.

At least three possible models exist for the driving force of constriction: (1) FtsZ provides the only force needed to constrict the inner membrane and septal peptidoglycan synthesis follows passively; (2) Septal peptidoglycan synthesis drives septum constriction and the Z ring follows passively; or (3) The Z ring and septal peptidoglycan synthesis both provide force to drive constriction. There is recent evidence from the Xiao group that supports the latter two models. Cells were imaged to view Z ring localization using PALM and ordered by their estimated stage in cell division by comparing septum constriction of brightfield images (Coltharp et al., 2016). From this analysis they were able to measure the rate of septum closure, and found that this was largely independent of the GTPase activity and Z ring density of FtsZ, but was slower in cells with a temperature sensitive allele of FtsI (Coltharp et al., 2016). As FtsI is involved in septal peptidoglycan synthesis (Botta & Park, 1981), these data support a model in which septal peptidoglycan synthesis is rate limiting for the force that drives constriction (Coltharp et al., 2016). These results do not exclude forces generated by FtsZ, which are supported by *in vitro* data that FtsZ can generate a constrictive force on liposomes when artificially fused to a membrane tether, or when tethered to the membrane by FtsA* (Osawa et al., 2008; Osawa & Erickson, 2013). There is *in vivo* evidence that FtsZ is not involved at the later stages of septum closure, as it delocalizes from a condensed focus in constricting daughter cells and re-localizes to sites of future divisions prior to sealing of the inner membrane, separating daughter cell cytoplasms (Söderström et al., 2014). Therefore, the most likely model is that both septal peptidoglycan synthesis and the Z ring generate forces to constrict the cell envelope.

6.4 FtsA forms rings *in vitro* similar to a functional homolog, SepF.

The oligomeric rings we observed for purified FtsA by transmission electron microscopy (TEM) are similar to rings formed by SepF, a functional homolog of FtsA. Nevertheless, we see a much wider range of ring diameters (from ~10 to 75 nm, vs. ~ 40 to 65 nm for SepF) (Gündoğdu et

al., 2011) as well as short straight filaments. Rings of purified SepF form whether or not SepF has its N-terminal MTS (Gündoğdu et al., 2011; Duman et al., 2013). We also observe rings of purified FtsA by TEM when the C-terminal MTS of FtsA is deleted, indicating that the MTS is not involved in polymer formation for either protein. Similar structures were observed for wild-type FtsA and other mutant proteins, including $FtsA_{G50E}$ and FtsA*, which show less self-interaction by *in vivo* assays (Herricks et al., 2014; Pichoff et al., 2012). Computational modeling of the curvature of FtsA dimers and tetramers has been used to suggest that FtsA polymers may curve on the membrane and have similar curvature to FtsZ polymers *in vivo* (Hsin et al., 2013). Furthermore, that study identified several residues likely to contribute to self-interaction, one of which was $FtsA_{G49}$; mutation of this amino acid has been suggested to have less self-interaction in the assay described below (Hsin et al., 2013; Pichoff et al., 2012).

One *in vivo* self-interaction assay for FtsA relies on overproducing proteins with a truncation of the C-terminal MTS, which causes wild-type FtsAΔC15 to form large cytoplasmic rods in cells when overproduced, while FtsA* or point mutants near the FtsA dimer interface that are predicted to be defective in self-interaction do not form these rods (Pichoff & Lutkenhaus, 2005; Pichoff et al., 2012). The rods (or lack thereof) have been detected by GFP fusions to the truncated FtsA proteins or using immunofluorescence with an antibody to FtsA (Herricks et al., 2014). Early bacterial two-hybrid data from our lab (Shiomi & Margolin, 2007b) suggested that FtsA* interacts more strongly with FtsZ than does wild-type FtsA (Geissler et al., 2007). However, more recent bacterial two-hybrid data from the Lutkenhaus lab showed that when mutated at a key residue for interaction with FtsZ, wild-type FtsA continued to self-interact, but FtsA* did not (Pichoff & Lutkenhaus, 2007; Pichoff et al., 2015). These data, along with the failure to form cytoplasmic rods, argue that FtsA* is truly defective in self-interaction on its own, but self-interaction can be driven by its strong affinity for FtsZ in the Z ring. As the majority of FtsA should be interacting with FtsZ in the cell when FtsA exerts its activity, it remains to be seen which assay best reflects the physiologically relevant

oligomerization state of FtsA. The two-hybrid and cytoplasmic rod assays may not reflect real FtsA activities because they involve fusions to adenylate cyclase or truncations of the MTS, respectively.

In contrast to the recent data from bacterial two-hybrid and cytoplasmic rod assays, we did not observe a decrease in polymerization of purified FtsA* relative to wild-type FtsA in our sedimentation and TEM analysis. The $FtsA_{G50E}$ mutation, which should affect the dimer interface directly, caused a small decrease in the amount of FtsA that pellets without added liposomes, but the mutant protein still formed rings and short filaments visualized by TEM. Clearly, more sensitive assays and physiological conditions are required to measure FtsA polymerization states *in vitro* and *in vivo*.

6.5 FtsA and FtsA mutant proteins polymerize and bind to liposomes without added ATP.

FtsA, FtsA*, and $FtsA_{G50E}$ bind to liposomes, which is not surprising given that they all function *in vivo* and contain the C-terminal MTS. However, it was surprising that they bound liposomes without the addition of ATP, and the addition of ATP did not change the structures of FtsA observed by TEM. ATP clearly affects FtsA activity in other contexts. For example, *Streptococcus pneumoniae* FtsA forms spiral polymers *in vitro* and binds membrane vesicles in an ATP-dependent manner (Lara et al., 2005; Krupka et al., 2014). Additionally, ADP/ATP addition is required for the dynamic behavior of FtsA and FtsZ on lipid bilayers (Loose & Mitchison, 2014). I detected ATP in our protein preparations, consistent with the *Thermotoga maritima* FtsA crystal structure having ATP bound (Szwedziak et al., 2012). Additionally, *T. maritima* FtsA can form polymers on a lipid monolayer without ATP added (Szwedziak et al., 2012). It is possible that enough ATP purifies with FtsA to allow it to polymerize and bind liposomes, or that bound ADP allows these assemblies, but we have not quantified the amount of ADP in our preparations. Given the role of ATP binding in some FtsA activities, it is unlikely that it is dispensable for polymerizing or binding the membrane, but our purification methods seem to result in protein that is already polymerized and nucleotide-bound. This suggests that another factor is needed for full responsiveness of *E. coli* FtsA to ATP, and

this factor is lost or inactivated in the purification. Isolating such a factor and/or a factor-independent mutant of FtsA are important goals for future studies. Crosslinking experiments may be helpful to identify additional proteins that bind to FtsA and are potential regulators.

FtsN has long been hypothesized to be a trigger for constriction, as it is the last known essential protein to localize to midcell (Corbin et al., 2004; Gerding et al., 2009; Lutkenhaus, 2009; Busiek et al., 2012). Future studies will aim to demonstrate this switch *in vitro* by analyzing structural changes in FtsZ in the presence of FtsA and FtsN and analyzing the effects of FtsN on FtsA assembly and ATPase activity. The activity of a mutant FtsA, $FtsA_{E124A}$, which bypasses the need for FtsN will also be evaluated (Bernard et al., 2007). Recently, other mutations that allow the bypass of FtsN were found in FtsB and FtsL, suggesting that there may be redundant signals to initiate constriction (Liu et al., 2015; Tsang & Bernhardt, 2015). The gain-of-function mutant FtsL* has a residue change in the periplasm and is able to bypass ZipA, similar to FtsA*. FtsL* also suppresses defects of FtsA depletion, but not the complete loss of FtsA (Tsang & Bernhardt, 2015). This data suggests that the FtsQBL complex may communicate signals between FtsA and downstream proteins (Tsang & Bernhardt, 2015). Investigation of potential protein-protein interactions between FtsA and downstream proteins in addition to characterizing their effects on FtsA and FtsZ should shed light on the mechanism of constriction. It is notable that apart from the FtsA-FtsN interaction, the protein partners needed for recruitment of downstream proteins such as FtsQBL to the Z ring are unknown.

Although purified FtsA, FtsA*, $FtsA_{G50E}$, and FtsAΔC15 all assemble into similar structures as visualized by TEM, it is possible that distinct structures might be observed on a membrane. This is true for *S. pneumoniae* FtsA, which forms spiral polymers in solution and straighter polymers on a lipid monolayer (Krupka et al., 2014). Therefore in the future we will assemble *E. coli* FtsA and FtsA mutant proteins on lipid monolayers, and this may aid in distinguishing differences among their assembly structures. Our eventual goal is to understand how FtsA influences FtsZ assembly, and by studying self-interaction mutants for their effects we hope to understand how FtsA functions at different stages of cell division. Soluble FtsA* can depolymerize FtsZ *in vitro* (Beuria et al., 2009),

suggesting that FtsA might aid in disassembly of the Z ring during constriction, but this has not yet been shown for wild-type FtsA. In normal cells, overproducing FtsA strongly inhibits cell division, whereas FtsA* does not. However, in cells with the more-highly assembled $FtsZ_{L169R}$ in place of FtsZ, excess FtsA is not toxic and even suppresses some of the defects of $FtsZ_{L169R}$, suggesting that perhaps it disassembles FtsZ more readily than does FtsA* (Haeusser et al., 2015).

6.6 Importance of reversible membrane binding.

Our laboratory has previously tested fusions of FtsA that should permanently tether FtsA to the inner membrane for their ability to complement a temperature sensitive mutant of FtsA, *ftsA12*. These fusions were able to complement *ftsA12* and allow growth at the non-permissive temperature, although some required higher expression levels to work (Shiomi & Margolin, 2008). These data suggested that reversible binding of the MTS of FtsA was not important, but recently we have made several attempts to transduce a null allele of *ftsA* into the fusion strains, and these have been unsuccessful. These results overturn our previous hypothesis that reversible membrane binding is not necessary, as these fusions cannot support division as the only copy of FtsA in cells. FtsA turns over very rapidly (Geissler et al., 2007) and reversible binding may be important for this turnover. A future goal is to deplete FtsA in cells producing FtsA-FtsN (or even better, FtsA fused to a transmembrane domain not associated with the divisome) to discern which steps in cell division are affected. The phenotype should shed light on which step(s) in cell division require reversible membrane binding by FtsA.

6.7 Targeting the divisome for novel antimicrobial therapies.

The rise in antibiotic resistant bacteria coupled with the lack of novel antibiotics is a growing problem in both hospital and community settings. Multidrug resistance has been observed in pathogens like *Staphylococcus aureus*, *Pseudomonas aeruginosa*, and *Enterococcus faecium*, among others (Nordmann et al., 2007). FtsZ has been proposed as a novel target for antimicrobial therapies

due to its high conservation and important role in cell division (Margolin, 2000; Vollmer, 2006; Erickson et al., 2010). In recent years, a large number of small molecule inhibitors of FtsZ have been identified (den Blaauwen et al., 2014). In 2008 the first *in vivo* evidence that targeting FtsZ could be an effective therapy was demonstrated in mice; a small molecule inhibitor of FtsZ allowed mice to survive even when challenged with a lethal dose of *S. aureus* (Haydon et al., 2008). Since then, several other inhibitors of FtsZ have been identified, but clinical trials are needed to demonstrate their efficacy. Because it is likely that resistance will arise, the use of multiple targets may be beneficial for reducing resistance (Silver, 2011; den Blaauwen et al., 2014). Other divisome proteins have also been proposed as good targets for antimicrobials. Peptide inhibitors of *P. aeruginosa* FtsA have been identified that bind to the ATP binding site and inhibit FtsA's ATPase activity (Paradis-Bleau et al., 2005). The interaction between FtsZ and ZipA has also been targeted, but there is no recent literature on targeting FtsA or ZipA (den Blaauwen et al., 2014). FtsZ seems to be the most promising target so far, and is likely to lead to effective novel antimicrobial therapies in the near future (Li & Ma, 2015).

In summary, these studies have refined our view of the organization of FtsZ and its membrane anchors FtsA and ZipA, viewed using 3D-SIM super-resolution for the first time. The proto-ring proteins largely overlap in patchy localization around the cell circumference. I also uncovered the mechanism behind jackknife divisions in cells producing an artificial fusion of MinCc-MinD. Finally, I have begun biochemical characterization of FtsA and FtsA mutant proteins that have altered properties *in vivo*. Together, these data add to our understanding of the mechanism of cell division in *E. coli* and have implications for other species, most of which divide using Z rings that rely on membrane tethers.

Bibliography

Aarsman, M.E., Piette, A., Fraipont, C., Vinkenvleugel, T.M., Nguyen-Distèche, M., and den Blaauwen, T. (2005) Maturation of the *Escherichia coli* divisome occurs in two steps. *Mol Microbiol* **55:** 1631–1645.

Adams, D.W., and Errington J. (2009) Bacterial cell division: assembly, maintenance and disassembly of the Z ring. *Nat Rev Microbiol* **7:** 642–653.

Addinall, S.G., and Lutkenhaus, J. (1996) FtsA is localized to the septum in an FtsZ-dependent manner. *J Bacteriol* **178:** 7167-7172.

Addinall, S.G., Bi, E., and Lutkenhaus, J. (1996) FtsZ ring formation in fts mutants. *J Bacteriol* 178: 3877–3884.

Adler, H.I., Fisher, W., Cohen, A., and Hardigree, A. (1967) Miniature *E. coli* cells deficient in DNA. *Proc Natl Acad Sci USA* **57:** 321–326.

Alexeeva, S., Gadella Jr., T.W.J., Verheul, J., Verhoeven, G.S., and den Blaauwen, T. (2010) Direct interactions of early and late assembling division proteins in *Escherichia coli* cells resolved by FRET. *Mol Microbiol* **77:** 384–398.

Anderson, D.E, Gueiros-Filho, F.J., and Erickson, H.P. (2004) Assembly dynamics of FtsZ rings in *Bacillus subtilis* and *Escherichia coli* and effects of FtsZ-regulating proteins. *J Bacteriol* **186:** 5775-5781.

Baba, T., Ara, T., Hasegawa, M., Takai, Y., Okumura, Y., Baba, M., Datsenko, K.A., Tomita, M., Wanner, B.L., and Mori, H. (2006) Construction of *Escherichia coli* K-12 in-frame, single-gene knockout mutants: the Keio collection. *Mol Syst Biol* **2:** 2006.0008.

Bailey, M.W., Bisicchia, P., Warren, B.T., Sherratt, D.J., and Männik, J. (2014) Evidence for divisome localization mechanisms independent of the Min system and SlmA in *Escherichia coli*. *PLoS Genet* **10:** e1004504.

Beall, B., and Lutkenhaus, J. (1992) Impaired cell division and sporulation of a *Bacillus subtilis* strain with the *ftsA* gene deleted. *J Bacteriol* **174:** 2398–2403.

Begg, K., Nikolaichik, Y., Crossland, N., and Donachie, W.D. (1998) Roles of FtsA and FtsZ in activation of division sites. *J Bacteriol* **180:** 881–884.

Bendezú, F.O., and de Boer, P.A.J. (2008) Conditional lethality, division defects, membrane involution, and endocytosis in *mre* and *mrd* shape mutants of *Escherichia coli*. *J Bacteriol* **190:** 1792–1811.

Bernard, C.S., Sadasivam, M., Shiomi, D., and Margolin, W. (2007) An altered FtsA can compensate for the loss of essential cell division protein FtsN in *Escherichia coli*. *Mol Microbiol* **64:** 1289-1305.

Bernhardt, T.G., and de Boer, P.A.J. (2005) SlmA, a nucleoid-associated, FtsZ-binding protein required for blocking septal ring assembly over chromosomes in *E. coli*. *Mol Cell* **18:** 555–564.

Bertsche, U., Kast, T., Wolf, B., Fraipont, C., Aarsman, M.E.G., Kannenberg, K., von Rechenberg, M., Nguyen-Distèche, M., den Blaawuen, T., Höltje, J.-V., and Vollmer, W. (2006) Interaction between two murein (peptidoglycan) synthases, PBP3 and PBP1B, in *Escherichia coli*. *Mol Microbiol* **61:** 675-690.

Beuria, T.K., Mullapudi, S., Mileykovskaya, E., Sadasivam, M., Dowhan, W., and Margolin, W. (2009) Adenine nucleotide-dependent regulation of assembly of bacterial tubulin-like FtsZ by a hypermorph of bacterial actin-like FtsA. *J Biol Chem* **284:** 14079–14086.

Bi, E., and Lutkenhaus, J. (1990) FtsZ regulates frequency of cell division in *Escherichia coli*. *J Bacteriol* **172:** 2765–2768.

Bi, E., and Lutkenhaus, J. (1991) FtsZ ring structure associated with division in *Escherichia coli*. *Nature* **354:** 161–164.

Bisicchia, P., Arumugam, S., Schwille, P., and Sherratt, D. (2013) MinC, MinD, and MinE drive counter-oscillation of early-cell-division proteins prior to *Escherichia coli* septum formation. *mBio* **4:** e00856-13.

Biteen, J.S., Goley, E.D., Shapiro, L., and Moerner, W.E. (2012) Three-dimensional super-resolution imaging of the midplane protein FtsZ in live *Caulobacter crescentus* cells using astigmatism. *Chemphyschem* **13:** 1007-1012.

Bork, P, Sander, C., and Valencia, A. (1992) An ATPase domain common to prokaryotic cell cycle proteins, sugar kinases, actin, and Hsp70 heat shock proteins. *Proc Natl Acad Sci USA* **89:** 7290–7294.

Botta, G.A., and Park, J.T. (1981) Evidence of penicillin-binding protein 3 in murein synthesis during septation but not during cell elongation. *J Bacteriol* **145:** 333–340.

Bramkamp, M., Emmins, R., Weston, L., Donovan, C., Daniel, R.A., and Errington, J. (2008) A novel component of the division-site selection system of *Bacillus subtilis* and a new mode of action for the division inhibitor MinCD. *Mol Microbiol* **70:** 1556-1569.

Buddelmeijer, N., and Beckwith, J. (2002) Assembly of cell division proteins at the *E. coli* cell center. *Curr Opin Microbiol* **5:** 553–557.

Buddelmeijer, N., and Beckwith, J. (2004) A complex of the *Escherichia coli* cell division proteins FtsL, FtsB and FtsQ forms independently of its localization to the septal region. *Mol Microbiol* **52:** 1315–1327.

Busiek, K.K., Eraso, J.M., Wang, Y., and Margolin, W. (2012) The early divisome protein FtsA interacts directly through its 1c subdomain with the cytoplasmic domain of the late divisome protein FtsN. *J Bacteriol* **194:** 1989–2000.

Busiek, K.K., and Margolin, W. (2014) A role for FtsA in SPOR-independent localization of the essential *Escherichia coli* cell division protein FtsN. *Mol Microbiol* **92:** 1212–1226.

Busiek, K.K., and Margolin, W. (2015) Bacterial actin and tubulin homologs in cell growth and division. *Curr Biol* **25:** 245–254.

Buss, J., Coltharp, C., Huang, T., Pohlmeyer, C., Wang, S.C., Hatem, C., and Xiao, J. (2013) *In vivo* organization of the FtsZ-ring by ZapA and ZapB revealed by quantitative super-resolution microscopy. *Mol Microbiol* **89:** 1099-1120.

Buss, J., Coltharp, C., Shtengel, G., Yang, X., Hess, H., and Xiao, J. (2015) A multi-layered protein network stabilizes the *Escherichia coli* FtsZ-ring and modulates constriction dynamics. *PLoS Genet* **11:** e1005128.

Camberg, J.L., Hoskins, J.R., and Wickner, S. (2009) ClpXP degrades the cytoskeletal protein FtsZ, and modulates FtsZ polymer dynamics. *Proc Natl Acad Sci USA* **106:** 10614-10619.

Cha, J.-H., and Stewart, G.C. (1997) The *divIVA* minicell locus of *Bacillus subtilis*. *J Bacteriol* **179:** 1671-1683.

Chen, Y., Milam, S.L., and Erickson, H.P. (2012) SulA inhibits assembly of FtsZ by a simple sequestration mechanism. *Biochemistry* **51:** 3100-3109.

Cho, H., and Bernhardt, T.G. (2013) Identification of the SlmA active site responsible for blocking bacterial cytokinetic ring assembly over the chromosome. *PLoS Genet* **9:** e1003304.

Cho, H., McManus, H.R., Dove, S.L., and Bernhardt, T.G. (2011) Nucleoid occlusion factor SlmA is a DNA-activated FtsZ polymerization antagonist. *Proc Natl Acad Sci USA* **108:** 3773–3778.

Coltharp, C., Buss, J., Plumer, T.M., and Xiao, J. (2016) Defining the rate-limiting processes of bacterial cytokinesis. *Proc Natl Acad Sci USA* **113:** E1044-E1053.

Conti, J., Viola, M..G., and Camberg, J.L. (2015) The bacterial cell division regulators MinD and MinC form polymers in the presence of nucleotide. *FEBS Lett* **589:** 201-206.

Corbin, B.D., Geissler, B., Sadasivam, M., and Margolin, W. (2004) A Z-ring-independent interaction between a subdomain of FtsA and late septation proteins as revealed by a polar recruitment assay. *J Bacteriol* **186:** 7736–44.

Corbin, B.D., Yu, X.-C., and Margolin, W. (2002) Exploring intracellular space: function of the Min system in round-shaped *Escherichia coli*. *EMBO J* **21:** 1998–2008.

Cordell, S.C., Anderson, R.E., and Löwe, J. (2001) Crystal structure of the bacterial cell division inhibitor MinC. *EMBO J* **20:** 2454–2461.

Dai, K., and Lutkenhaus, J. (1992) The proper ratio of FtsZ to FtsA is required for cell division to occur in *Escherichia coli*. *J Bacteriol* **174:** 6145–6151.

Dajkovic, A., Lan, G., Sun, S.X., Wirtz, D., and Lutkenhaus, J. (2008) MinC spatially controls bacterial cytokinesis by antagonizing the scaffolding function of FtsZ. *Curr Biol* **18:** 235–244.

de Boer, P.A.J., Crossley, R.E., and Rothfield, L.I. (1989) A division inhibitor and a topological specificity factor coded for by the minicell locus determine proper placement of the division septum in *E. coli*. *Cell* **56:** 641–649.

de Boer, P.A.J., Crossley, R.E., Hand, A.R., and Rothfield, L.I. (1991) The MinD protein is a membrane ATPase required for the correct placement of the *Escherichia coli* division site. *EMBO J* **10:** 4371–4380.

de Boer, P.A.J. (2010) Advances in understanding *E. coli* cell fission. *Curr Opin Microbiol* **13:** 730-737.

den Blaauwen, T., de Pedro, M.A., Nguyen-Distèche, M., and Ayala, J.A. (2008) Morphogenesis of rod-shaped sacculi. *FEMS Microbiol Rev* **32:** 321–344.

den Blaauwen, T., Andreu, J.M., and Monasterio, O. (2014) Bacterial cell division proteins as antibiotic targets. *Bioorg Chem* **55:** 27-38.

Di Lallo, G., Fagioli, M., Barionovi, D., Ghelardini, P., and Paolozzi, L. (2003) Use of a two-hybrid assay to study the assembly of a complex multicomponent protein machinery: bacterial septosome differentiation. *Microbiology* **149:** 3353–3359.

Donachie, W.D., and Begg, K.J. (1989) Cell length, nucleoid separation, and cell division of rod-shaped and spherical cells of *Escherichia coli*. *J Bacteriol* **171:** 4633-4639.

Du, S., and Lutkenhaus, J. (2014) SlmA antagonism of FtsZ assembly employs a two-pronged mechanism like MinCD. *PLoS Genet* **10:** e1004460.

Duman, R., Ishikawa, S., Celik, I., Strahl, H., Ogasawara, N., Troc, P., Löwe, J., and Hamoen, L.W. (2013) Structural and genetic analyses reveal the protein SepF as a new membrane anchor for the Z ring. *Proc Natl Acad Sci USA* **110:** E4601-E4610.

Durand-Heredia, J., Rivkin, E., Fan, G., Morales, J., and Janakiraman, A. (2012) Identification of ZapD as a cell division factor that promotes the assembly of FtsZ in *Escherichia coli*. *J Bacteriol* **194:** 3189-3198.

Durand-Heredia, J.M., Yu, H.H., De Carlo, S., Lesser, C.F., and Janakiraman, A. (2011) Identification and characterization of ZapC, a stabilizer of the FtsZ ring in *Escherichia coli*. *J Bacteriol* **193:** 1405-1413.

Erickson, H.P., Anderson, D.E., and Osawa, M. (2010) FtsZ in bacterial cytokinesis: cytoskeleton and force generator all in one. *Microbiol Mol Biol Rev* **74:** 504–528.

Erickson, H.P., Taylor D.W., Taylor, K.A., and Bramhill, D. (1996) Bacterial cell division protein FtsZ assembles into protofilament sheets and minirings, structural homologs of tubulin polymers. *Proc Natl Acad Sci USA* **93:** 519–523.

Espéli, O., Borne, R., Dupaigne, P., Thiel, A., Gigant, E., Mercier, R., and Boccard, F. (2012) A MatP-divisome interaction coordinates chromosome segregation with cell division in *E. coli*. *EMBO J* **31:** 3198–3211.

Edwards, D.H., and Errington, J. (1997) The *Bacillus subtilis* DivIVA protein targets to the division septum and controls the site specificity of cell division. *Mol Microbiol* **24:** 905-915.

Fleurie, A., Lesterlin, C., Manuse, S., Zhao, C., Cluzel, C., Lavergne, J.-P., Franz-Wachtel, M., Macek, B., Combet, C., Kuru, E., VanNieuwenhze, M.S., Brun, Y.V., Sherratt, D., and Grangeasse, C. (2014) MapZ marks the division sites and positions of FtsZ rings in *Streptococcus pneumoniae*. *Nature* **516:** 259-262.

Fu, G., Huang, T., Buss, J., Coltharp, C., Hensel, Z., and Xiao, J. (2010) *In vivo* structure of the *E. coli* FtsZ-ring revealed by photoactivated localization microscopy (PALM). *PLoS ONE* **5:** e12682.

Fu, X., Shih, Y.-L., Zhang, Y., and Rothfield, L.I. (2001) The MinE ring required for proper placement of the division site is a mobile structure that changes its cellular location during the *Escherichia coli* division cycle. *Proc Natl Acad Sci USA* **98:** 980–985.

Geissler, B., Elraheb, D., and Margolin, W. (2003) A gain-of-function mutation in *ftsA* bypasses the requirement for the essential cell division gene *zipA* in *Escherichia coli*. *Proc Natl Acad Sci USA* **100:** 4197–4202.

Geissler, B., Shiomi, D., and Margolin, W. (2007) The *ftsA** gain-of-function allele of *Escherichia coli* and its effects on the stability and dynamics of the Z ring. *Microbiology* **153:** 814–825.

Gerding, M.A., Liu, B., Bendezú, F.O., Hale, C.A., Bernhardt, T.G., and de Boer, P.A.J. (2009) Self-enhanced accumulation of FtsN at division sites and roles for other proteins with a SPOR domain (DamX, DedD, and RlpA) in *Escherichia coli* cell constriction. *J Bacteriol* **191:** 7383–7401.

Gerding, M.A., Ogata, Y., Pecora, N.D., Niki, H., and de Boer, P.A.J. (2007) The trans-envelope Tol-Pal complex is part of the cell division machinery and required for proper outer-membrane invagination during cell constriction in *E. coli*. *Mol Microbiol* **63:** 1008–1025.

Ghosal, D., Trambaiolo, D., Amos, L.A., and Löwe, J. (2014) MinCD cell division proteins form alternating copolymeric cytomotive filaments. *Nat Commun* **5:** 5431.

Goehring, N.W., and Beckwith, J. (2005) Diverse paths to midcell: assembly of the bacterial cell division machinery. *Curr Biol* **15:** 514–526.

Gola, S., Munder, T., Casonato, S., Manganelli, R., and Vicente, M. (2015) The essential role of SepF in mycobacterial division. *Mol Microbiol* **97:** 560–576.

Gray, A.N., Egan, A.J.F., van't Veer, I.L., Verheul, J., Colavin, A., Koumoutsi, A., Biboy, J., Altelaar, A.F.M., Damen, M.J., Huang, K.C., Simorre, J.-P., Breukink, E., den Blaauwen, T., Typas, A., Gross, C.A., and Vollmer, W. (2015) Coordination of peptidoglycan synthesis and outer membrane constriction during *Escherichia coli* cell division. *eLife* **4:** e07118.

Gregory, J.A., Becker, E.C., and Pogliano, K. (2008) *Bacillus subtilis* MinC destabilizes FtsZ-rings at new cell poles and contributes to the timing of cell division. *Genes Dev* **22:** 3475–3488.

Gündoğdu, M.E., Kawai, Y., Pavlendova, N., Ogasawara, N., Errington, J., Scheffers, D.-J. and Hamoen, L.W. (2011) Large ring polymers align FtsZ polymers for normal septum formation. *EMBO J* **30:** 617-626.

Gupta, S., Kaushik, Banerjee, S.K., Chatterjee, A., Sharma, A.K., Kundu, M., and Basu, J. (2015) Essential protein SepF of mycobacteria interacts with FtsZ and MurG to regulate cell growth and division. *Microbiology* **161:** 1627-1638.

Haeusser, D.P., Hoashi, M., Weaver, A., Brown, N., Pan, J., Sawizke, J.A., Thomason, L.C., Court, D.L., and Margolin, W. (2014) The Kil peptide of bacteriophage λ blocks *Escherichia coli* cytokinesis via ZipA-dependent inhibition of FtsZ assembly. *PLoS Genet* **10:** e1004217.

Haeusser, D.P., Rowlett, V.W., and Margolin, W. (2015) A mutation in *Escherichia coli ftsZ* bypasses the requirement for the essential division gene *zipA* and confers resistance to FtsZ assembly inhibitors by stabilizing protofilament bundling. *Mol Microbiol* **97:** 988-10005.

Hale, C.A., and de Boer, P.AJ. (1997) Direct binding of FtsZ to ZipA, an essential component of the septal ring structure that mediates cell division in *E. coli*. *Cell* **88:** 175–185.

Hale, C.A., Rhee, A.C., and de Boer, P.A.J. (2000) ZipA-induced bundling of FtsZ polymers mediated by an interaction between C-terminal domains. *J Bacteriol* **182:** 5153-5166.

Hale, C.A., Shiomi, D., Liu, B., Bernhardt, T.G., Margolin, W., Niki, H., and de Boer, P.A.J. (2011) Identification of *Escherichia coli* ZapC (YcbW) as a component of the division apparatus that binds and bundles FtsZ polymers. *J Bacteriol* **193:** 1393-1404.

Hamoen, L.W., Meile, J.-C., de Jong, W., Noirot, P., and Errington, J. (2006) SepF, a novel FtsZ-interacting protein required for a late step in cell division. *Mol Microbiol* **60:** 1364-1380.

Haydon, D.J., Stokes, N.R., Ure, R., Galbraith, G., Bennett, J.M., Brown, D.R., Baker, P.J., Barynin, V.V., Rice, D.W., Sedelnikova, S.E., Heal, J.R., Sheridan, J.M., Aiwale, S.T., Chauhan, P.K., Srivastava, A., Taneja, A., Collins, I., Errington, J., and Czaplewski, L.G. (2008) An inhibitor of FtsZ with potent and selective anti-Staphylococcal activity. *Science* **321:** 1673–1675.

Herricks, J.R., Nguyen, D., and Margolin, W. (2014) A thermosensitive defect in the ATP binding pocket of FtsA can be suppressed by allosteric changes in the dimer interface. *Mol Microbiol* **94:** 1393-1404.

Hill, N.S., Buske, P.J., Shi, Y., and Levin, P.A. (2013) A moonlighting enzyme links *Escherichia coli* cell size with central metabolism. *PLoS Genet* **9:** e1003663.

Holden, S.J., Pengo, T., Meibom, K.L., Fernandez Fernandez, C., Collier, J., and Manley, S. (2014) High throughput 3D super-resolution microscopy reveals *Caulobacter crescentus in vivo* Z-ring organization. *Proc Natl Acad Sci USA* **111:** 4566-4571.

Holečková, N., Doubravová, L., Massida, O., Molle, V., Buriánková, K., Benda, O., Kofroňová, O., Ulrych, A., and Branny, P. (2014) LocZ is a new cell division protein involved in proper septum placement in *Streptococcus pneumoniae*. *mBio* **6:** e01700-e01714.

Holmes, W.M., Platt, T., and Rosenberg, M. (1983) Termination of transcription in *E. coli*. *Cell* **32:** 1029-1032.

Hsieh, C.-W., Lin, T.-Y., Lai, H.-M., Lin, C.-C., Hsieh, T.-S., and Shih, Y.-L. (2010) Direct MinE-membrane interaction contributes to proper localization of MinDE in *E. coli*. *Mol Microbiol* **75:** 499-512.

Hsin, J., Fu, R., and Huang, K.C. (2013) Dimer dynamics and filament organization of the bacterial cell division protein FtsA. *J Mol Biol* **425:** 4415–4426.

Hu, Z., and Lutkenhaus, J. (1999) Topological regulation of cell division in *Escherichia coli* involves rapid pole to pole oscillation of the division inhibitor MinC under the control of MinD and MinE. *Mol Microbiol* **34:** 82–90.

Hu, Z., and Lutkenhaus, J. (2000) Analysis of MinC reveals two independent domains involved in interaction with MinD and FtsZ. *J Bacteriol* **182:** 3965–3971.

Hu, Z., and Lutkenhaus, J. (2003) A conserved sequence at the C-terminus of MinD is required for binding to the membrane and targeting MinC to the septum. *Mol Microbiol* **47:** 345–355.

Hu, Z., Gogol, E.P., and Lutkenhaus, J. (2002) Dynamic assembly of MinD on phospholipid vesicles regulated by ATP and MinE. *Proc Natl Acad Sci USA* **99:** 6761–6766.

Hu, Z., Mukherjee, A., Pichoff, S., and Lutkenhaus, J. (1999) The MinC component of the division site selection system in *Escherichia coli* interacts with FtsZ to prevent polymerization. *Proc Natl Acad Sci USA* **96:** 14819–14824.

Huang, K.-H., Durand-Heredia, J., and Janakiraman, A. (2013) FtsZ ring stability: of bundles, tubules, crosslinks, and curves. *J Bacteriol* **195:** 1859–1868.

Huang, K.C., Meir, Y., and Wingreen, N.S. (2003) Dynamic structures in *Escherichia coli*: spontaneous formation of MinE rings and MinD polar zones. *Proc Natl Acad Sci USA* **100:** 12724–12728.

Huisman, O., and D'Ari, R. (1981) An inducible DNA replication-cell division coupling mechanism in *E. coli*. *Nature* **290:** 797–799.

Ishikawa, S., Kawai, Y., Hiramatsu, K., Kuwano, M., and Ogasawara, N. (2006) A new FtsZ-interacting protein, YlmF, complements the activity of FtsA during progression of cell division in *Bacillus subtilis*. *Mol Microbiol* **60:** 1364–1380

Iwaya, M., Goldman, R., Tipper, D.J., Feingold, B., and Strominger, J.L. (1978) Morphology of an *Escherichia coli* mutant with a temperature-dependent round cell shape. *J Bacteriol* **136:** 1143-1158.

Jennings, P.C., Cox, C.G., Monahan, L.G., and Harry, E.J. (2011) Super-resolution imaging of the bacterial cytokinetic protein FtsZ. *Micron* **42:** 336-341.

Jensen, S.O., Thompson, L.S., and Harry, E.J. (2005) Cell division in *Bacillus subtilis*: FtsZ and FtsA association is Z-ring independent, and FtsA is required for efficient midcell Z-ring assembly. *J Bacteriol* **187:** 6536–6544.

Jiménez, M., Martos, A., Vicente, M., and Rivas, G. (2011) Reconstitution and organization of *Escherichia coli* proto-ring elements (FtsZ and FtsA) inside giant unilamellar vesicles obtained from bacterial inner membranes. *J Biol Chem* **286:** 11236-11241.

Johnson, J.E., Lackner, L.L., and de Boer, P.A.J. (2002) Targeting of ^{D}MinC/MinD and ^{D}MinC/DicB complexes to septal rings in *Escherichia coli* suggests a multistep mechanism for MinC-mediated destruction of nascent FtsZ rings. *J Bacteriol* **184:** 2951–2962.

Judd, E.M., Comolli, L.R., Chen, J.C., Downing, K.H., Moerner, W.E., and McAdams, H.H. (2005) Distinct constrictive processes, separated in time and space, divide *Caulobacter* inner and outer membranes. *J Bacteriol* **187:** 6874-6882.

Karimova, G., Pidoux, J., Ullmann, A., and Ladant, D. (1998) A bacterial two-hybrid system based on a reconstituted signal transduction pathway. *Proc Natl Acad Sci USA* **95:** 5752–5756.

Karimova, G., Dautin, N., and Ladant, D. (2005) Interaction network among *Escherichia coli* membrane proteins involved in cell division as revealed by bacterial two-hybrid analysis. *J Bacteriol* **187:** 2233–2243.

Katzmann, E., Müller, F.D., Lang, C., Messerer, M., Winklhofer, M., Plitzko, J.M., and Schüler, D. (2011) Magnetosome chains are recruited to cellular division sites and split by asymmetric septation. *Mol Microbiol* **82:** 1316–1329.

Kiekebusch, D., Michie, K.A., Essen, L.O., Löwe, J., and Thanbichler, M. (2012) Localized dimerization and nucleoid binding drive gradient formation by the bacterial cell division inhibitor MipZ. *Mol Cell* **46:** 245–259.

Król, E., and Scheffers, D.J. (2013) FtsZ polymerization assays: simple protocols and considerations. *J Vis Exp* **81:** e50844.

Król, E., van Kessel, S.P., van Bezouwen, L.S., Kumar, N., Boekema, E.J., and Scheffers, D.J. (2012) *Bacillus subtilis* SepF binds to the C-terminus of FtsZ. *PLoS One* **7:** e43293.

Krupka, M., Cabré, E.J., Jiménez, M., Rivas, G., Rico, A.I., and Vicente, M. (2014) Role of the FtsA C terminus as a switch for polymerization and membrane association. *mBio* **5:** e02221-14.

Kuchibhatla, A., Bhattacharya, A., and Panda, D. (2011) ZipA binds to FtsZ with high affinity and enhances the stability of FtsZ protofilaments. *PLoS One* **6:** e28262.

Lackner, L.L., Raskin, D.M., and de Boer, P.A.J. (2003) ATP-dependent interactions between *Escherichia coli* Min proteins and the phospholipid membrane *in vitro*. *J Bacteriol* **185:** 735–749.

Lan G., Daniels, B.R., Dobrowsky, T.M., Wirtz, D., and Sun, S.X. (2009) Condensation of FtsZ filaments can drive bacterial cell division. *Proc Natl Acad Sci USA* **106:** 121-126.

Land, A.D., Tsui, H.-C.T., Kocaoglu, O., Vella, S.A., Shaw, S., Keen, S.K., Sham, L.-T., Carlson, E.E., and Winkler, M.E. (2013) Requirement of essential Pbp2x and GpsB for septal ring closure in *Streptococcus pneumoniae* D39. *Mol Microbiol* **90:** 939-955.

Lara, B., Rico, A.I., Petruzzelli, S., Santona, A., Dumas, J., Biton, J., Vicente, M., Mingorance, J., and Massidda, O. (2005) Cell division in cocci: localization and properties of the *Streptococcus pneumoniae* FtsA protein. *Mol Microbiol* **55:** 699–711.

Levin, P.A. (2002) Light microscopy techniques for bacterial cell biology. In *Molecular Cellular Microbiology*, Sansonetti, P.J., and Zychlinsky, A. (eds) London: Academic Press pp. 115-132.

Li, X., and Ma, S. (2015) Advances in the discovery of novel antimicrobials targeting the assembly of bacterial cell division protein FtsZ. *Eur J Med Chem* **95:** 1-15.

Li, Y., Hsin, J., Zhao, L., Cheng, Y., Shang, W., Huang, K.C., Wang, H.W., and Ye, S. (2013) FtsZ protofilaments use a hinge-opening mechanism for constrictive force generation. *Science* **341:** 392–395.

Li, Z., Trimble, M.J, Brun, Y.V., and Jensen, G.J. (2007) The structure of FtsZ filaments *in vivo* suggests a force-generating role in cell division. *EMBO J* **26:** 4694–4708.

Liu, B., Persons, L., Lee, L., and de Boer, P.A.J. (2015) Roles for both FtsA and the FtsBLQ subcomplex in FtsN-stimulated cell constriction in *Escherichia coli*. *Mol Microbiol* **95:** 945–970.

Loose, M., and Mitchison, T.J. (2014) The bacterial cell division proteins FtsA and FtsZ self-organize into dynamic cytoskeletal patterns. *Nat Cell Biol* **16:** 38-46.

Loose, M., Fischer-Friedrich, E., Herold, C., Kruse, K., and Schwille, P. (2011) Min protein patterns emerge from rapid rebinding and membrane interaction of MinE. *Nat Struct Mol Biol* **18:** 577-583.

Lu, C., Reedy, M., and Erickson, H.P. (2000) Straight and curved conformations of FtsZ are regulated by GTP hydrolysis. *J Bacteriol* **182:** 164–170.

Lutkenhaus, J. (2009) FtsN—trigger for septation. *J Bacteriol* **191:** 7381-7382.

Lutkenhaus, J., Pichoff, S., and Du, S. (2012) Bacterial cytokinesis: from Z ring to divisome. *Cytoskeleton* **69:** 778–790.

Ma, X., and Margolin, W. (1999) Genetic and functional analyses of the conserved C-terminal core domain of *Escherichia coli* FtsZ. *J Bacteriol* **181:** 7531-7544.

Ma, L., King, G.F., and Rothfield, L. (2003) Mapping the MinE site involved in interaction with the MinD division site selection protein of *Escherichia coli*. *J Bacteriol* **185:** 4948-4955.

Ma, L., King, G.F., and Rothfield, L. (2004) Positioning of the MinE binding site on the MinD surface suggests a plausible mechanism for activation of the *Escherichia coli* MinD ATPase during division site selection. *Mol Microbiol* **54:** 99–108.

Maggi, S., Massidda, O., Luzi, G., Fadda, D., Paolozzi, L., and Ghelardini, P. (2008) Division protein interaction web: identification of a phylogenetically conserved common interactome between *Streptococcus pneumoniae* and *Escherichia coli*. *Microbiology* **154:** 3042–3052.

Männik, J. and Bailey, M.W. (2015) Spatial coordination between chromosomes and cell division proteins in *Escherichia coli*. *Front Microbiol* **6:** 306.

Männik, J., Wu, F., Hol F.J., Bisicchia, P., Sherratt, D.J., Keymer, J.E., and Dekker, C. (2012) Robustness and accuracy of cell division in *Escherichia coli* in diverse cell shapes. *Proc Natl Acad Sci USA* **109:** 6957–6962.

Margolin, W. (2000) Themes and variations in prokaryotic cell division. *FEMS Microbiol Rev* **24:** 531–548.

Margolin, W. (2005) FtsZ and the division of prokaryotic cells and organelles. *Nat Rev Mol Cell Biol* **6:** 862–871.

Margolin, W. (2012) The price of tags in protein localization studies. *J Bacteriol* **194:** 6369–6371.

Martos, A., Monterroso, B., Zorrilla, S., Reija, B., Alfonso, C., Mingorance, J., Rivas, G., and Jiménez, M. (2012) Isolation, characterization and lipid-binding properties of the recalcitrant FtsA division protein from *Escherichia coli*. *PLoS ONE* **6:** e39829.

Miroux, B., and Walker, J.E. (1996) Over-production of proteins in *Escherichia coli*: mutant hosts that allow synthesis of some membrane proteins and globular proteins at high levels. *J Mol Biol* **260:** 289-298.

Miyagishima, S.-Y., Wolk, C.P., and Osteryoung, K.W. (2005) Identification of cyanobacterial cell division genes by comparative and mutational analyses. *Mol Microbiol* **56:** 126–143.

Mohammadi, T., Karczmarek, A., Crouvoisier, M., Bouhss, A., Mengin-Lecreulx, D., and den Blaauwen, T. (2007) The essential peptidoglycan glycosyltransferase MurG forms a complex with proteins involved in lateral envelope growth as well as with proteins involved in cell division in *Escherichia coli*. *Mol Microbiol* **65:** 1106-1121.

Monahan, L.G., and Harry, E.J. (2013) Identifying how bacterial cells find their middle: a new perspective. *Mol Microbiol* **87:** 231–34.

Monahan, L.G., and Harry, E.J. (2016) You are what you eat: metabolic control of bacterial division. *Trends Microbiol* **24:** 181-189.

Monahan, L.G., Liew, A.T.F., Bottomley, A.L., and Harry, E.J. (2014) Division site positioning in bacteria: one size does not fit all. *Front Microbiol* **5:** 19.

Mosyak, L., Zhang, Y., Glasfeld, E., Haney, S., Stahl, M., Seehra, J., and Somers, W.S. (2000) The bacterial cell-division protein ZipA and its interaction with an FtsZ fragment revealed by X-ray crystallography. *EMBO J* **19:** 3179-3191.

Moy, F.J., Glasfeld, E., Mosyak, L., and Powers, R. (2000) Solution structure of ZipA, a crucial component of *Escherichia coli* cell division. *Biochemistry* **39:** 9146–9156.

Mukherjee, A., and Lutkenhaus, J. (1994) Guanine nucleotide-dependent assembly of FtsZ into filaments. *J Bacteriol* **176:** 2754-2758.

Nanninga, N. (1991) Cell division and peptidoglycan assembly in *Escherichia coli*. *Mol Microbiol* **5:** 791–795.

Niki, H., Jaffé, A., Imamura, R., Ogura, T., and Hiraga, S. (1991) The new gene *mukB* codes for a 177-kD protein with coiled-coil domains involved in chromosome partitioning of *Escherichia coli*. *EMBO J* **10:** 183–94.

Nishida, Y., Takeuchi, H., Morimoto, N., Umeda, A., Kadota, Y., Kira, M., Okazaki, A., Matsumura, Y., and Sugiura, T. (2016) Intrinsic characteristics of Min proteins on the cell division of *Helicobacter pylori*. *FEMS Microbiol Lett* [Epub ahead of print].

Niu, L., and Yu, J. (2008) Investigating intracellular dynamics of FtsZ cytoskeleton with photoactivation single-molecule tracking. *Biophys J* **95:** 2009-2016.

Nordmann, P., Naas, T., Fortineau, N., and Poirel, L. (2007) Superbugs in the coming new decade; multidrug resistance and prospects for treatment of *Staphylococcus aureus*, *Enterococcus* spp. and *Pseudomonas aeruginosa* in 2010. *Curr Opin Microbiol* **10:** 436-440.

Osawa, M., Anderson, D.E., and Erickson, H.P. (2008) Reconstitution of contractile FtsZ rings in liposomes. *Science* **320:** 792–394.

Osawa, M., and Erickson, H.P. (2011) Inside-out Z rings—constriction with and without GTP hydrolysis. *Mol Microbiol* **81:** 571-579.

Osawa, M., and Erickson, H.P. (2013) Liposome division by a simple bacterial division machinery. *Proc Natl Acad Sci USA* **110:** 11000–11004.

Paradis-Bleau, C., Sanschagrin, F., and Levesque, R.C. (2005) Peptide inhibitors of the essential cell division protein FtsA. *Protein Eng Des Sel* **18:** 85–91.

Park, K.T., Wu, W., Battaile, K.P., Lovell, S., Holyoak, T., and Lutkenhaus, J. (2011) The Min oscillator uses MinD-dependent conformational changes in MinE to spatially regulate cytokinesis. *Cell* **146:** 396–407.

Patrick, J.E., and Kearns, D.B. (2008) MinJ (YvjD) is a topological determinant of cell division in *Bacillus subtilis*. *Mol Microbiol* **70:** 1166-1179.

Pazos, M., Natale, P., and Vicente, M. (2013) A specific role for the ZipA protein in cell division: stabilization of the FtsZ protein. *J Biol Chem* **288:** 3129-3226.

Pettersen, E.F., Goddard, T.D., Huang, C.C., Couch, G.S., Greenblatt, D.M., Meng, E.C., and Ferrin, T.E. (2004) UCSF Chimera--a visualization system for exploratory research and analysis. *J Comput Chem* **25:** 1605-1612.

Pichoff, S., and Lutkenhaus, J. (2001) *Escherichia coli* division inhibitor MinCD blocks septation by preventing Z-ring formation. *J Bacteriol* **183:** 6630–6635.

Pichoff, S., and Lutkenhaus, J. (2002) Unique and overlapping roles for ZipA and FtsA in septal ring assembly in *Escherichia coli*. *EMBO J* **21:** 685–693.

Pichoff, S., and Lutkenhaus, J. (2005) Tethering the Z ring to the membrane through a conserved membrane targeting sequence in FtsA. *Mol Microbiol* **55:** 1722–1734.

Pichoff, S., and Lutkenhaus, J. (2007) Identification of a region of FtsA required for interaction with FtsZ. *Mol Microbiol* **64:** 1129–1138.

Pichoff, S., Du, S., and Lutkenhaus, J. (2015) The bypass of ZipA by overexpression of FtsN requires a previously unknown conserved FtsN motif essential for FtsA-FtsN interaction supporting a model in which FtsA monomers recruit late cell division proteins to the Z ring. *Mol Microbiol* **95:** 971-987.

Pichoff, S., Shen, B., Sullivan, B., and Lutkenhaus, J. (2012) FtsA mutants impaired for self-interaction bypass ZipA suggesting a model in which FtsA's self-interaction competes with its ability to recruit downstream division proteins. *Mol Microbiol* **83:** 151–167.

Potluri, L.P., Kannan, S., and Young, K.D. (2012) ZipA is required for FtsZ-dependent preseptal peptidoglycan synthesis prior to invagination during cell division. *J Bacteriol* 194, no. 19: 5334–5342.

Raskin, D.M., and de Boer, P.A.J. (1997) The MinE ring: an FtsZ-independent cell structure required for selection of the correct division site in *E. coli*. *Cell* **91:** 685–694.

Raskin, D.M., and de Boer, P.A.J. (1999a) MinDE-dependent pole-to-pole oscillation of division inhibitor MinC in *Escherichia coli*. *J Bacteriol* **181:** 6419–6424.

Raskin, D.M., and de Boer, P.A.J. (1999b) Rapid pole-to-pole oscillation of a protein required for directing division to the middle of *Escherichia coli*. *Proc Natl Acad Sci USA* **96:** 4971–4976.

RayChaudhuri, D. (1999) ZipA is a MAP-Tau homolog and is essential for structural integrity of the cytokinetic FtsZ ring during bacterial cell division. *EMBO J* **18:** 2372-2383.

Ricard, M., and Hirota, Y. (1973) Process of cellular division in *Escherichia coli*: physiological study on thermosensitive mutants defective in cell division. *J Bacteriol* **116:** 314-322.

Rico, A.I., Garcia-Ovalle, M., Mingorance, J., and Vicente, M. (2004) Role of two essential domains of *Escherichia coli* FtsA in localization and progression of the division ring. *Mol Microbiol* **53:** 1359–1371.

Robichon, C., Luo, J., Causey, T.B., Benner, J.S., and Samuelson, J.C. (2011) Engineering *Escherichia coli* BL21(DE3) derivative strains to minimize *E. coli* protein contamination after purification by immobilized metal affinity chromatography. *Appl Environ Microbiol* **77:** 4634-4646.

Robinson, A.C., Kenan, D.J., Hatfull, G.F., Sullivan, N.F., Spiegelberg, R., and Donachie, W.D. (1984) DNA sequence and transcriptional organization of essential cell division genes *ftsQ* and *ftsA* of *Escherichia coli*: evidence for overlapping transcriptional units. *J Bacteriol* **160:** 546–555.

Robinson, A.C., Kenan, D.J., Sweeny, J., and Donachie, W.D. (1986) Further evidence for overlapping transcriptional units in an *Escherichia coli* cell envelope-cell division gene cluster: DNA sequence and transcriptional organization of the *ddl ftsQ* region. *J Bacteriol* **167:** 809–817.

Romberg, L., and Levin, P.A. (2003) Assembly dynamics of the bacterial cell division protein FtsZ: poised at the edge of stability. *Annu Rev Microbiol* **57:** 125-154.

Rowlett, V.W., and Margolin, W. (2013) The bacterial Min system. *Curr Biol* **23:** R553–556.

Rowlett, V.W., and Margolin, W. (2014a) Asymmetric constriction of dividing *Escherichia coli* cells induced by expression of a fusion between two Min proteins. *J Bacteriol* **196:** 2089–2100.

Rowlett, V.W., and Margolin, W. (2014b) 3D-SIM super-resolution of FtsZ and Its membrane tethers in *Escherichia coli* cells. *Biophys J* **107:** L17–L20.

Rowlett, V.W., and Margolin, W. (2015a) The Min system and other nucleoid-independent regulators of Z ring positioning. *Front Microbiol* **6:** 478.

Rowlett, V.W., and Margolin, W. (2015b) The bacterial divisome: ready for its close-up. *Phil Trans R Soc B* **370:** 20150028.

Ruiz, N. (2016) Lipid flippases for bacterial peptidoglycan biosynthesis. *Lipid Insights* **8(S1):** 21-31.

Schaechter, M., Maaløe, O., and Kjeldgaard, N.O. (1958) Dependency on medium and temperature of cell size and chemical composition during balanced growth of *Salmonella typhimurium*. *J gen Microbiol* **19:** 592-606.

Sanchez, M., Dopazo, A., Pla, J., Robinson, A.C., and Vicente, M. (1994) Characterisation of mutant alleles of the cell division protein FtsA, a regulator and structural component of the *Escherichia coli* septator. *Biochimie* **76:** 1071–1074.

Schneider, C.A., Rasband, W.S., and Eliceiri, K.W. (2012) NIH Image to ImageJ: 25 years of image analysis. *Nat Methods* **9:** 671–675.

Schumacher, M.A., Zeng, W., Huang, K.-H., Tchorzewski, L., and Janakiraman, A. (2016) Structural and functional analysis reveal insights into the molecular properties of the *Escherichia coli* Z ring stabilizing protein, ZapC. *J Biol Chem* **291:** 2485-2498.

Shen, B., and Lutkenhaus, J. (2009) The conserved C-terminal tail of FtsZ is required for the septal localization and division inhibitory activity of $MinC^{c}$/MinD. *Mol Microbiol* **72:** 410–424.

Shen, B., and Lutkenhaus, J. (2010) Examination of the interaction between FtsZ and $MinC^N$ in *E. coli* suggests how MinC disrupts Z rings. *Mol Microbiol* **75:** 1285–1298.

Shiomi, D., and Margolin, W. (2007a) The C-terminal domain of MinC inhibits assembly of the Z ring in *Escherichia coli*. *J Bacteriol* **189:** 236–243.

Shiomi, D., and Margolin, W. (2007b) Dimerization or oligomerization of the actin-like FtsA protein enhances the integrity of the cytokinetic Z ring. *Mol Microbiol* **66:** 1396-1415.

Shiomi, D., and Margolin, W. (2008) Compensation for the loss of the conserved membrane targeting sequence of FtsA provides new insights into its function. *Mol Microbiol* **67:** 558–569.

Si, F., Busiek, K., Margolin, W., and Sun, S.X. (2013) Organization of FtsZ filaments in the bacterial division ring measured from polarized fluorescence microscopy. *Biophys J* **105:** 1976-1986.

Silhavy, T.J., Kahne, D., and Walker, S. (2010) The bacterial cell envelope. *Cold Spring Harb Perspect Biol* **2:** a000414.

Silver, L.L. (2011) Challenges of antibacterial discovery. *Clin Microbiol Rev* **24:** 71-109.

Söderström, B., Skoog, K., Blom, H., Weiss, D.S., von Heijne, G., and Daley, D.O. (2014) Disassembly of the divisome in Escherichia coli: evidence that FtsZ dissociates before compartmentalization. *Mol Microbiol* **92:** 1-9.

Spratt, B.G. (1975) Distinct penicillin-binding proteins involved in the division, elongation and shape of *Escherichia coli* K-12. *Proc Natl Acad Sci USA* **72:** 2999–3003.

Spratt, B.G. (1977) Temperature-sensitive cell division mutants of *Escherichia coli* with thermolabile penicillin-binding proteins. *J Bacteriol* **131:** 293–305.

Strauss, M.P., Liew, A.T., Turnbull, L., Whitchurch, C.B., Monahan, L.G., and Harry, E.J. (2012) 3D-SIM super resolution microscopy reveals a bead-like arrangement for FtsZ and the division machinery: implications for triggering cytokinesis. *PLoS Biol* **10:** e1001389.

Stricker, J., and Erickson, H.P. (2003) *In vivo* characterization of *Escherichia coli ftsZ* mutants: effects on Z-ring structure and function. *J Bacteriol* **185:** 4796–4805.

Suefuji, K., Valluzzi, R., and RayChaudhuri, D. (2002) Dynamic assembly of MinD into filament bundles modulated by ATP, phospholipids, and MinE. *Proc Natl Acad Sci USA* **99:** 16776–1681.

Sun, Q., and Margolin, W. (1998) FtsZ dynamics during the division cycle of live *Escherichia coli* cells. *J Bacteriol* **180:** 2050–2056.

Sun, Q., and Margolin, W. (2001) Influence of the nucleoid on placement of FtsZ and MinE rings in *Escherichia coli*. *J Bacteriol* **183:** 1413–1422.

Szeto, T.H., Rowland, S.L., Habrukowich, C.L., and King, G.F. (2003) The MinD membrane targeting sequence is a transplantable lipid-binding helix. *J Biol Chem* 278: 40050–40056.

Szeto, T.H., Rowland, S.L., Rothfield, L.I., and King, G.F. (2002) Membrane localization of MinD is mediated by a C-terminal motif that is conserved across eubacteria, archaea, and chloroplasts. *Proc Natl Acad Sci USA* **99:** 15693–15698.

Szwedziak, P., and Löwe, J. (2013) Do the divisome and elongasome share a common evolutionary past? *Curr Opin Microbiol* **16:** 745–751.

Szwedziak, P., Wang, Q., Bharat, T.A.M, Tsim, M., and Löwe, J. (2014) Architecture of the ring formed by the tubulin homologue FtsZ in bacterial cell division. *eLife* **3:** e04601.

Szwedziak, P., Wang, Q., Freund, S.M. Löwe, J. (2012) FtsA forms actin-like protofilaments. *EMBO J* **31:** 2249-2260.

Thanbichler, M., and Shapiro, L. (2006) MipZ, a spatial regulator coordinating chromosome segregation with cell division in *Caulobacter*. *Cell* **126:** 147–162.

Thanedar, S., and Margolin, W. (2004) FtsZ exhibits rapid movement and oscillation waves in helix-like patterns in *Escherichia coli*. *Curr Biol* **14:** 1167–1173.

Thanky, N.R., Young, D.B., and Robertson, B.D. (2007) Unusual features of the cell cycle in mycobacteria: polar-restricted growth and the snapping-model of cell division. *Tuberculosis* **87:** 231–236.

Tonthat, N.K., Arold, S.T., Pickering, B.F., Van Dyke, M.W., Liang, S., Lu, Y., Beuria, T.K., Margolin, W., and Schumacher, M.A. (2011) Molecular mechanism by which the nucleoid occlusion factor, SlmA, keeps cytokinesis in check. *EMBO J* **30:** 154–164.

Tonthat, N.K., Milam, S.L., Chinnam, N., Whitfill, T., Margolin, W., and Schumacher, M.A. (2013) SlmA forms a higher-order structure on DNA that inhibits cytokinetic Z-ring formation over the nucleoid. *Proc Natl Acad Sci USA* **110:** 10586 –10591.

Treuner-Lange, A., Aguiluz, K., van der Does, C., Gómez-Santos, N., Harms, A., Schumacher, D., Lenz, P., Hoppert, M., Kahnt, J., Muñoz-Dorado, J., and Søgaard-Andersen, L. (2013) PomZ, a ParA-like protein, regulates Z-ring formation and cell division in *Myxococcus xanthus*. *Mol Microbiol* **87:** 235-253.

Tsang, M.-J., and Bernhardt, T.G. (2015) A role for the FtsQLB complex in cytokinetic ring activation revealed by an *ftsL* allele that accelerates division. *Mol Microbiol* **95:** 925–944.

Tsui, H.-C.T., Boersma, M.J., Vella, S.A., Kocaoglu, O., Kuru, E., Peceny, J.K., Carlson, E.E., VanNieuwenhze, M.S., Brun, Y.V., Shaw, S.L., and Winkler, M.E. (2014) Pbp2x localizes separately from Pbp2b and other peptidoglycan synthesis proteins during later stages of cell division in *Streptococcus pneumoniae* D39. *Mol Microbiol* **94:** 21-40.

van Baarle, S., and Bramkamp, M. (2010) The MinCDJ system in *Bacillus subtilis* prevents minicell formation by promoting divisome disassembly. *PLoS ONE* **5:** e9850.

van den Ent, F., Amos, L.A., and Löwe, J. (2001) Prokaryotic origin of the actin cytoskeleton. *Nature* **413:** 39–44.

van den Ent, F., and Löwe, J. (2000) Crystal structure of the cell division protein FtsA from *Thermotoga maritima*. *EMBO J* **19:** 5300–5307.

Vendyaykin, A.D., Vishnyakov, I.E., Polinovskaya, V.S., Khodorkovskii, M.A., and Sabantsev, A.V. (2016) New insights into FtsZ rearrangements during the cell division of *Escherichia coli* from single-molecule localization microscopy of fixed cells. *Microbiologyopen* doi: 10.1002/mbo3.336.

Vicente, M., and Rico, A.I. (2006) The order of the ring: assembly of *Escherichia coli* cell division components. *Mol Microbiol* **61:** 5–8.

Vicente, M., Rico, A.I., Martinez-Arteaga, R., and Mingorance, J. (2006) Septum enlightenment: assembly of bacterial division proteins. *J Bacteriol* **188:** 19–27.

Vollmer, W. (2006) The prokaryotic cytoskeleton: a putative target for inhibitors and antibiotics? *Appl Microbiol Biotechnol* **73:** 37-47.

Wang, X., and Lutkenhaus, J. (1993) The FtsZ protein of *Bacillus subtilis* is localized at the division site and has GTPase activity that is dependent upon FtsZ concentration. *Mol Microbiol* **9:** 435–442.

Weart, R.B., Lee, A.H., Chien, A.C., Haeusser, D.P., Hill, N.S., and Levin, P.A. (2007) A metabolic sensor governing cell size in bacteria. *Cell* **130:** 335–347.

Weiss, D.S. (2004) Bacterial cell division and the septal ring. *Mol Microbiol* **54:** 588–597.

Weiss, D.S., Chen, J.C., Ghigo, J.-M., Boyd, D., and Beckwith, J. (1999) Localization of FtsI (PBP3) to the septal ring requires its membrane anchor, the Z ring, FtsA, FtsQ, and FtsL. *J Bacteriol* **181:** 508–520.

Willemse, J., Borst, J.W., de Waal, E., Bisseling, T., and van Wezel, G.P. (2011) Positive control of cell division: FtsZ is recruited by SsgB during sporulation of *Streptomyces*. *Genes Dev* **25:** 89–99.

Wojtkowiak, D., Georgopoulos, C., and Zylicz, M. (1993) Isolation and characterization of ClpX, a new ATP-dependent specificity component of the Clp protease of *Escherichia coli*. *J Biol Chem* **268:** 22609-22617.

Woldringh, C.L. (1976) Morphological analysis of nuclear separation and cell division during the life cycle of *Escherichia coli*. *J Bacteriol* **125:** 248–257.

Yi, Q.-M., Rockenbach, S., Ward, J.E., Jr., and Lutkenhaus, J. (1985) Structure and expression of the cell division genes *ftsQ*, *ftsA* and *ftsZ*. *J Mol Biol* **184:** 399–412.

Yim, L., Vandenbussche, G, Mingorance, J, Rueda, S., Casanova, M., Ruysschaert, J.-M., and Vicente, M. (2000) Role of the carboxy terminus of *Escherichia coli* FtsA in self-interaction and cell division. *J Bacteriol* **182:** 6366–6373.

Yu, X.-C., and Margolin, W. (1999) FtsZ ring clusters in min and partition mutants: role of both the Min system and the nucleoid in regulating FtsZ ring localization. *Mol Microbiol* **32:** 315–326.

Zhou, H., and Lutkenhaus, J. (2005) MinC mutants deficient in MinD- and DicB-mediated cell division inhibition due to loss of interaction with MinD, DicB, or a septal component. *J Bacteriol* **187:** 2846–2857.

Vita

Veronica Wells Rowlett was born in El Paso, Texas on June 16, 1986, the daughter of Phyllis Morin Wells and Russel Wayne Wells. After graduation from Americas High School, El Paso, Texas in 2004, she attended The University of Texas at El Paso and earned a Bachelor of Science degree with a major in biological sciences and a minor in chemistry in May, 2010. In August of 2010 she entered The University of Texas Graduate School of Biomedical Sciences at Houston.